MECHANICAL BEHAVIOUR OF ULTRAFINE GRAINED Al-Mg-Si ALLOY PROCESSED THROUGH SPD

Ph.D. THESIS

by

MARUFF HUSSAIN

DEPARTMENT OF METALLURGICAL AND MATERIALS ENGINEERING
INDIAN INSTITUTE OF TECHNOLOGY ROORKEE
ROORKEE-247667, INDIA
OCTOBER, 2015

MECHANICAL BEHAVIOUR OF ULTRAFINE GRAINED Al-Mg-Si ALLOY PROCESSED THROUGH SPD

A THESIS

Submitted in partial fulfillment of the requirements for the award of the degree of

DOCTOR OF PHILOSOPHY

in

METALLURGICAL AND MATERIALS ENGINEERING

by

MARUFF HUSSAIN

DEPARTMENT OF METALLURGICAL AND MATERIALS ENGINEERING
INDIAN INSTITUTE OF TECHNOLOGY ROORKEE
ROORKEE-247 667, INDIA
OCTOBER, 2015

INDIAN INSTITUTE OF TECHNOLOGY ROORKEE ROORKEE

CANDIDATE'S DECLARATION

I hereby certify that the work which is being presented in the thesis entitled "**MECHANICAL BEHAVIOUR OF ULTRAFINE GRAINED Al-Mg-Si ALLOY PROCESSED THROUGH SPD"** in partial fulfilment of the requirements for the award of the Degree of Doctor of Philosophy and submitted in the Department of Metallurgical and Materials Engineering of the Indian Institute of Technology Roorkee is an authentic record of my own work carried out during a period from December, 2009 to October, 2015 under the supervision of Dr. R. Jayaganthan, Professor, Metallurgical and Materials Engineering Department, Indian Institute of Technology Roorkee, Roorkee.

The matter presented in this thesis has not been submitted by me for the award of any other degree of this or any other institute.

(MARUFF HUSSAIN)

This is to certify that the above statement made by the candidate is correct to the best of my knowledge.

Date: _____

(R. JAYAGANTHAN)
(Supervisor)

ABSTRACT

The thesis presents the effect of various thermo mechanical treatments on the microstructure evolution and its influence on the precipitation hardening behavior of Al-Mg-Si alloy. The starting material with grain size of several microns has been processed through various thermo mechanical routes to realize ultrafine grained (UFG) structure in it. To ensure the UFG structure in the processed alloy, Electron back scattered diffraction (EBSD), Transmission electron microscopy (TEM), X-ray diffraction (XRD) techniques are used. The mechanical properties of UFG material and its bulk coarse grained counterpart are evaluated through hardness testing and tensile testing at room temperature. The precipitation evolution in UFG material is monitored through differential scanning calorimetry (DSC), hardness testing and TEM.

Al-6061 alloy after solution treatment (ST) was processed through cryorolling (CR) and room temperature rolling (RTR) up to ~90% thickness reduction. Effect of low temperature ageing (at 125 °C) on microstructure and mechanical properties was investigated. The results evidenced that, in as-rolled conditions, RTR material has shown higher hardness than the CR material, which can be attributed to the formation of nanoclusters due to dynamic ageing effect during RTR. Low temperature ageing has resulted simultaneous increment in the strength and ductility in both CR and RTR alloys. However the hardening behavior of RTR material is found to be superior to the CR material. The natural ageing behavior of CR and RTR alloy is found to be similar as observed through hardness testing. Transmission electron microscopy analysis revealed the formation of ultrafine grains (UFG) filled with dislocations and nanosized precipitates in the CR and RTR conditions after ageing treatment. The size of the nano sized precipitates found in optimized condition of RTR material is finer than that in CR material.

To investigate the effect of warm rolling temperature and % deformation after cryorolling on the mechanical properties and microstructural evolution of Al 6061 alloy, the alloy was subjected to cryorolling followed by warm rolling at 100°C, 145 °C and 175 °C with various % reductions (67%, 75%, 80%). The thermal behavior of processed alloy was investigated through DSC. The microstructural features were characterized by adopting Electron back scattered diffraction (EBSD) and Transmission electron microscopy (TEM) techniques. It was observed that the combination of cryorolling and warm rolling is more effective than cryorolling alone. With increasing WR temperature and % of deformation, the alloy has shown significant

improvement in tensile strength (415 MPa) and partial improvement in ductility (6%) as measured from tensile testing. After subsequent low temperature ageing of CR +WR samples at 125 °C has resulted simultaneous improvement in strength and ductility. Dynamic ageing effect during warm rolling has resulted by the formation of nanosized precipitates (clusters) which is evident from the DSC thermograms. Remarkable improvement in hardness and strength of CR +WR sample is attributed to the combined effect of precipitation hardening, dislocation strengthening and partial solid solution strengthening.

To investigate the effect of pre-ageing temperature on the hardening behavior of Al-Mg-Si alloys processed by cryorolling, the alloy was subjected to natural ageing for 2days and pre-ageing at 100 °C, 130°C and 170 °C for 4 hours, 2 hours and 30 minutes respectively. The present investigation revealed that, the natural ageing and pre-ageing before cryorolling is useful to introduce solute clusters in the material to enhance the dislocation density during cryorolling. However artificial ageing of cryorolled samples is not influenced much with pre-ageing. It is also observed that, maturing of CR samples at room temperature for 30 days has resulted better hardening response in subsequent artificial ageing. The optimum heat treatment condition for better mechanical properties may be preferred as "Natural ageing for 2 days + cryorolling 90% + Natural ageing for 30 days followed by artificial ageing at 125 °C for 48 hours.

To understand the evolution of microstructure at larger strains and its influence on the precipitation behavior and mechanical properties, Al-Mg-Si alloy was deformed through cryoforging followed by cryorolling. The bulk Al-Mg-Si alloy, with initial grain size 400 μm, was subjected to solid solution treatment (ST) followed by water quenching at room temperature. The ST treated alloy was subjected to ageing at 100 °C for 4 hours and 8 hours prior to cryoforging. The cryoforged alloy was subjected to cryorolling up to 2.4 true strain for producing long sheets. Finally, the deformed alloy was subjected to low temperature ageing at 120 °C to improve the tensile properties of the alloys. Microstructure and mechanical properties were evaluated through Vickers hardness testing, tensile testing and electron back scattered diffraction (EBSD). The results indicate that combined cryoforging + cryorolling followed by ageing led to remarkable improvement in strength (UTS- 452 MPa) and ductility (8%). The average grain size the alloy was found to be 240 nm, with increased fraction of high angle grain boundaries. Low temperature differential scanning calorimetry (DSC) was used to study thermal behavior of bulk and severely deformed alloy. The thermal behavior of this particular alloy is different as

compared the behavior of the Al-Mg-Si alloys reported in literature. Employing pre-ageing (100 ℃ for 4 h and 8h) has resulted significant improvement in strength and hardness in the forged material. The combination of cryoforging and cryorolling can be used as a simple and cost effective technique to produce high strength Al alloy sheets with UFG structure. Scheduling suitable heat treatments in precipitation hardenable alloys aids to achieve proper combination of properties.

Acknowledgments

I am using this opportunity to thank my supervisor Prof. ***R. Jayaganthan*** for assigning this work to me, his inspiring guidance, and for giving his expertise to this thesis. I am sincerely grateful to him for being patiently with me during the research work and the extra care shown on me. It was pleasure to work under him.

I express my sincere gratitude to Prof. S. K. Nath (Head - MMED, Chairman-SRC), Dr. Vivek Pancholi (Internal member, SRC), Dr. Ramesh Chandra (External member, SRC), Prof. Anjan Sil (Chairman, DRC) for their valuable suggestions to improve this thesis.

I would like to give my special thanks to Prof. Ramesh Chandra (Head, IIC) for providing the TEM and EBSD facilities, which are very essential to carry out this work. I would like to express my sincere thanks to Mr. T.K. Sharma, Mr. B.D. Sharma, Mr. Shakthi Guptha, Mr. Rajendra Sharma and Mr. R.K. Sharma Technical staff of MMED for their great support during the research period.

Furthermore my heartiest thanks to P.Nageswara Rao, Dr. Dharmendra Singh and Dr. Vinod kumar Jeenager for their help at difficult times and friendly advices and inspiring technical inputs. The time I spent with them is memorable. Without their support completing this thesis would have been impossible.

I would like to express my gratitude to all the friends Dr. Sankalp Goel,Nikhil Kumar,Amit Joshi,Yogessha K.K (Research Scholar, MMED) who are supported directly or indirectly to complete this thesis.

My sincere thanks to my wife *Aazra* for her great patience, love and support during my thesis work. I cannot appreciate her in terms of words. My heartiest thank goes to my brothers Warish Hussain and sister Fatma.

I am deeply grateful to Dr. V. N. Shukla and Dr.Sudhakar Pandey for the inspiration given to do Ph.D. Without them I would not have thought about doing Ph.D.

At last, my gratitude to goes to my parents *Ismail Hussain* and *Aisha Khatun*, who supported me always and looking forward patiently for me to complete my thesis work. I dedicate this work to them.

(M. Hussain)

Table of Contents

List of Figures

List of Tables

Definitions and abbreviations

ARB	Accumulative roll bonding
ECAP	Equal channel angular pressing
HPT	High pressure torsion
CR	Cryorolling
WR	Warm rolling
FSP	Friction stir processing
EBSD	Equal channel angular pressing
IQ	Image Quality
MAF	Multi axial forging
MDF	Multi directional forging
B	Burgers vector
SPD	Severe plastic deformation
IPF	Inverse pole figure
DSC	Differential scanning calorimetry
CG	Coarse grained
EDS	Energy dispersive spectroscopy
FCC	Face centered cubic
GND	Geometrically necessary dislocations
MEMS	Microelectromechanical systems
OM	Optical microscopy
SEM	Scanning electron microscopy
TE	Twist extrusion
UTS	Ultimate tensile strength
YS	Yield strength
XRD	X-ray diffraction
A	Constant
β	Poisson ratio
C	Average value of LAGB misorientations
B	Grain boundary spacing

List of publications

A) Refereed International Journals (Published/ Under review): 5 papers

1) **Maruff Hussain,** P.Nageswara rao, R.Jayaganthan, Development of Ultrafine-grained Al– Mg–Si Alloy through SPD processing, "*Metallography, Microstructure and Analysis*"
   (2015), Vol. 4, Issue 3, pp. 219-228.

2) **Maruff Hussain,** P.Nageswara rao, Dharmendra Singh, R.Jayaganthan, Surendra Singh "Comparative study of Microstructure and Mechanical properties of Al 6063 alloy Processed by Multi axial forging at 77K and Cryorolling" *Proceedia Engineering*, (2014), Vol. 75, pp. 129-133.

3) **Maruff Hussain,** P.Nageswara rao, R.Jayaganthan "Precipitation hardening behaviour of Al-Mg-Si alloy Processed by Cryorolling and Room temperature rolling" *Journal of Alloys and Compounds*. (Under review).

4) **Maruff Hussain,** P.Nageswara rao, R.Jayaganthan "Effect of cryorolling followed by warm rolling at various temperatures on microstructure and mechanical properties of Al 6061 alloy.
   Journal of Materials Engineering and Performance. (Under review).

5) **Maruff Hussain,** P.Nageswara rao, R.Jayaganthan "Effect of pre-ageing and natural ageing on hardening behavior of cryorolled Al 6061 alloy. *Materials Physics and Chemistry*, 2014 (Under review)**.**

B) International Conferences (Presented): 1

1. **Maruff Hussain**, P.Nageswara rao**,** R.Jayaganthan,, Comparative study of Microstructure and Mechanical properties of Al 6063 alloy Processed by Multi axial forging at 77K and Cryorolling 7nth International conference on Materials for Advanced technologies (**ICMAT 2013**), 30 June to 5 July 2013, Suntec Singapore.

Chapter 1

Introduction

High strength to weight ratio, high corrosion resistance and easy machinability of the aluminium alloy makes it useful in aerospace, automobile and construction engineering sectors[1]. Various mechanisms used for strengthening aluminium alloys are strain hardening, solid solution strengthening and precipitation hardening. The cost effective method to strengthen the Al alloys is through precipitation hardening achieved by ageing treatment. The precipitates hinder the motion of dislocations during deformation due to which strength is achieved. The evolution of solutes in the form of nano clusters along with different intermediate metastable phases takes place during ageing. The interaction of metastable phases with matrix leads to strengthening during straining of the alloy. The contribution of fortifying from the precipitates is determined by nature, size, volume fraction and their distribution in precipitation hardenable Al alloys. Al 6061 and 6063 are medium strength age hardenable alloys and are used extensively for the fabrication of food containers and various structural components in aircraft industries.

Due to, the ever growing demand for high strength materials with lesser weight in the aerospace and automotive industry as well as to reduce the fuel cost, materials engineers are continuously involved in developing materials with high mechanical properties and corrosion resistance. Nanostructured (grain size < 100 nm) and ultrafine grained (grain size < 1000 nm) materials compared to their coarse grain counterpart have created immense interests in academic institutions and industries due to its substantial improvement in mechanical and corrosion properties. Severe Plastic deformation (SPD) is identified as one of the potential techniques to produce ultrafine and nanostructured materials. Large plastic strain applied on the materials can produce ultrafine grained microstructures in Al alloys [2]. In SPD process, high strain is imposed over the material without any change in the overall dimension and the shape is retained by preventing the free flow of the material using special tool geometries. The hydrostatic pressure applied produces high defects and thus producing better grain refinement. There are various SPD processes used to produce UFG structure in Al alloys such as equal channel angular pressing (ECAP)[2], high pressure torsion (HPT)[3], multi axial forging (MAF), hydrostatic extrusion (HE), twist extrusion (TE) [4][5], Accumulative roll

bonding (ARB)[6],[7] friction stir processing (FSP) [8] and severe cold rolling [9][10][11]. Although deformation strain is important but type of processing and temperature also plays a very important role in achieving grain refinement in aluminium alloys. The mechanism of grain refinement involves continuous generation and multiplication of dislocation in coarse grains and their rearrangement, leading to the formation of subgrain boundaries and finally reorientation of the structures forming ultrafine grained structure. The formation of shear bands due to shear localization at low temperatures could also result in forming high angle grain boundaries in the refined microstructures.

The strength and ductility are important parameters for the materials to be used in structural application. After SPD, materials show high strength but low ductility due to poor work hardenability. Many researchers in last two decades have focused on strategies to develop high strength ultrafine grained materials without losing their ductility. In pure metals, ductility can be achieved by losing slight strength. Ductility in UFG Al alloys can be achieved by processing below the artificial ageing temperatures followed by low temperature ageing. During this type of processing, the drop in strength due to recovery is compensated by precipitation hardening effect. The ductility is increased by increasing the ability to accumulate dislocations surrounding the precipitates. The strengthening of precipitation hardenable UFG/NS aluminium alloys, is due to grain size strengthening (σ_{GS}), solid solution strengthening (σ_{SS}), precipitation strengthening (σ_{PS}), and dislocation strengthening (σ_{DS}). The influence of precipitation hardening on aluminium alloys is most efficient strengthening mechanism in coarse grains as well as in SPD processed Al alloys. Therefore, a thorough investigation is needed to study the effect of precipitation by various SPD processes. However, in case of cryorolling, the precipitation phenomenon is controlled by suppression of diffusion during the deformation process.

Processing at cryo temperature has been found to be an ideal condition for Al alloys to produce ultrafine grained (UFG) materials. At this very low temperature, the strain required to produce UFG is substantially reduced due to suppression of dynamic recovery, resulting in very high dislocation density. Multi directional forging (MAF) is also used to produce UFG structures in the bulk metals and alloys without changing dimension of the work piece. It facilitates to impart very large strain (higher than 6.0) to the materials at different temperatures and thus the effect of precipitation hardening can be studied very easily. The literature is limited on mechanical and precipitation kinetics of Al-Mg-Si alloys processed by combined cryorolling and cryoforging.

Owing to the above mentioned views, the present work has been focused to produce UFG Al-Mg-Si alloys through cryorolling and multiaxial forging and investigate their mechanical and microstructural characteristics. The effect of deformation strain on the microstructure was characterized by using TEM, FE-SEM/EBSD. Optimization of annealing temperature for the deformed Al alloy was made to achieve a better combination of strength and ductility in the alloy in the present work.

CHAPTER 2

Literature Review

2.1 Introduction

Present chapter highlights a brief description of aluminium and their alloys, strengthening mechanisms, ultrafine grained/nano-crystalline materials, material development and different techniques used for producing ultrafine and nano-crystalline grained materials. Cryogenic applications can be possible due to its high toughness at low temperature. Literature related to cryorolling and different severe plastic deformation techniques used for producing UFG microstructure in aluminium are discussed in this chapter. Properties like Light weight, softness of the material with non-poisonous and colorless oxide layer over the surface is well utilized by the packaging industry. Naval applications required good corrosion resistance property which can be possible with aluminium alloy, which forms thin oxide layer which is adherent to the surface and possible to enhance the corrosion resistance by anodizing the surface.

2.2 Severe Plastic Deformation

Severe plastic deformation (SPD) is a technique of producing ultrafine grained material by help of employing large amount of plastic strain. Grain size has a great effect on the mechanical properties in the polycrystalline metals plays a very crucial role. In conventional material the grains size is of several micrometer and a lot of knowledge about the mechanical and physical behaviour has already been understood. The exceptional physical, mechanical and chemical properties shown by ultrafine grained materials are well known. Ultrafine have grain size range (100-1000nm) and Nano grained structure have grain size range (1-100 nm) [12], [13], [14].

There are two methods for producing Bulk UFG/NC grained materials, one is the Bottom up approach in which atom by atom is assembled like a building blocks to produce nano crystalline materials. Examples are inert gas condensation, electro deposition, chemical and physical deposition etc[15]

The second method is known as top-down approach, in which bulk material is refined to produce a ufg material. The large amount of plastic strain generated provides the high amount of dislocation density. The beauty of this technique is such that the original form and

dimension of the specimen remains the same. There are several advantages of top down approach over bottom up approaches as given below.

i) Bulk UFG/NC grained materials can be obtained through SPD.
ii) Defects produced during casting as well as grain size both can be eliminated without effecting the dimensions of the specimen. .
iii) The metal forming techniques are used for SPD techniques and can be used easily in the industry.

A lot of work explaining the various SPD techniques by various researchers has been done. The various SPD techniques are

1. Equal channel angular pressing (ECAP)[16, 17]
2. High pressure torsion (HPT) [18]
3. Multi axial forging (MAF) [19]
4. Twist extrusion (TE) [20]
5. Accumulative roll bonding (ARB) [21]

Derivative process

6. Repetitive side extrusion [22]
7. Rotary die ECAP [23]
8. Cone cone method (CCM) [24]
9. Cryo rolling [25]
10. Transverse rolling [26]
11. Asymmetric rolling (ASR) [27]
12. Cyclic extrusion compression (CEC) [28]
13. Cyclic close die forging(CCDF) [29]
14. Repetitive corrugation and straightening (RCS) [30]
15. Super short interval multi-pass rolling (SSMR)[31]
16. Helical rolling [32]
17. Torsion extrusion[33]
18. Simple shear extrusion [34]
19. Vortex extrusion [35]
20. ECAP with rotation tooling in which the conventional fixed die is replaced by rotating tools [36]
21. Continuous frictional angular extrusion (CFAE)[37]
22. Friction stir processing (FSP)[38]

23. Severe torsion straining (STS) [39]
24. Reversed shear spinning [17]
25. High-pressure tube twisting (HPTT) for thin-walled tubes [40]
26. Cyclic expansion–extrusion CEE—a modified CEC process[41]
27. High-pressure sliding [42]
28. Non-equal channel angular pressing (NECAP) for plate shaped billets [43]
29. Tube channel pressing [44]
30. KOBO forming [45]

Integrated process

31. Integrated extrusion + ECAP [46]
32. Parallel channel ECAP [47]

Continuous process

33. Continuous repetitive corrugation and straightening[48]
34. Incremental ECAP [49]
35. Continuous high pressure torsion [50]
36. Continuous manufacturing of bolts [51]

2.2.1 Equal channel angular pressing: This process is one of widely used SPD process. This method was devised by Segal et al. (1997).ECAP is a process in which material underwent an intense plastic straining through simple shear. In this method sample is placed in a die ,which is in the form of channel. Sample is pressed by the help of plunger. The pressings may be repeated to obtain exceptionally high strains. There are four different methods in ECAP and these methods introduce different shear routes during the pressing operation so that they provides significant differences in the microstructures produced by ECAP.The sample is pressed without rotation in route A. The sample is rotated by 90°in alternate directions during consecutive passes (route B_A). The sample is rotated by 90° either in clockwise or counterclockwise direction between each pass (route B_C). The sample is rotated by 180°between passes (route B_C). This technique is much suitable SPD technique because load requirement is very less and simple tool geometry resulting low tool pressure to develop microstructure and strength in material at applied strain [52]. Figure 2.10 shows the schematic of various ECAP techniques.

Later on, ECAP was corrected by various research groups. Lee et al. (2003) have developed modified equal channel angular rolling (ECAR), the process is represented schematically in Figure 2.10b. Here between the two rollers the strip is made to fed and extruded in order to reduce its strip thickness. In this case sample is made to drive in forward direction by frictional forces, which is applied on the contact surfaces by the help of forward by these forces on the three contact interface.

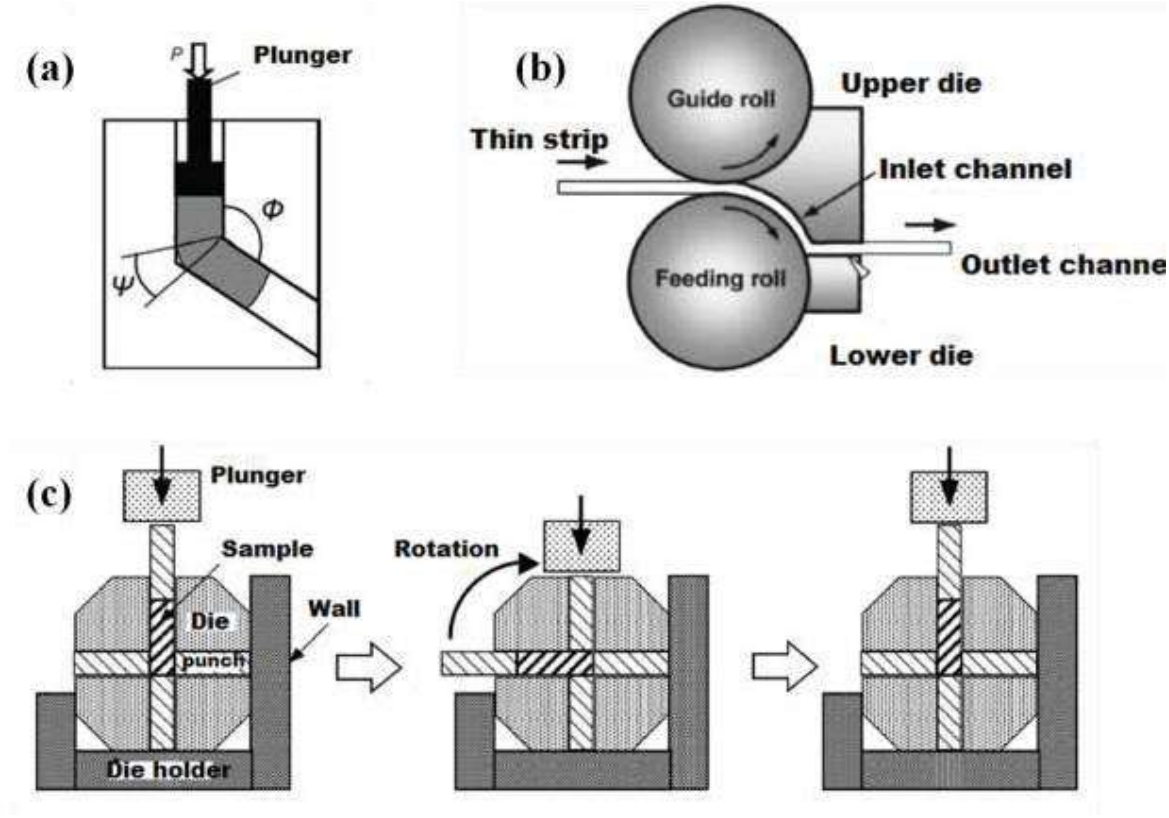

Figure 2.1: Schematic representation of equal channel angular processing (ECAP)[17]; (a) Conventional ECAP[19], (b) Conventional Equal channel angular rolling (ECAR)[53], (c) Rotary die ECAP[17]

2.2.2 Accumulative roll bonding (ARB) : Accumulative roll bonding (ARB) was devised by Saito et al. (1998), shown in figure 2.11a, where the two sheets to be roll bonded were cleaned by acetone and wire-brushed by steel wire. The sheets were then stacked together to form a thick sheet. The two stacked sheets are rolled to 50% of their initial thickness, and then cut into two halves, cleaned thoroughly with wire brushing, stacked together, and rolled again. This sequence is continued for several times till to achieve desired strain. The strength

of the ARB processed material critically depends on the quality of the bond, which may be difficult to achieve. The process may be performed at room temperature or at some elevated temperature. Basic mechanism of grain refinement in ARB takes place due to pure shear. Several researchers have shown that the process may be repeated several times, if some precautions like removing the edge cracks are taken into account. UFG materials produced through ARB exhibit high strength and ductility [54]. Nowadays, this technique is being used to develop composite materials with aim to have qualities of both the material [55], [56].

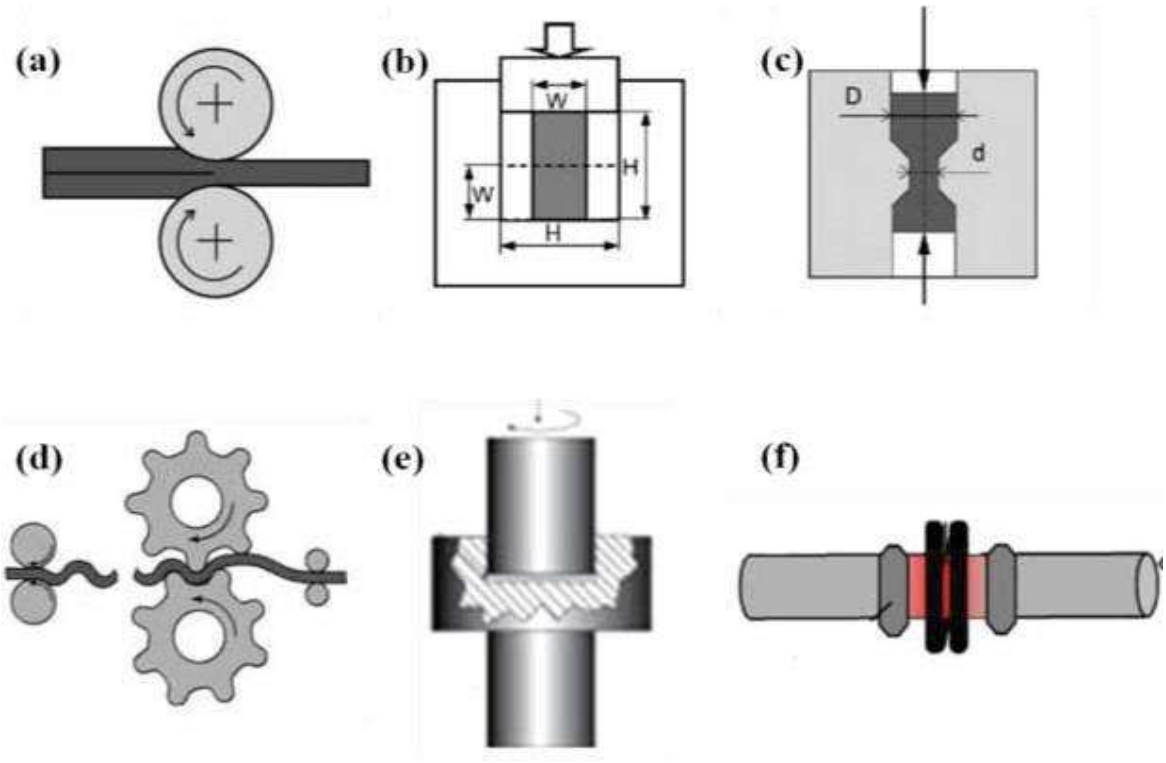

Figure 2.2: Schematic representation of few common SPD processes; (a) ARB[17], (b) MAF[19], (c) CEC[28], (d) RCS[17], (e) HPT[12], (f) STS[17].

2.2.3 Cyclic Extrusion Compression (CEC): Cyclic extrusion compression (CEC) is well known process to produce UFG materials devised by Richert et al. (1986), and represented schematically in Figure 2.11c. RE involves the cyclic flow of metal between the blinking extrusion and compression chambers. The sufficient counter-pressure is given to the samples to cause plastic deformation by alternating extrusion and compression by touching the workpiece cyclically between the two die chambers to build up desired plastic strain. The accumulated equivalent strain is approximately given by;

$$\varepsilon = 4n\ ln\ (\frac{D}{d}) \quad (2.1)$$

Where; 'D'is the chamber diameter, 'd' is the channel diameter and 'n' the number of deformation cycles. A elevated hydrostatic pressure is imposed due to cyclic extrusion and compression, resulting in higher loads, which require special tooling. This process is most appropriate for processing of soft material such as aluminium alloys.

2.2.4 Repetitive Corrugation and Straightening (RCS): This method was developed by Huang et al. (2001), and represented schematically in Figure 2.11d. The method consists of continually bending and straightening of a billet with ridged tools and then straightening the billet with flat tools without changing the cross-sectional area of the billet imposing high strain into the material. The equivalent strain per one sequence is given by;

$$\varepsilon = 4\ ln\ \frac{[\frac{r+t}{r+0.5t}]}{\sqrt{3}} \quad (2.2)$$

Where, 't' is the thickness of sample and 'r' is the curvature of bent zone. By repeating this process in a cyclic manner, severe plastic strain can be introduced in to the work piece, which results in grain refinement.

2.2.5 High Pressure Torsion: The high pressure torsion (HPT) process was first investigated by Bridgman et al. (1935). Later on, Erb et al. (1993) reported that there are formation of ufg and nano grain with high angle boundary in this process. Sample in HPT is in the form of small ring, which is having a conical face as shown in Figure 2.11e. The sample is pressed between anvil and burrs are formed at the edges. Then, one anvil is rotated with respect to another one and the speed of rotation is varied over a large range. The deformation of the sample takes place through simple shear. The high pressure suppresses the formation of cracks and therefore, it is possible to apply extremely high strain without failure of the deformed sample, and very fine grains of the order of nanometer range (100 nm) may be produced. The major drawback of this process is that, it process the specimens in the form of relatively small discs, therefore, it is not applicable for bulk material.

2.2.6 Severe Torsion straining (STS): This process was developed by Nakamura et al. (2004), which is shown schematically in Figure 2.11f.in this process one end is rotated with respect to another. Due to which severe torsion strain is induced . The rod is moved along the longitudinal axis of apparatus creating the local strain. Therefore, a severe plastic strain can

be induced continuously all through the rod. To create competent STS, the locally heated region should be thin and rod should be rotated faster with respect to its moving speed. A amendment can be made for the cooling system so that the heated region is more limited to a small area to create torsion strain. The severe torsional straining (STS) procedure can be used for consolidation of powders to produce metal-ceramic and nano-composites having high density, and to produce ultrafine grain size and high strength materials.

All of the above explained procedures can introduce large plastic strain into the material leading to significant refinement in microstructure of bulk crystalline solids. Some of them are well established and being used by different research groups to fabricate bulk nanostructured or ultrafine grain samples of different materials, while others are under development stage and not fully commercialized for large-scale industrial applications due to their limited production rates.

It can be observed that all the methods stated above are developed newly with in 10 to 12 years, so there is a scope for more routes. Cryo rolling, because of its simplicity, less expensive process, no die design requirement, lesser wear problems during processing, low maintenance cost, easy to produce in ultrafine and nanocrystalline materials in bulk lure scientist to do research on this process. Cryo rolling was first introduced by Wang et.al. (2002), they rolled copper plate in liquid nitrogen temperature up to 93% and developed both nanocrystalline and ultrafine grains ranging <300nm with high yield strength. He also reported that annealing at low temperature and at optimized time period, multimodal grain structure with bulk, ultrafine and nanocrystalline grains with large ductility can be obtained without losing strength. A lot of papers are already been published on the cryorolling of copper, aluminium, Titanium, Zirconium ,Steel, zinc, Magnesium, Nickel and their alloys [57], [58], [59], [60], [61], [62].

2.3 Aluminium alloys

Pure form of aluminium has low strength and highly ductile, good corrosion resistant along with good electrical conductivity Hence, it is widely used for applications in foil and conductor cables. For the application purpose, it is needed to alloying aluminum with other elements in order to increases it strength. It has face centered cubic (FCC) structure which is stable up to its melting point temperature (657 $^{\circ}$C). Yield strength of pure aluminium is 7-11 MPa, while its alloys have yield strengths ranging from 200 MPa to 600 MPa. For low

temperature application, aluminium alloys can be used suitably. Aluminium is very reactive to oxygen due to which it forms a very thin oxide layer over its surface which is very stable and works as insulator as well as protects aluminium from external environment. Aluminium Alloys are classified as wrought alloys which are formed by rolling, forging and extrusion and cast aluminium alloys those are directly casted in required shape. Further classification falls into two distinct categories as shown in Figure 2.1.

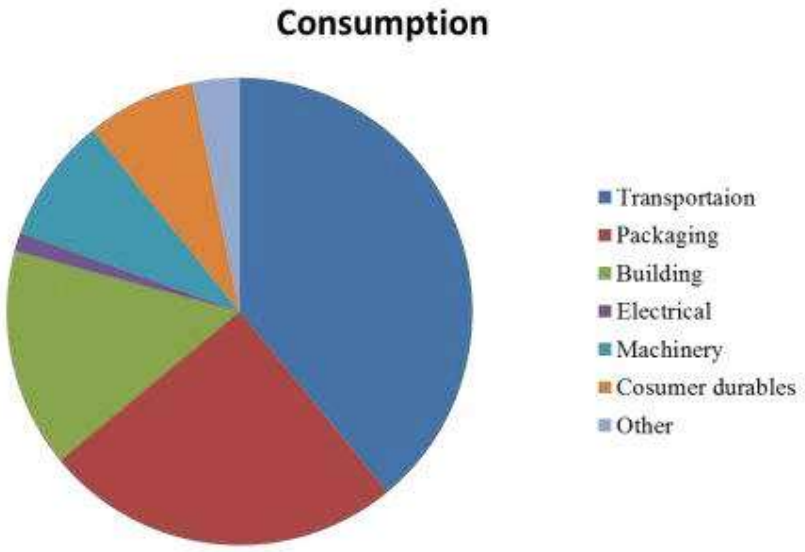

Figure 2.3:Consumption of Aluminium in various sectors (Data plotted based on 2013reports)

a. Heat treatable alloys

Few Aluminium alloys in which improvement in strength is achieved by heat treatment and age hardening. 2xxx, 6xxx, 7xxx series contains solute elements in the concentrations that exceed their equilibrium solubility at room temperature. After solution treatment (dissolution of soluble phase) and water quenching (development of super saturation phase) followed by low temperature ageing, the solute atoms precipitates which significantly strengthen the materials. This strengthening mechanism is called precipitation hardening.

b. Non-heat treatable alloys

These are the materials which derive their properties from work hardening and solid solution strengthening. The enhancement in properties of 1xxx, 3xxx, 4xxx and 5xxx series alloys is achieved through cold working usually by cold rolling and annealing along with thermal treatment required for their stabilization. They are not sufficient for load bearing structural applications because the strengthening properties obtained for the cold worked structures are lost at elevated temperatures. The alloys above mentioned are non-heat treatable alloys. The strengthening of these alloys is primarily through solid solution strengthening and strain hardening. The cold working is achieved by rolling, drawing, stretching, forging or similar operations. Moreover these alloys will not show any hardening response due to precipitation hardening through heat treatment.

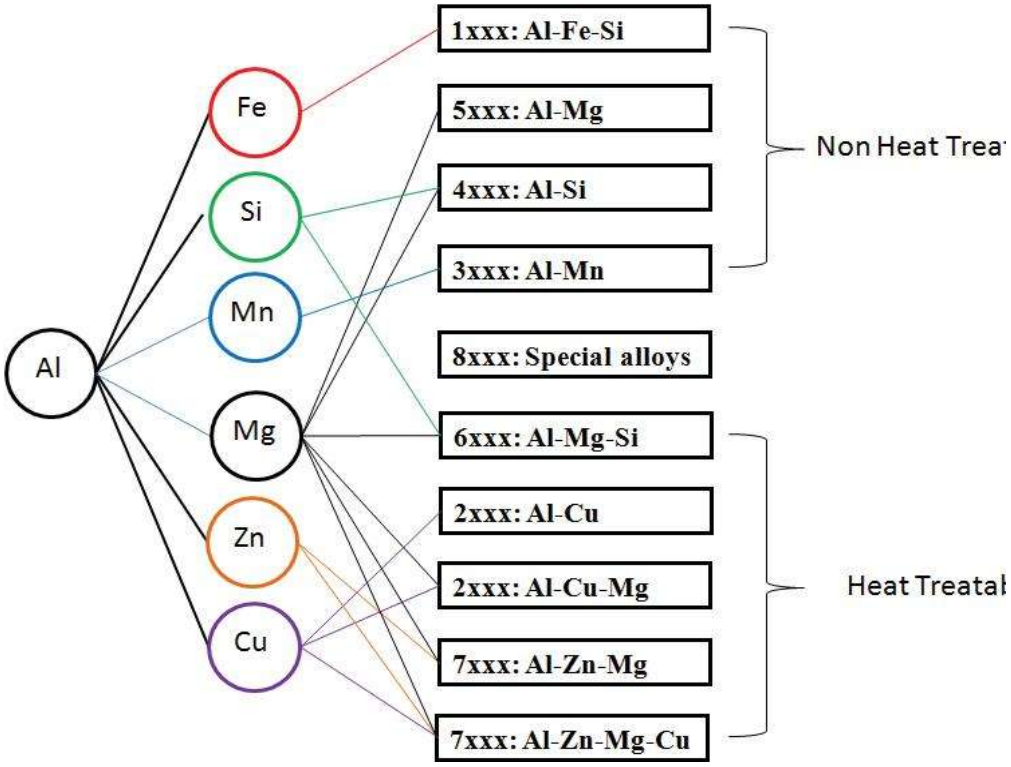

Figure 2.4: Principal alloying elements and the families of alloy derived from them (Hatch, 1984).

2.4 Strengthening mechanisms for aluminium alloys

Strengthening of aluminium alloys is of great interest because of low density of the alloy, and various people have reported the strengthening through grain refinement of aluminium alloy [63] [64], [65][66][67][68][69][70] It is already known that the strength of the material can be enhanced by restricting the motion of dislocation during loading. The

motion of dislocations can be blocked in different ways within the microstructure, such as precipitates, crystal lattice itself, solute atoms, strain hardening and grain boundaries, thus increasing dislocation density in the matrix [71].Strengthening by, solid-solution strengthening, grain-size reduction, and strain hardening apply for single-phase metals. While, fiber strengthening, dispersion hardening and precipitation hardening is in multi-phase metallic materials.

2.4.1 Strengthening by Grain Size Reduction

In polycrystalline materials, orientation of grain changes abruptly on moving from one grain to another across the grain boundary. During deformation it becomes difficult for the dislocations to move from one grain to another grain due to a particular slip plane. Due to this reasons the dislocation during deformation initially piles up near the grain boundary. This pile up of dislocations will be more rapid in smaller grain. This restriction of dislocation motion in small grain makes it strain hardened due to which the strength increases. If the grain boundary is low angle grain boundary hindering of dislocations is less, while high angle grain boundary completely hinders the dislocation motion thus strength of the material increases. The Fig 2.2 a shows dislocation moving along a slip plane approaching grain boundary. Fig 2.2 b shows low and high-angle grain boundaries with respect to atom positions adjacent to it.

As the grain size reduces, the mean distance travelled by dislocation decreases, and pile up of dislocations starts at grain boundaries. This results the increase in yield strength of the material, which is explained from relation known as Hall-Petch relation between yield strength (σ_y) and grain size (d) (Hall, 1951, Petch, 1953 and Hansen, 2004).

$$\sigma_y = \sigma_{o+kd}^{-1/2} \qquad (2.3)$$

Where; 'σ_o' is the friction stress representing the resistance of the crystal lattice to dislocation movement, 'k' is the locking parameter that measures the hardening contribution made by grain boundaries and 'd' is the average grain diameter. The yield strength of the material is inversely proportional to its grain size; this means that as the grain size decreases the strength of the material will increase. The above relation is not valid on coarse grain and extremely fine grain polycrystalline materials.

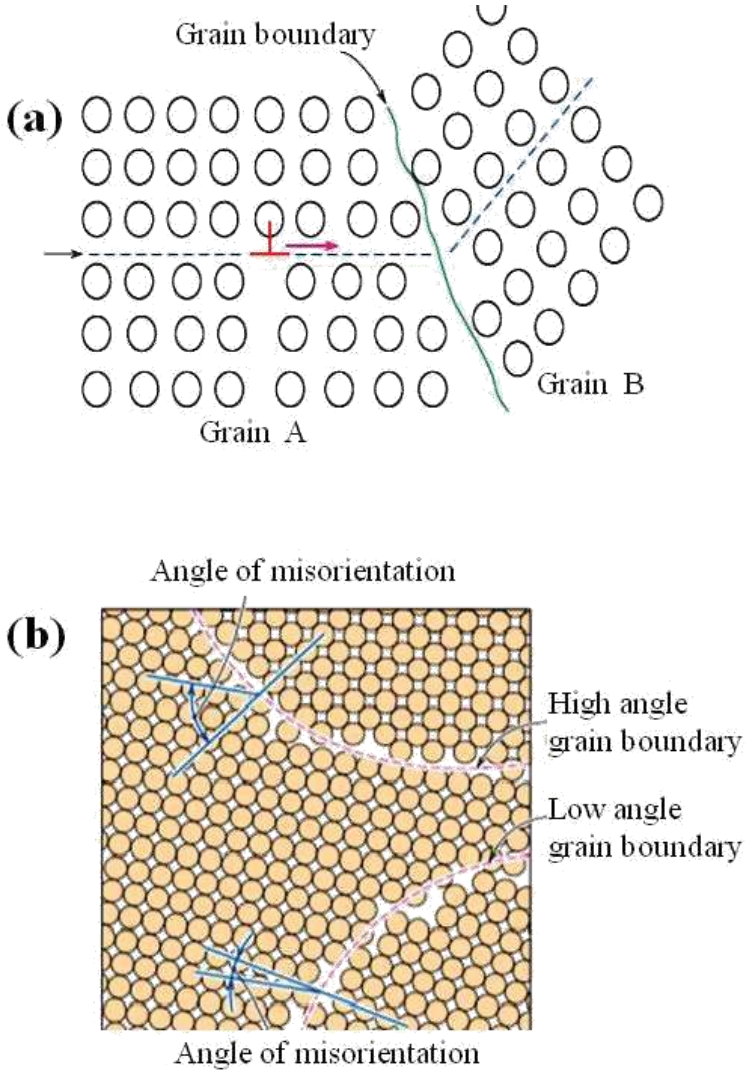

Figure 2.5:(a) Dislocation motion approaching a grain boundary,(b) Low and high-angle grain boundaries with respect to adjacent atom positions[72]

2.4.2 Solid solution strengthening

Solid solution hardening is a very successful method for improving the strength of a material. Adding stronger atoms of another element stronger than the parental method occupies interstitial or substitutional sites in lattice and increases the strength of parent material as shown in Figure 2.3. The stress fields generated around the solute atoms interact with the stress fields of a moving dislocation and thus restricting the motion thereby increasing the stress required for plastic deformation. Solid solution strengthening depends on: concentration of solute atoms, size of solute atoms, valency of solute atoms and shear modulus of solute

atoms, The strengthening increment by a solute '$\Delta \sigma_{ss}$', due to concentration 'C' of a solute atom, is defined as;

$$\Delta\sigma_{ss} = HC_{\alpha} \quad (2.4)$$

Where 'α' and 'H' are constants. A higher concentration of solute atoms will obstruct more dislocation as compared to low solute concentration, thus increasing strength [73].

The alloy which is strengthened by solid solution strengthning coupled with cold working is aluminium-magnesium alloy containing magnesium in range from 0.5 to 6 wt%. Some other elements in small quantities such as manganese or chromium, zirconium controls the grain or subgrain structure, silicon and iron are impurities present as intermetallic particles. Al -Mn acts as point defects and impedes dislocation movement. Figure 2.4 shows the effect of magnesium in solid solution on the strength and elongation for some of the common aluminium- magnesium alloys.

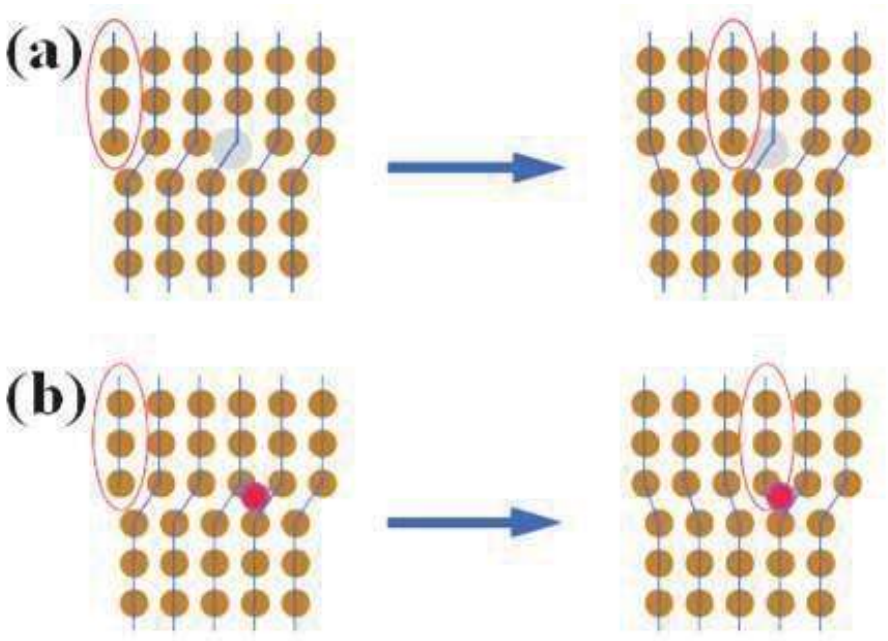

Figure 2.6: Representation of a dislocation stopped by; (a) Substitutional atom (b) Interstitial atom[75].

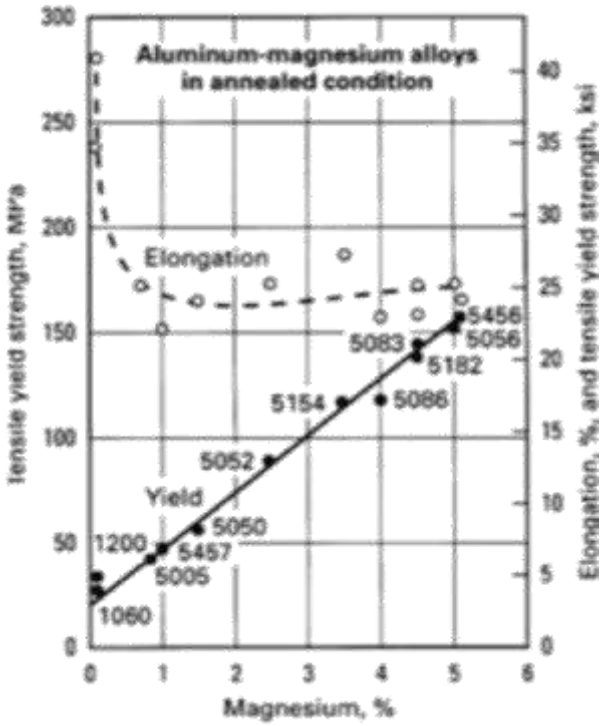

Figure 2.7: Effect of Magnesium (wt %) in solid solution on mechanical properties[74]

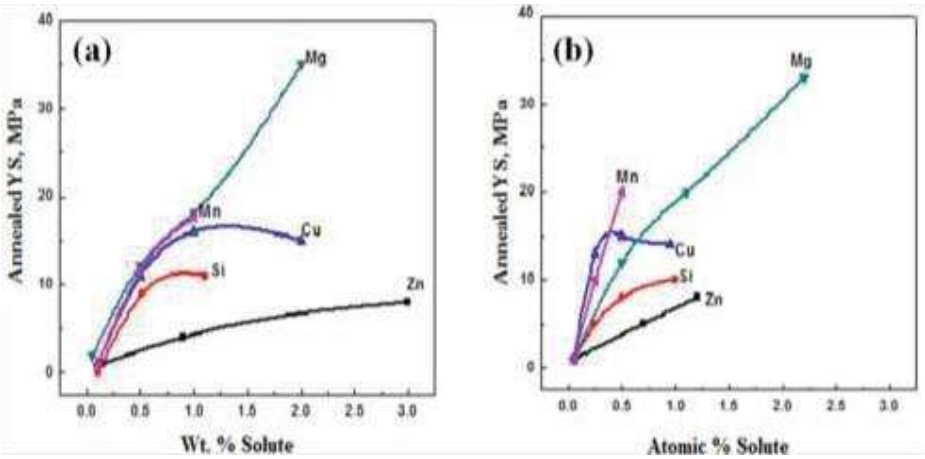

Figure 2.8: Effect of various alloying elements and their concentration on yield strength as a function of; (a) weight % solute, (b) atomic % solute. [75]

From Figure 2.5 (a) and 2.5 (b) it can be seen that alloying the elements in aluminium the yield strength of annealed aluminium sheet increases. On varying the concentration of the alloying element the effect is not linear; similarly, the various types of solute elements are not equally effective in strengthening mechanism. A concentration less than 0.5% of Cu and Mn are more effective in strengthening as can be seen from figure 2.5 a. Addition of Magnesium on weight % basis is more effective compared to atomic % basis. The effect of magnesium is more in solid solution strengthening of aluminium alloys. Cu and Si affects presents in small effects the amount of Mg retained in solution, as Al-Cu-Mg, Al-Mg-Si phases. (13) (14) Alloying of Cu results in age hardening behaviour, while Zinc is highly soluble at low temperature and has very less effect on strength due to its high density of 7.14 g/cm^3.

2.4.3 Strain hardening

Strain hardening is a method which has been used from ages by various blacksmiths to increase the strength of the materials. Wrought alloys are mostly strengthened by strain hardening. The material is cold worked at ambient temperatures, where the dislocations multiply at a faster rate than destroyed by dynamic recovery**.** With increase in dislocation density, dislocations come together and interaction between dislocations takes place which produce obstacles in the motion of other dislocation. This leads to an increase in the yield strength of the material at the expense of ductility. Orowan Type equation shows the strength contribution of dislocation structures to the macroscopic flow stress [76]

$$\sigma_0 = \alpha G b \rho \qquad (2.5)$$

Where, ‘σ’ is macroscopic flow stress, ‘σ ، is friction stress, ‘α’ is constant, ‘G’ is shear modulus, ‘b’ is Burger’s vector and ‘ρ’ is total dislocation density. From equation (2.3), it can be seen that yield strength is directly proportional to dislocation density. Therefore, with the increase in dislocation density during plastic deformation, the yield strength of the material increases significantly. The influence of cold working on the yield stress and ductility of the material is shown in Figure 2.6.

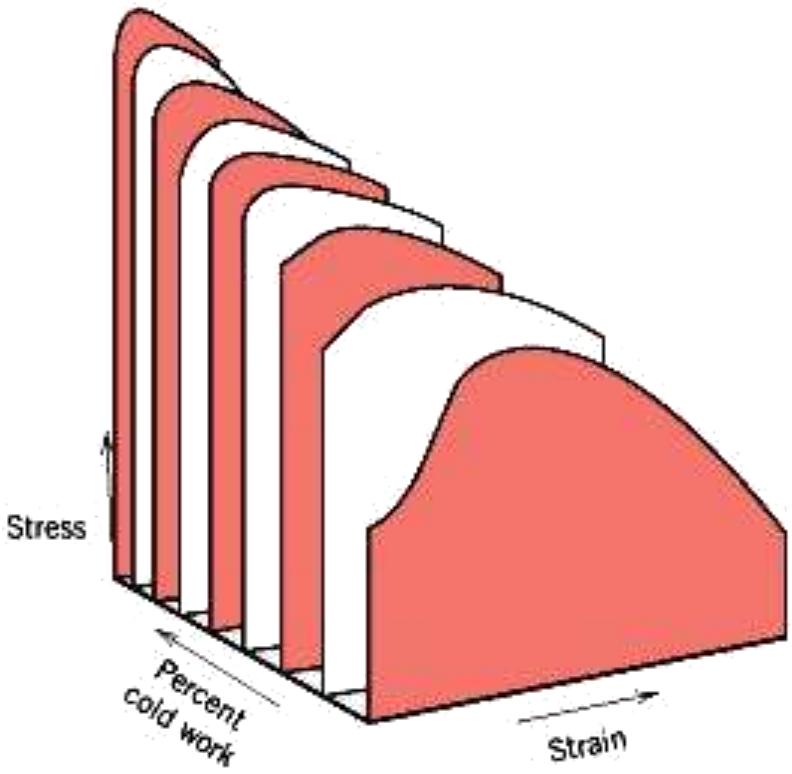

Figure 2.9: The influence of cold working on yield stress and ductility of a material [72].

2.4.4 Precipitation hardening

Precipitation hardening is most useful strengthening mechanisms of aluminium alloys in 2xxx, 6xxx and 7xxx series, where the strength of aluminium alloys is improved by the formation of fine and uniformly dispersed second-phase particles of the solute atoms in matrix. The fine precipitates restrict the motion of dislocations and strengthen the heat-treated alloys. The process is mainly of three steps; i) Homogenization or Solution heat treatment of the alloy, where the alloy is heated above the solvus temperature and soaked, until solute dissolves properly and homogeneous solid solution is produced; ii) Quenching, where this solid solution cools rapidly to a lower temperature forming a supersaturated solid solution and the solute does not immediately able to diffuse out of a phase.; iii) Finally ageing is done where the supersaturated solid solution is heated below the solvus temperature to produce a finely dispersed precipitate. The solvus temperature is the temperature above which the soild1+solid2 will become a single solid phase. It corresponds to the particular composition of interest. Figure 2.7 shows temperature vs time plot for precipitation hardening mechanism. The fine precipitates in the alloy are more helpful in preventing movement of dislocations. Various modes of interaction between precipitates and dislocations proposed by [77] can be seen from the schematic shown in Figure 2.8.

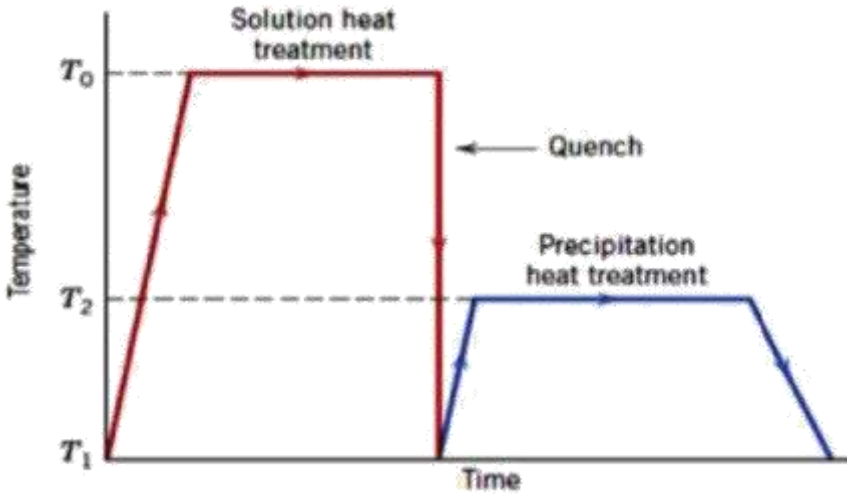

Figure 2.10: Schematic of temperature-time plot showing precipitation hardening mechanism[77].

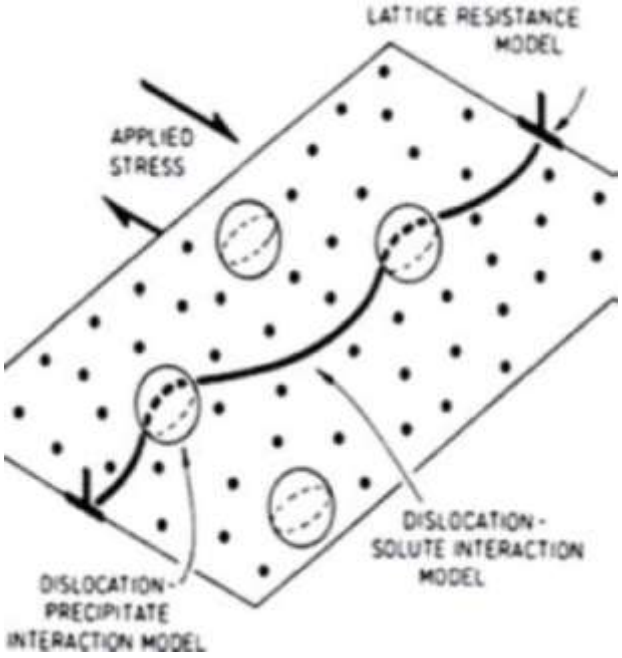

Figure 2.11: Schematic of interaction of dislocation line with precipitates [77]

2.4.5 Dispersion hardening

The strength and hardness in metal and alloys can also be improved by the help of extremely small and uniformly dispersed particles usually less than 0.1μm size within the matrix. These particles can hinder the motion of dislocation and can increase the strength of a material. By simple mixing and consolidation or as precipitates in a solid state these second phase particles can be added in the matrix, even at higher temperatures. The strengthening of the alloy can be controlled by size, shape, and amount of second phase particles, for example hard fine particles of Al_2O_3 in soft ductile matrix of aluminium. When there is an abrupt change in orientation and the solid solutions are non-deformable dislocations are not able to cut though the precipitate particles at even high value of applied stress. The moving dislocations bow instead of cutting through the precipitate. When the dislocation moves forward leaving a dislocation loop around each particle, it is known as Orowan mechanism [78] Schematic showing the Orwan mechanism of dispersion hardening can be seen from Figure 2.9.

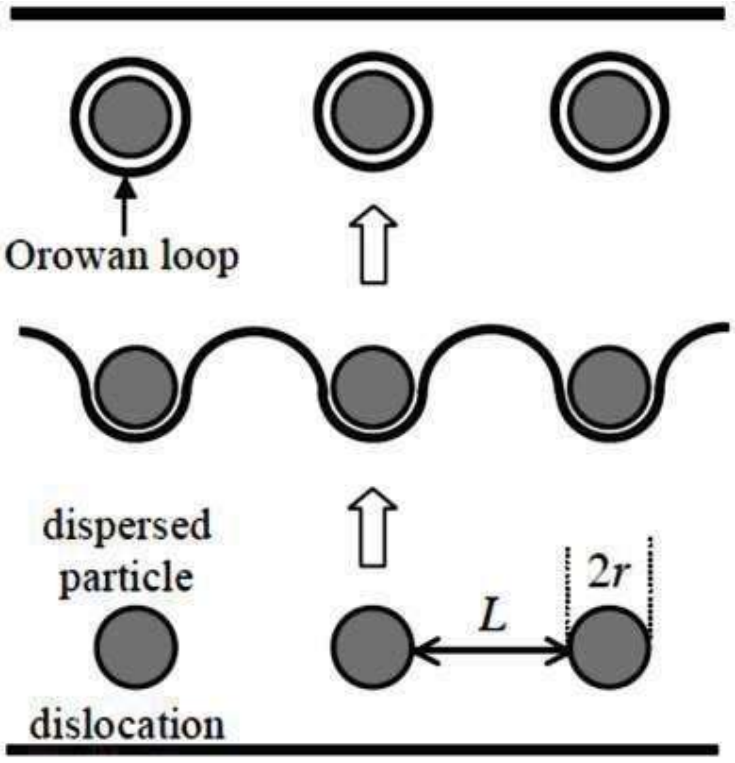

Figure 2.12: Schematic of Orwan mechanism for dispersion hardening [78]

2.4.6 Strengthening mechanisms in ultrafine grained Aluminium alloys

i) Grain boundary strengthening

Grain boundary is the area where the lot of lattice perturbation occurs. When the dislocation faces grain boundary, its motion gets hindered. It leads to pile up of dislocations at the grain boundaries. Therefore, the distance moved by dislocation before reaching grain boundary reduces with decreasing size resulting in higher strength [79]. This effect is called as grain boundary strengthening. In coarse grained aluminium alloy, the grain size is in the range of few microns to several microns (three digits). Coarse grained aluminium alloys shows normal yielding and work hardening behavior, whereas UFG materials shows sharp yield point [80]. In the early 1950s, Hall and Petch have proposed a relation between yield stress ($\sigma_{y)}$ to the grain size (d) of the undeformed material [81][82].

$$\sigma_y = \sigma_o + Kd^{-m} \quad (2.6)$$

where σ_o is the Peierls or frictional stress, '*K'* a coefficient and an exponent '*m'* is ½.

Peierls equation is as follows:

$$T_{\rho} = [2G/1-\mu]\, e^{-2\pi w/b} \quad (2.6)\ (a)$$

Above equation shows that with the increasing dislocation width (w), the corresponding shear stress would decrease.

It was observed from (*Figure 2.12*), that this relation is also well valid for UFG (grain size 100-1000 nm) in Al alloys [83]. However, in the materials developed through severe plastic deformation, microstructure contains grain boundaries with different misorientation angle. The resistance provided to the dislocation pileup by grain boundary depends on its nature, and the nature of the grain boundaries depends on method of synthesis [84]. A grain boundary with low angle misorientation provides less resistance to the dislocation motion as compared to the grain boundaries with high angle misorientation. Later, the Hall-Petch relation has been modified to include the grain boundary character, and the proposed modified Hall-Petch relation by Niels Hansen [84] is

$$\sigma_f = \sigma_0 + [M\alpha\sqrt{3b\theta LAGB\,(1-f)} + K_1\sqrt{f}]D_B^{-1/2} = \sigma_0 + k_2 D_B^{-1/2} \quad (2.7)$$

Where σ_f – is flow stress, M- Taylor's factor, α- Material dependent constant, G- Shear modulus, b- Burgers vector, D_B - Grain boundary spacing, k_1- constant, f- Fraction of HAGB. In micro crystalline and UFG materials, the pile-up of dislocations at grain boundaries is a key mechanistic process underlying an enhanced resistance to plastic flow from grain refinement [85].

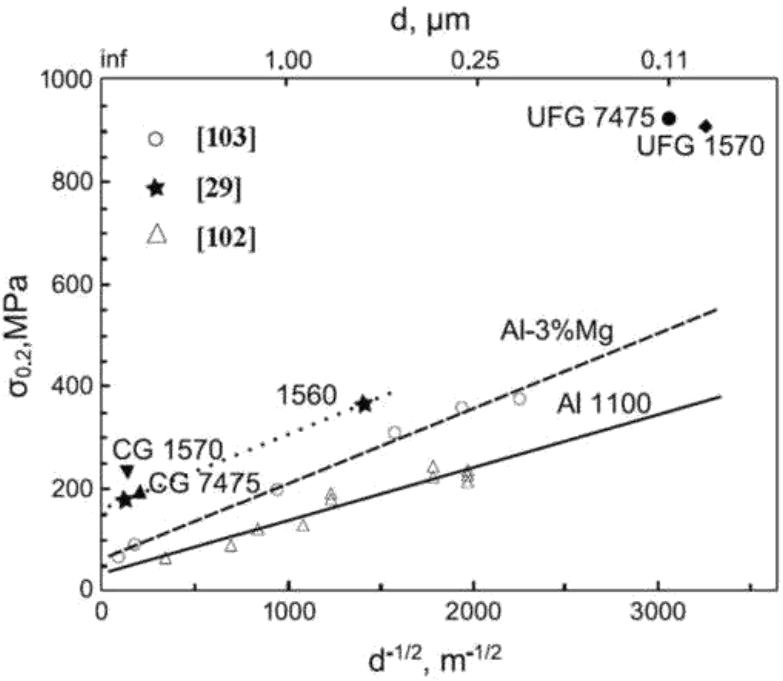

Figure 2.13: The Hall-Petch relation for the Al alloys: AA 1100, Al-3% Mg, 1570 and AA 7475 [83][79].

ii) Solid solution strengthening

In the category of non-heat treatable aluminium alloys, the strengthening mainly comes from solid solution strengthening and grain boundary strengthening. Al 1xxx (Al-small amounts of Fe and Si), 3xxx (Al-Mn) and the 5xxx (Al-Mg) alloys comes under this category. These alloys are widely used in the range of applications where a low to medium strength, a good formability, and a good corrosion resistance are desirable [86]. A systematic work has been carried out on the effect of solid solution on strengthening of the matrix in coarse grained Al alloys. It has been observed that the strength by solid solution is directly proportional to the concentration (C) of solute in the matrix.

The relation is

$$\sigma_{ss} = HC^{n} \qquad (2.8)$$

Where H and n are constants. The value of n can be in the range of 0.5-0.75 [86]. This is very much valid for coarse grained Al alloys. However, the recent observation in UFG/NS Al alloys, produced by SPD indicates the breakdown of the relationship shown in equitation (2.3) due to solute atom segregations at the grain boundaries. The atom probe tomography analysis of Al 6061 alloy processed through HPT [87] has shown segregation of Mg, Si, and Cu along

the new grain boundaries. In the similar way, Al 7075 processed through HPT has shown solute segregations at the grain boundaries (*Figure 2.13*) [88].

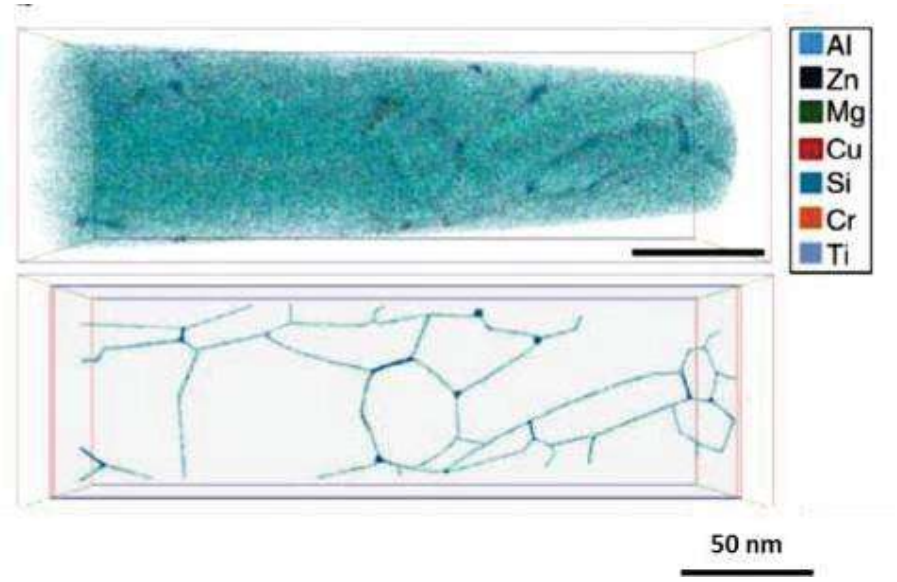

Figure 2.14: Alloy grain structure in the HPT processed AA7075 (scale bar: 50 nm).

UFG/NS material possesses large volume fraction of grain boundaries. This may lead to segregation of large fraction of solute at the grain boundaries, which is a different phenomenon as compared to coarse grained material [89]. Solute segregations in UFG/NS Al alloys are due to increased diffusion coefficient of the material by increasing dislocation densities and vacancy concentrations. Solute segregation also depends on the grain boundary character. Non equilibrium grain boundaries are often observed in UFG/NS material developed through SPD. These boundaries possess increased excess energy and act as sinks for solute atoms [90]. Due to solute segregations, the estimated strength from the grain boundaries in nanostructured material processed through HPT is less than the experimentally obtained value[87]. It is attributed to retardation of dislocation initiation at the grain boundaries [91][83].

iii) Precipitation hardening

A German metallurgist, Alfred Wilm (1869-1937), has invented the new aluminium alloy known as "Duralumin", which has extensive applications in air crafts[92][93][94][95][96] He has published an article on age hardening in aluminium alloys in 1911 by mentioning "*My studies of aluminum alloys at the central office for scientific-technical investigations in Neubabelberg, which I have been conducting since 1903, have shown that even a small amount of magnesium added to aluminum enables hardening by a thermal*

treatment."[97][98]. This phenomenon has brought revolution in the aluminium alloys and led to development of several age hardenable aluminium alloys with medium strength to high strength. There are several studies in conventional coarse grained aluminium alloys on precipitation hardening effect. Coming to UFG/NS Al alloys, the precipitation hardening response is different as compared to the coarse grained counterparts [79]. Overlapping of two strengthening mechanisms makes it difficult in UFG/NS Al alloys to understand the actual hardening effect through precipitation. Different strategies have been implemented to optimize the precipitation hardening effect in UFG/NS Al alloys. It includes SPD processing i) At elevated temperatures after solid solution treatment, ii) At room temperatures after solid solution treatment, followed by low temperature ageing, iii) After solid solution treatment followed by various ageing conditions viz., natural ageing, artificial ageing and over ageing.

The selection of strategy depends on the feasibility of processing. Cryorolling and cryomilling process facilitate to perform deformation at desired heat treated condition. Whereas in other SPD processes (ECAP, HPT, ARB, FSP, HE), design of the technique makes it necessary to perform processing at room temperature or above room temperature. UFG structure evolution through SPD processing involves continuous generation of dislocations and its transformation to UFG. SPD processing at room temperature or above room temperature of solid solution treated material leads to simultaneous evolution of precipitates and UFGs. The process involves complex phase transformations such as nucleation, growth, fragmentation and segregation of second phase precipitate [99][100][101] [102][103][104][105][106][107][108]. This makes it very difficult to understand the precipitation evolution in UFG/NS aluminium alloys. Due to poor ductility, alloys after SPD processing are subjected to post heat treatment processes. However, the alloys which are SPD processed at elevated temperatures have shown poor mechanical properties after post SPD ageing treatments. This is attributed to coarsening of precipitates, which are already formed during SPD processing. Whereas, the alloys which are deformed under cryogenic temperature or at room temperature have shown significant improvement in strength and ductility as compared to as deformed alloys after post SPD ageing at low temperatures. Hence, that it can be considered as an effective approach to enhance the strength and ductility.

2.4.7 Strategies to enhance the ductility in UFG Al alloys

i) Bimodal Grain size distribution

Wang et al.,[109] have reported the effect of bimodal structure on ductility without affecting the strength of nanostructured Cu produced by cryorolling. The applied recipe is "developing UFG/NS structure which renders high strength to the material, by heavily deforming at cryogenic temperature followed by annealing for a short time. Annealing leads to formation of micron sized grains in matrix of UFG/NS, which attributes for increased tensile ductility. Since then, there are several attempts made on different metals to achieve the similar effect. However, the improvement in ductility was observed with the expense of strength. Whereas, Panigrahi and Jayagnathan [110] have successfully developed UFG Al 6063 alloy with enhanced strength and ductility. The proposed strategy is "Solid solution treatment followed by water quenching to room temperature → Cryorolling → short annealing at 155 °C for 5 minutes → low temperature (125 °C) ageing for 12 hours.

Cryorolling after solid solution treatment results in improved strength by accumulation of high density of dislocations and formation of subgrain boundaries in the material. Short annealing leads to formation of recovered or partially recrystallized grains, which would act as empty rooms for newly generate dislocations to accommodate plastic deformation. Further, low temperature ageing leads to increase in strength by precipitation hardening effect. The selection of short annealing temperature and time is critical to observe the enhanced ductility without affecting strength. However, it is obvious that by performing short annealing results in restoration process through recovery and recrystallization. It will have definite negative influence on strength. In precipitation hardenable alloys, it is not observable due to nullifying effect by cluster strengthening effect. There are several other reports where bimodal or inhomogeneous grain structure synthesized by consolidation of mixture of various range of sized powders has shown improved tensile ductility [111] [112] [113] [114] [115] [116] [117] [118] [119][120]. During extrusion, the coarse grains elongate along the extrusion direction. It was reported that presence of duplex or bimodal structure of elongated coarse and fine grains have both advantages and disadvantages [115]. The advantages are, presence of coarse grained regions may contribute in enhancing the ductility and fracture toughness by interfering with the crack and shear banding. The disadvantage is, due to elongated structures, the material possesses anisotropy in its properties. When the stress is applied normal to extrusion direction, both the strength and ductility are reduced in engineered bimodal extrusions. Apart from increase in ductility with the presence of coarse grain structure in the

microstructure, the coarser grains possess lower strength compared to fine grains. It can be noted that the increase in ductility through this route is with the cost of ductility.

ii) Introducing nano-sized precipitates

Introducing nano-sized precipitates in to the matrix is found to be an effective approach to enhance the ductility of the UFG Aluminium alloys. Firstly Zhao et al., [121] have reported significant improvement in the ductility of UFG Al 7075 alloy without the expense of ductility. The recipe is (i) Allowing second phase particles to dissolve in to the matrix in coarse grained material; ii) Producing UFG structure through deformation at supersaturated solid solution state, and (iii) Proper ageing treatments to form nano sized precipitates in the UFG microstructure. Generation of nano precipitates alone will not help to enhance the ductility of the material. During ageing process, the microstructure undergo recovery process, thus the dislocation density will be reduced. The annihilation of dislocations during recovery process will leave a space for dislocations that generate during deformation. Thus, ductility of the material is increased. To enable the material to undergo stable plastic flow, the nano-sized precipitates play a major role and also they accumulate more dislocations; thus the work hardening rate of the material gets improved. The drop in strength due to annihilated dislocations is compensated by the nano sized precipitates, but it also enhances the strength further. The simultaneous improvement in strength and ductility has not been achieved earlier [122][123][124][125][126][127]. Later Cheng et al., [128] have slightly modified the strategy proposed by Zhao et al.,[121] approach and successfully achieved improvement in both strength and ductility in Al 2014 alloy. It indicates that to achieve simultaneous strength and ductility in the Al alloys, effective control of precipitation process is required. Compared to room temperature or elevated temperature SPD processing, cryogenic deformation after solid solution treatment of the alloy facilitates no phase transformation during the process, due to suppressed diffusion of solute atoms. Nucleation and growth of the precipitates can be effectively controlled by post deformation heat treatments. However, there are some issues with the above said approach. As discussed in the previous section (Non-equilibrium grain boundaries), SPD processed material contains non-equilibrium grain boundaries, which are at high energy state. In Al alloys which are more prone to intergranular precipitation such as Al-Cu, Al-Cu-Zn, during post SPD precipitation process, these non-equilibrium grain boundaries promote intergranular precipitation, which leads to intergranular fracture with poor ductility[129]. In recent studies by Jiang et al.,[130], they have observed enhanced ductility in micro alloyed- Al-Cu material after ECAP followed by artificial ageing. *Figure 2.14* shows the stress strain diagram of UFG Al-Cu-Sc alloy by micro alloying.

Addition of Sc in Al-Cu alloy has suppressed the intergranular precipitation of θ- Al_2.Cu phase and by promoting intragranular precipitation of θ'-Al_2.Cu phase.

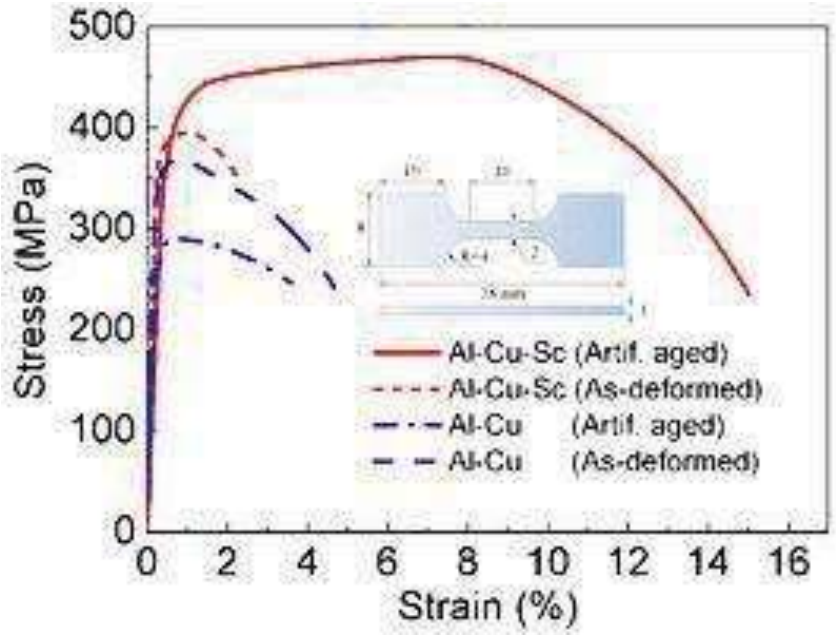

Figure 2.15: Typical tensile engineering stress-strain curves of the as-processed Al-Cu-Sc (short-dash curve), Al-Cu (dash curve), and artificially aged Al-Cu-Sc (solid curve), Al-Cu (dash-dot curve) UFG alloys [130].

iii) Modifying Grain boundary characters

The microstructure that develops during SPD generally is characterized by nature of the grain boundaries. If the misorientation with the neighbor grains is less than 15°, then it is called as low angle grain boundaries (LAGB). If it is greater than 15°, then it is called high angle grain boundaries (HAGB). It has been observed that the misorientation of the adjacent grains directly influences the mechanical properties[131][132][133] Grain boundaries render strength to the material by behaving as an obstacle to the gliding of mobile dislocations. However, the amount of strength that can be imparted to the material is dependent on the grain boundary character. In the material with HAGBs, activation of slip between the adjacent grains is difficult and it requires more energy [131]. Thus, the strength of the material increases. Increase in strength with the expense of ductility is not desirable as high strength with reasonable ductility of materials is essential for engineering applications. In contrast to

HAGB, LAGBs shows poor resistance to the gliding of mobile dislocation [131]. This property can be utilized to improve the ability of plastic deformation in UFG/NS materials. Hu et al.,[131] have recently reported increased ductility and uniform elongation while retaining high strength by engineering the relative proportion of LAGBS in the Al alloys.

2.4.8 Applications of UFG material

UFG/NS materials could serve as potential materials for structural and functional applications in many engineering sectors such as aerospace, automotive, defense, electronics, constructions, biomedical, etc. [134][79][135][136][137] The process of commercialization of UFG/NS materials is hindered due to small size of SPD processed material and their cost of production[79]. However, the recent developments in SPD techniques, allowed scaling up of the processing up to industry production level.

A) Biomedical applications

The metals such as Fe, Mg, and Ti are widely used for biomedical applications as body implants. The field of biomaterials is significantly growing due to ever increasing demand for bio implants. The physical properties that are generally considered for biomaterials includes hardness, tensile strength, modulus, elongation, fatigue strength, impact properties, wear, dimension stability, biodegradability, biocompatibility [138][139][140][141]. Materials for permanent implants such as bone and tooth replacements should possess inert behavior in body fluids, whereas for temporary implants, material must degrade at a suitable rate for the targeted application [142]. Titanium alloys are widely using as permanent body implants due to its excellent combination of physical and electrochemical properties. Implants with pure Fe and Mg are highly biodegradable. Recent studies have proven that UFG materials processed through SPD can be used as suitable candidates for biomedical applications [143][144][145][146][147][148][149][150][151][152]. The reported literature shows that the commercial pure Ti with UFG structure developed through SPD will be better replacement for Ti alloys. By nano-sizing the microstructure of CP Ti, the mechanical behaviour and biocompatibility have increased [149][148]. The materials processed through SPD have shown better corrosion resistance in body fluids over coarse grained materials. Fine grained Mg has shown significant enhancement of fatigue life and endurance limit as well as reduction in corrosion rate in Hanks solution [153]. In particular biomedical applications, high dissolution rate of materials might require. Instance UFG copper

processed through ECAP, with grain size 380 nm has shown higher corrosion current than coarse grained Cu in Hanks's solution[144]. Fine grained Cu is excellent material for contraception application [144],

B) Microelectromechanical systems (MEMS)

In order to have a better mechanical strength of the micro parts in MEMS, the average grain size should be less than the part dimension. UFG/NS materials are suitable candidates for these applications. Latest developments in SPD by miniaturizing the processing technique allows to produce micron scale products with desired grain size to enhance the strength and fracture toughness of the material [154]. For instance, UFG AA 1050 produced through ECAP has shown better surface finish and thermal conductivity as compared to coarse grained material in micro heat exchanger applications [155][156]. *Figure 2.7* shows the surface morphology of hot embossed UFG Al-1050 and coarse grained Al 1050 alloy. The top surface of micro channels of the coarse grained alloy is rougher than UFG alloy [155].

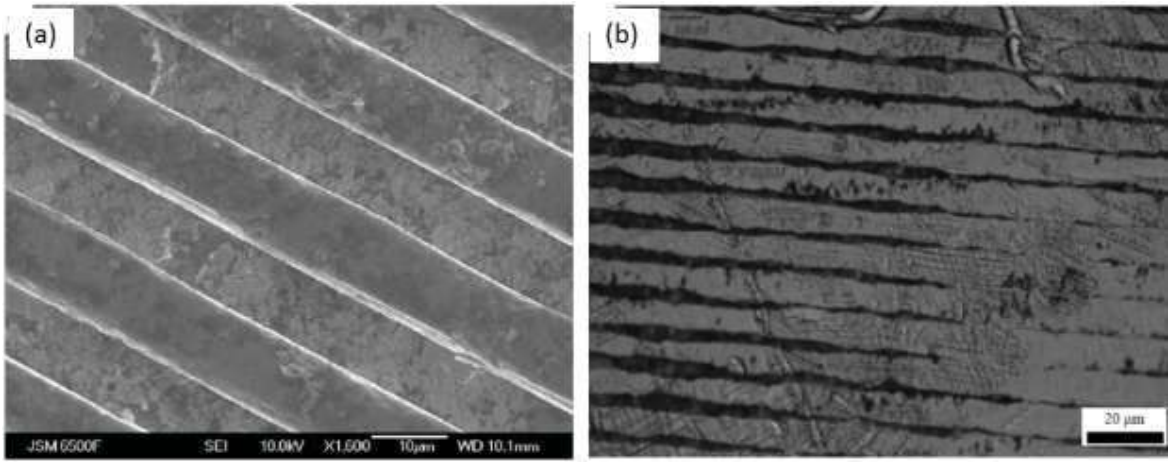

Figure 2.16: a) SEM micrograph of top surface of hot embossed UFG Al 1050 alloy; b) Optical micrograph of top surface of hot embossed coarse grained Al 1050 alloy[155].

2.5 Multi directional forging (MDF)

Armstrong et al group was first who have studied the formation of ultrafine grain by multi-axially forged commercial purity aluminum in 1982. They have conducted the MAF test on Aluminum alloy 1100. They observed that considerable increase in strength of Al 1100 with increasing the cumulative strain. In this paper Armstrong discussed and compares the various studies conducted by various authors on copper and alpha iron. Another study on MAF has

been done by Salischev et al. (1993) in early 90's. They produced ultrafine grain in bulk billets of Ti alloy by multiple forging.

Cherukeri et al [2006] [157] provides the comparative study of grain size and tensile properties of AA 6061 processed by MAF, ECAP and ARB techniques. The texture and micro texture development was studied in an Al-3Mg-Sc (Zr) alloy deformed by MAF Ringeval et al. (2006).

The altering strain path associated with MDF and its higher deformation rates can significantly influence the microstructure development, especially in Aluminum alloy 6xxx series which are light weight medium strength alloy, such studies are scarce in literature.

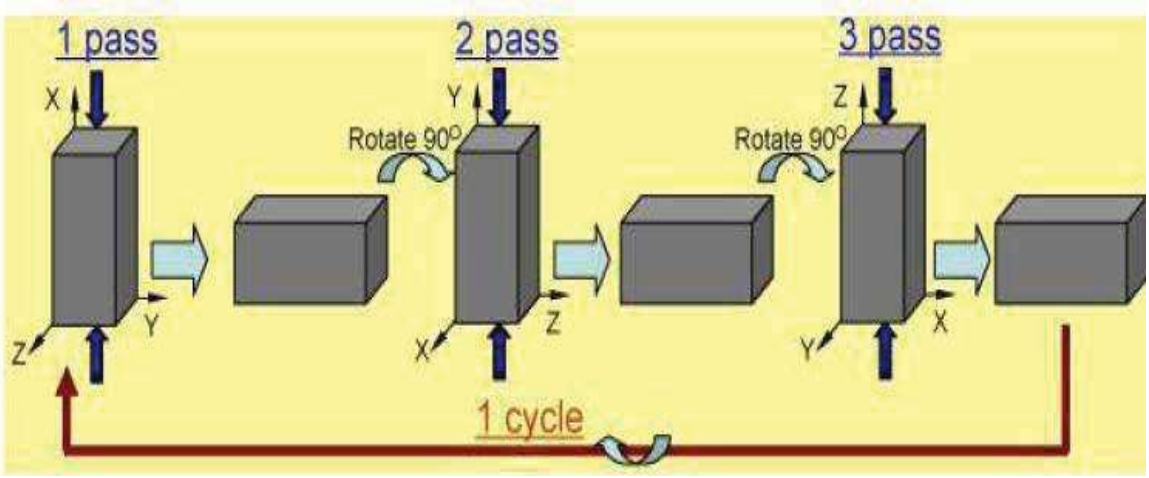

Figure.2.17: Principle of Multi axial forging[157]

Later on Multiaxial forging (MAF) was developed by Noda et al. (2005), where the samples were cut to cubic shape generally prepared in ratio of 1.5:1.22:1.0, as shown in Figure 2.11b. It is the simplest method to achieve larger strains with minimum distraction from its original shape and allows processing of bulk products. Strains were applied to the test materials alternately in three directions by rotating the test materials by 90° after each pass up to a required true strain. Working temperature and deformation rates influences the microstructure evolution and mechanical properties of MAFed material. Severe strain induced in material resulted in increasing the active slip systems and the deformation bands, high-misorientation grain boundaries (94.8%), and ultrafine grains with a grain diameter of 0.8 μm were formed.

Therefore, the MAF technique is an effective working method for producing ultrafine grains in the bulk materials.

2.6 Cryo Rolling

Aluminium due to its corrosion resistance and strength is the most promise light weight material for industrial applications. Aluminium alloys is used in the form of tubes and sheets in most industrial applications due to which different rolling techniques have been developed to increase efficiency and even the strength of the sheets and tubes. straight rolling at room temperature and above is not appropriate for mass production of bulk ultrafine-grained Al alloys due to its high stacking fault energy, which provides the dynamic recovery through climb and cross-slip of dislocations and thus avoids grain refinement in the alloys. The SFE can be reduced by deforming at low temperature and even alloying the metal [158]

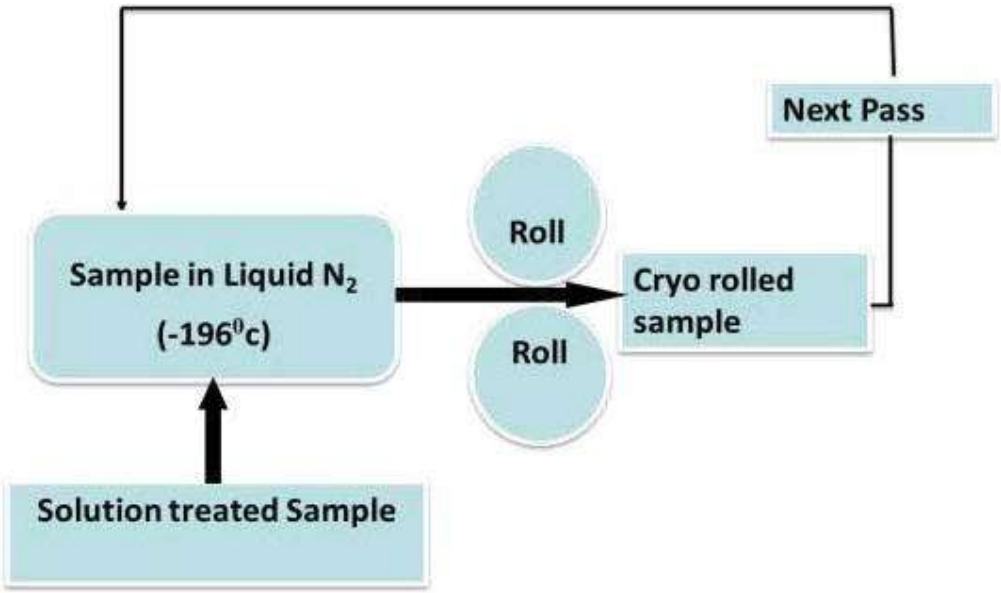

Figure.2.18: Schematic illustration of principle of rolling at liquid nitrogen temperature [159]

To overcome the above explained subject conventional rolling at liquid nitrogen temperature (cryorolling) is performed which suppresses dynamic recovery and allow the development of ultrafine grained structures by rearranging the high dislocation density produced in the alloy during rolling. For performing cryorolling the samples are dipped into liquid nitrogen (-196 ℃) till it gets uniform temperature and then rolled and dipped immediately for consecutive passes. This process is performed continuously till required strain is obtained. Secondary phase particles increase the rate of dislocation production and dislocation accumulation, improving the grain refinement. The reliance of grain refinement on SFE of aluminium alloy results in high raise in strength at cryo temperature rolled as

- compared to room temperature rolled, thus SFE controls dynamic recovery [158].The SFE of the metal decreases with addition of alloying elements as observed in the alloys such Al-Mg, Al-Cu, Cu-Zn and as a result, there is an enlarged separation in partial dislocations, which causes decrease in dynamic recovery rate.

Asymmetric rolling [160] and cryorolling followed by warm rolling [161], has been reported to produce bulk NC/UFG in aluminium alloys.

Cryorolling followed by subsequent annealing at low temperature produced duplex microstructure with an average grain size of 200 nm in 5083 Al alloy with better strength and ductility, 10% more than room temperature rolled material. Annealing above 300 ^{o}C leads to coarsening of recrystallized grains, which has little influence on hardness.

Cherukuri et al. (2006) [162]compared the properties of AA 6061 Al Alloy at room temperature up to accumulated strain 4, processed by ECAP, MAF, and ARB. Ultrafine grain structure with submicron grain size was obtained in all three techniques. They have found that multi axial forging followed by rolling gives significant improvement of mechanical properties.

Mironov et al. **(2006**) investigated properties of pure titanium processed by warm MAF. They have found that warm MAF provides an effective way of grain refinement. In the lower strain majority of boundaries are LAGB, while development of HAGB strongly depends upon twins.

Satishchev et al. (2004) produced ultrafine grain in Ti-6Al-4V sheets. They have investigated the microstructure, texture, room temperature properties and super plastic properties of the Ti-6A1-4V sheets with ultrafine grain structure. They shows that ufg Ti-6Al-4V have a very good mechanical properties as well as super plastic properties.

Rao et al. [2014] [163] investigated the properties of AA 6061 alloy processed by MDF. They have found that there is a significant improvement of mechanical properties of aluminum alloy 6061 with increasing strain steps of MDF at liquid nitrogen temperature. This is due to the high dislocation density. At cryogenic temperature there is a formation of dislocation cells structure with high dislocation density at lower strains. With increasing strain there was a significant improvement in dislocation density.

Zherebtsov et al. [2012] investigated the mechanical properties of Ti-6A1-4V alloy processed via MAF. They have shown that there is a 33% increment in strength of this alloy.

They observed that with decreasing temperature from (700°C to 450°C); tensile ductility, impact and fracture toughness get decreases.

Xinxing et al. [2013] observed the mechanical behavior of AZ21 Mg alloy processed by MDF and reported that mechanical twinning is responsible for improvement in strength in MAFed AZ21 Mg alloy at RT. Annealing temperature plays an important role of improving ductility of MAFed alloy.

Weilin et al. **[2013]** reported that strength of AA 6061 is augmented after MAF at 130°C .it is due to dispersed ultrafine precipitates within the grains. After ageing treatment ultrafine precipitate particles spread within the grains which increase the work hardening of the material accumulated resisted dislocations.

Panigrahi et al. (2008, 2010, 2011) [10] [163] [164] have reported 6063 Al alloy subjected to cryorolling at different strains, shows the development of recrystallized ultrafine grains structure with the high angle grain boundaries at 3.8 true strain. He also investigated the development of precipitates, during annealing of cryorolled 6063 Al alloy. The precipitates followed a sequence i.e., the formation of GP zones (spherical), β'' phase (needle), β' phase (rod), and stable β phase (plate) shaped morphology after annealing in temperature range of 150 - 250 ℃ for 1 hr respectively. The DSC analysis of cryorolled 6063 Al alloy at different heating rate was used to assess activation energies of precipitates using Kissinger analysis. In cryorolled Al 6063 samples, activation energy observed was less for the formation and dissolution of precipitates as compared to solution treated and water quenched condition. This may be attributed to an excess free energy linked with higher volume fraction of low angle grain boundaries in Al 6063 alloy, that promotes precipitation kinetics by providing high diffusion path due to precipitation growth and reducing activation energy of precipitates by providing improvement in nucleation sites..

Gang et al. (2009) [163] have studied that combined treatment of cryogenic-rolling with warm rolling (175 ℃) was found more effective than a single cryogenic-rolling alone in 5052 Al alloy and remarkable increment in ultimate tensile strength (452 MPa) observed was attributed to the formation of fine precipitates during warm-rolling. Enhanced ductility observed after annealing at 175 ℃ for 48 hr was recognized to the formation of fine equiaxed grains (100-200 nm) as well as the reduction in dislocation density.

Rao et al. (2009, 2013) [163] [164] have studied the effect of annealing and ageing on strength and ductility of UFG Al 6061 alloy, and reported that short annealing before ageing has significant effect on enhancement in ductility without decreasing strength. Later, they reported microstructural evolution in 6061 with combined effect of cryorolling followed by

warm rolling performed at 145 ℃. Considerable improvement in strength (376 MPa) and partial improvement in ductility (5%) was observed in cryorolled followed by warm rolled sample as compared to CR samples alone. Further enhancement in UTS (406 MPa) and ductility (7.9%) of cryorolling followed by warm rolling followed by peak ageing sample was reported on ageing at 125 ℃ for 45 hr.

Krishna et al (2014) performed cryorolling of Al-4%Cu-3%TiB_2 in situ composite followed by short annealing at 175 ℃ and ageing at 125 ℃. The yield strength of about 800 MPa with 9% total elongation was obtained. The strengthening assistance were from solid solution strengthening, grain refinement, dislocation strengthening, precipitation hardening and dispersion strengthening.

The literature reported above is mainly concentrated on the cryorolling of pure aluminium or precipitation hardenable alloys. Lee et al. (2004) and Kang et al. (2009) have reported formation of ultrafine grained material on cryorolling of non-heat treatable aluminium alloys. The present research work is focused to develop ultrafine grained (UFG) microstructure in bulk 5083 Al alloy sheets for high strength structural applications through grain refinement. The microstructural characteristics, mechanical properties, high cycle fatigue behaviour and corrosion behaviour of Al alloys processed through cryorolling were investigated.

2.7 Problem formulation

2.7.1 Current Literature on Bulk ultrafine grained & nanostructured materials

A detailed literature survey has been carried out on the development of high strength Al alloys processed through SPD techniques. The important findings from the literature are as given below.

- Bulk SPD processing techniques have been found to be lucrative approach for the development of advanced high strength materials.
- SPD processing also leads to, the strengthening of bulk ultrafine grained and nanostructured materials by structural features such as non-equilibrium grain boundaries, grain boundary segregation of solute atoms, nano twins, and nano particles in addition to grain boundary strengthening.
- The introduction of nanosized precipitates in to the UFG structure has been found to be an effective approach to resolve the problem of poor tensile ductility in UFG material.

2.7.2 Objectives

The following objectives in Al-Mg-Si alloys were formulated based on the current literature in UFG Al alloys

(i) To produce ultrafine grained Al-Mg-Si alloy from its bulk by cryorolling and room temperature rolling and to study its ageing behavior.

(ii) To investigate the effect of warm rolling temperature and % of deformation after cryorolling on strength and ductility of Al-Mg-Si alloy.

(iii) To investigate the effect of natural ageing and pre-ageing on the hardening behavior of cryorolled Al-Mg-Si alloy.

(iv) To investigate the evolution of ultrafine grain structures and precipitation behaviour of UFG Al-Mg-Si alloy developed though cryoforging followed by cryorolling.

2.7.3 Work plan and Layout of the thesis

To accomplish the above objectives, a systematic work plan has been made and carried out. The layout of the thesis is as follows;

The **Chapter 1** gives a brief introduction about several SPD processing techniques, role of Al alloys for light metal applications and need of UFG materials. It is followed by literature survey of Aluminium alloys, various strengthening mechanisms in Aluminium alloys, its applications in various sectors and various SPD techniques used to produce UFG structure in Al alloys and its principles are discussed in the **Chapter 2**. In **Chapter 3**, materials and experimental procedures are described. **Chapter 4** presents the effect of cryorolling and room temperature rolling on microstructure and mechanical properties of Al 6061 alloy. The effect of cryorolling followed by warm rolling in Al 6061 is described in **Chapter 5**. In **Chapter 6**, a detailed investigation of the effect of natural ageing and pre-ageing on the hardening behavior of cryorolled Al-6061 alloy. **Chapter 7** investigates the effect of cryoforging followed by cryorolling on microstructural evolution, ageing behaviour, and mechanical properties in Al 6061 alloy. The overall conclusions and the scope of future work are given in **Chapter 8** and **Chapter 9** respectively.

CHAPTER 3

Experimental Details: Material and Methods

In this chapter, material selection, experimental techniques employed in processing for grain refinement and characterization techniques to understand the phenomenon of grain refinement are discussed.

3.1 Material Selection

Commercially available Al-Mg-Si alloy with thickness 60 mm and chemical composition as shown in Table 3.1 was procured from Hindalco industries private limited India in the plate form and was used in the present work. The samples were cut from procured plate and solutionised at (550˚C/3 hr) followed by quenching in water. The solutionised samples were free from any defects. Homogenised microstructure with an average grain size of 85 µm was obtained.

Initial condition	Elements	Mg	Si	Fe	Cu	Mn	Cr	Zn	Al
Material in the as cast form	Wt.%	1.2	0.7	0.22	0.3	0.02	0.19	0.014	Balance
Material in the wrought form	Wt.%	1.01	0.67	0.28	0.2	0.04	0.05	0.06	Balance

Table 3.1 Chemical composition of the Al 6061 alloy

3.2 Experimental techniques

3.2.1 Experimental set up for cryorolling

Ultrafine grains can be produced by different techniques but cryorolling (CR) is the easiest and cost effective method. The dimensions used for cryorolling (CR) were 40 × 30 × 10 mm^3. The samples after solutionizing were cryorolled with different thickness reduction as 30%, 50%, and 90% with a true strain of 0.35, 0.69 and 2.3, respectively. Initial thickness was same for all conditions. The experimental set up used to carry out cryorolling in the present study is shown in Figure 3.1. The accessories and equipments used during cryorolling are given below:

- two high laboratory rolling mill having rolling speed of 8rpm and roll diameter of 110 mm was used

- molybdenum disulphide is used as lubricant to reduce the frictional force and heat generated between the sample and the rollers,.
- Liquid nitrogen was stored in cryocans.
- The containers covered with glass wool and asbestoses sheet to minimize the evaporation of liquid nitrogen was used to dip the samples in liquid nitrogen during rolling.
- To measure reduction in each pass, digital vernier caliper was used. Gloves were used for handling the samples during rolling.

3.2.2 Cryorolling Procedure

The samples were machined and surfaces grounded according to the required dimension and were subjected to solution treatment to roll at different temperature. The schematic of the setup used to perform cryorolling is shown in Figure 3.1.

Figure 3.1: Schematic of experimental setup for cryorolling.

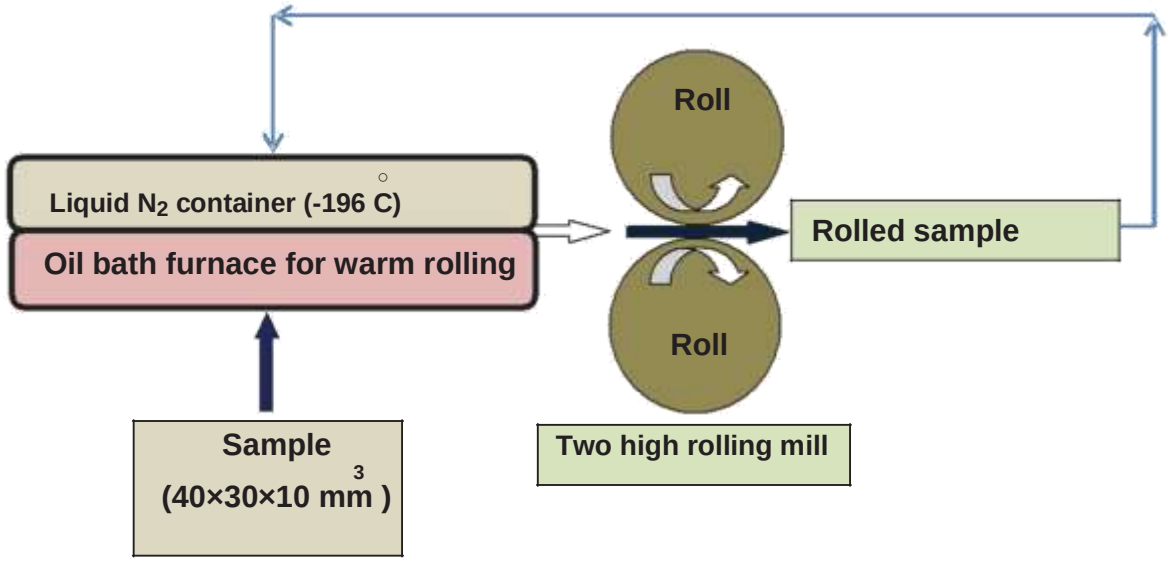

Figure 3.2: Schematic diagrams of cryorolling and cryorolling followed by warm rolling.

The procedures adopted for cryorolling is given below.

The rolling mill was cleaned thoroughly by using emery papers and acetone to remove rust, burrs, oxides and oil or grease, if any. The samples were also surface polished and cleaned properly.

To perform cryorolling samples were dipped into liquid nitrogen (-196 °C) kept for 15 min for the successive passes. The process is repeated continuously till required strain is achieved. The temperature is measured before and after each rolling pass was found to be -150 °C and -75 °C, respectively. After every rolling pass the sample thickness was measured.

True strain per pass (e) is calculated by using the following formula:

$$e = \ln \frac{\text{Thickness after cryorolling}}{\text{Initial thickness before cryorolling}} \quad (3.1)$$

3.2.3 Cryoforging

3.2.4 Experimental setup and procedure for cryoforging

Friction screw forging press was used in the present work for performing multiaxial forging at liquid nitrogen temperature (77K) which is also described as cryoforging, at an approximate strain rate of $10s^{-1}$. Rectangular samples having dimensions 27 X 30.5 X 33 mm^3 were machined from the as received plate and were subjected to solution treatment at a

temperature of 520°C for 2 hours followed by water quenching. The first forging axis chosen was parallel to the rolling direction of the starting sample. After every forging pass, the sample was rotated through 90° for the next pass. The sample dimension ratio of 1:1.13:1.22 was maintained after every pass and throughout the processing. Cryoforging was carried out by filling the die with liquid nitrogen up to the height of the sample. Initially, the samples were dipped in liquid nitrogen for about 15 minutes and were allowed to attain thermal equilibrium by soaking it for about 5-10 mins after every pass. The schematic diagram showing experimental setup for MAF at liquid nitrogen temperature is shown in Figure 3.3. A true strain of 0.061 per pass and a cumulative strain of 0.5 after one cycle was fixed throughout the process. The samples were MAF up to cumulative strains of 1.5 corresponding to 3 number of cycles. In order to study the microstructural and mechanical properties after MAF, the samples were sectioned along the highest dimension i.e., along the plane perpendicular to the last forging axis.

Figure 3.3: Friction screw forging press used for cryoforging

3.3 Characterization techniques

3.3.1 Optical microscopy (OM)

Optical Microscopy was used to investigate the microstructure of the samples obtained after processing. The samples after solution treatment, cryorolling and cryoforging were characterized using optical microscope (LEICA DMI5000 M) to examine the processing effect and evolution of microstructure. The photograph of the LEICA DMI5000 M optical microscope can be seen from Figure 3.4 which was used in the present study.

Figure 3.4: The Photograph of LEICA DMI5000 M optical microscope.

For the preparation of samples, the selected part of the material was cut on diamond cutter. The sample was then mounted and grounded using SiC abrasive papers of different grit sizes, usually 320 to 2000 grit. Water was used to eliminate the embedding of abrasive particles into soft aluminium alloys. These polished samples were then cloth polished using paste of magnesium oxide with water. The cloth polished samples were then dried and etched with 50 ml of Poulton's reagent mixed with 25 ml HNO_3, 40 ml solution of 3 g chromic acid per 10 ml of water. After etching for 1 min, these samples were examined under Leica optical microscope under the polarized light.

3.3.2 Electron backscatter diffraction (EBSD)

Electron backscatter diffraction (EBSD) is a microstrutural characterization technique which uses backscatter kikuchi pattern to examine the misorientation of grains and texture or preferred orientation of grains in a polycrystalline material. The machine is equipped with a high resolution field emission gun scanning electron microscope (FEGSEM). It furnishes the information about the orientations of the subgrains and grains in a polycrystalline material

that cannot be easily obtained from the TEM. The deformation mechanism and the structure of the deformed alloys can be analyzed through quantitative measurement of low and high angle grain boundaries present and their distribution in deformed state. Therefore, in the present study, samples after ST, CR, MAFed and after annealing were characterized using the EBSD technique. The photograph of the FEG-SEM equipped with EBSD can be seen from Figure 3.5.

EBSD measurement was done by placing a flat/electropolished crystalline specimen in the SEM chamber tilted at an angle (~70° from horizontal) towards the diffraction camera. The SEM was equipped with an EBSD detector consisting of a phosphor screen, a CCD camera and a compact lens. The phosphor screen is placed inside the specimen chamber of the SEM which is at an angle of about 90° to the pole piece and is attached to a compact lens for focusing the image on the CCD camera. This arrangement of the instrument allows some of the electrons entering the sample to backscatter and escape. These electrons might leave the sample surface, at the Bragg condition and diffract to produce kikuchi bands Inside the SEM. The schematic of EBSD setup is shown in Figure 3.6. The obtained Kikuchi lines are collected by CCD camera and analyzed using specialized computer software using an optimized Hough transform.

To get a good diffraction patterns/Kikuchi bands, the sample surface should be well prepared. The selected section of the material was cut using diamond cutter using lubricant to avoid heating in the sample. The sample is then mechanically ground using SiC abrasive papers of different grit sizes, usually varying from 320-2000. To avoid embedding of abrasive particles water was used as a coolant as well as to flush away abrasives. These samples were then cloth polished using colloidal solution of magnesisum oxide and water. Electro polishing of the cloth polished samples was then performed at -15 °C using 80:20 solution of methanol: perchloric acid at a potential of 11 volts.

Figure 3.5: The Photograph of FEI Quanta 200 FEG-SEM.

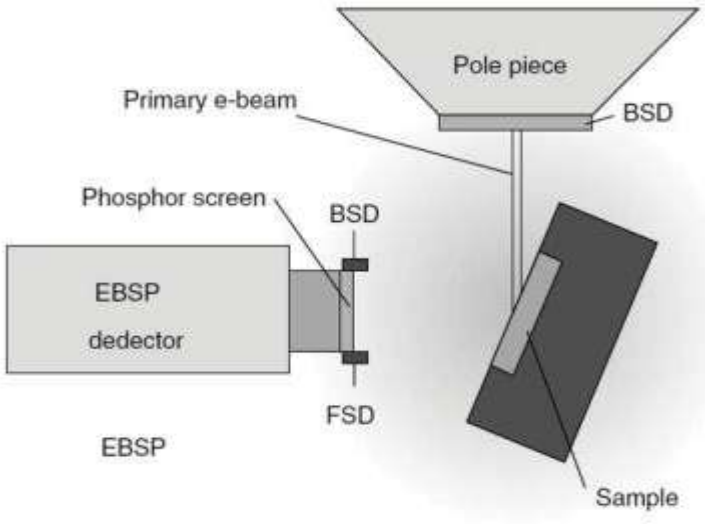

Figure 3.6: Schematic diagram of a typical EBSD sample installation (A. P. Day et al. Channel 5 User Manual, HKL Technology A/S, Hobro, Denmark (2001).

The samples for EBSD measurement were cut from the mid center of the rolled sheet and forged block respectively. The step size (1 μm) of the solution treated was kept higher, while for the deformed samples the step size (0.1 μm) were kept low to track the misorientation. EBSD of the samples were performed on FEI, Quanta 200 F machine and

analysis of the data was done on TSL OIM analysis 3.5 software developed by TEXSEM laboratories Inc.

3.3.3 Field emission gun scanning electron microscopy (FEG-SEM)/ SEM

The fractography of the Al alloys deformed at different strains was studied using field emission gun scanning electron microscope FEG-SEM (FEI Quanta 200) in the present work. The fractured samples after tensile test were ultrasonicated and then used in SEM for fractography analysis. Photograph of FEG-SEM used for investigation of fractured surface morphology is shown in Figure 3.5.

3.3.4 Transmission electron microscopy (TEM)

To get the information, which is not accessible using optical microscopy and SEM, transmission electron microscopy (TEM) was used. It can magnify the specimens in the region of 10^{-6} m to 10^{-9} m by diffraction and imaging techniques. TEM is used to determine the grain size, crystal structures, specimen orientations, chemical compositions of phases, dislocation density and precipitation morphology through diffraction pattern. In present work TEM analysis were carried out by using a FEI Technai 20 TEM operated at 200 KV. Figure 3.7 shows the photograph of the FEI Technai 20 TEM.

Figure 3.7 Photograph of the TEM unit (FEI Tecnai-20)

TEM samples were prepared by initially cutting into 10 mm × 10 mm dimension and then thinned up to 100 µm thicknesses through mechanically polishing from both sides by using silicon carbide emery papers. 3 mm diameter disk were punched and then cleaned using acetone. The punched samples were further thinned by a twin-jet electro polishing unit using a solution of 20% perchloric acid and 80% methanol at a temperature of -40 $^{\circ}$C and 40 volts potential.

3.3.5 X-ray diffraction

XRD is a technique used to get quantitative estimation of various phases of a crystalline material and provides information about the unit cell dimensions. The X-ray diffraction technique was utilized in the present study to study the different phases present in the ST, CR and MAFed samples. Bruker AXS D8 Advance instrument having Cu Kα radiation as the target was used for X-ray diffraction measurements in the present study. Figure 3.8 shows the photograph of the Bruker AXS D8 XRD equipment.

Figure 3.8: Photograph of the XRD unit /2 (Bruker AXS D8 Advance diffractometer

The X-rays are produced by cathode ray tube and are filtered to produce monochromatic radiation. These radiations are collimated and directed towards the sample.

The working principal can be seen in Figure 3.9. Whenever, the Bragg condition (2d sin = n) was satisfied, constructive interference took place and peak with high intensity was generated. The high intensity X-ray signals were detected and recorded by the detector. The Bruker D8 Advance diffractometer uses NaI scintillation counter as detector.

3.3.6 Differential scanning calorimetry (DSC)

Differential scanning calorimetry (DSC) is a thermoanalytical practice for measuring the temperatures and heat flows (into and out of the material) associated with phase transformation and chemical reactions taking place in materials as a function of temperature and time in a controlled atmosphere. Although 6061 Al alloy is non-heat treatable alloy, some of the second phase constituents may affect the reactions. Several studies related with the effect of precipitation during CR, WR and annealing treatments were investigated and reported through DSC. The energy related with the formation or deliquescence of various precipitate reactions was observed to be within few joules per gram. Further, the DSC technique can also be used for the investigation of recovery, recrystallization and grain growth phenomenon. Thus, in the present work the thermal behaviors of the above mentioned samples were estimated using Perkin Elmer paris Diamond DSC with pure nitrogen atmosphere at the rate of 100 ml per min. The photograph of Perkin Elmer paris Diamond DSC unit is shown in Figure 3.9.

The experimental setup of DSC consist two holders, one for holding the sample and the other for a reference. The holder further consists of a resistance heater and a temperature sensor. To increase the temperature, Currents were applied to the heaters with the selected rate. The temperature of both the holders was kept same; however, power required for maintaining the temperature was different and was used to calculate the difference in heat flow between the sample and the reference ($\Delta dH/dt$). The recorded difference gives an insight about the exothermic or endothermic reactions related with the formation or deliquescence of different reactions in the samples. Peak observed in pattern corresponds to heat effect associated with different processes, such as crystallization as an exothermic process or melting as endothermic process. The area under the endothermic or exothermic peaks over layered on the baseline is proportional to ΔdH i.e., the heat absorbed or released by the material, and also the temperature scan rate.

The samples for DSC study were prepared for different conditions by thinning down to 0.8 mm using the silicon carbide emery papers (water proof) up to 1000 grit sizes. Heating

of the sample was avoided during grinding by continuously pouring the water. Finally, the thin samples were then punched to 5mm diameter disks by using a specially prepared set of punch and die and were cleaned using acetone.

Figure 3.9: The Photograph of Perkin Elmer Paris Diamond DSC instrument.

3.4 Mechanical testing 3.4.1

Vickers hardness test

Hardness is defined as the property of a material which measures the resistance offered by it to plastic deformation. The hardness machine consists of a diamond indenter with a right pyramid shape having a square base and an angle of 136° between its opposite faces. The hardness tests were performed to evaluate hardness values (HV) of ST samples, CR samples and MAF samples. Figure 3.10 shows a photograph of Vickers hardness testing machine, used in the present study.

The sample preparation was done by cutting 15 mm × 15 mm block from the processed material. The samples were then mechanically polished by using silicon carbide emery papers. These samples were further cloth polished on a rotating cloth polisher using a colloidal solution of magnesium oxide and water. Vickers hardness testing was performed with load of 5 kg having dwell time of 15 s. An average of ten readings was taken to obtain a hardness (HV) value of samples.

Figure 3.10: The Photograph of Vickers hardness testing machine.

3.4.2 Tensile test

Mechanical behavior of ST, CR and MAFed samples were investigated by performing tensile tests at room temperature. The tensile tests were performed on S-Series, H25K-S testing machine operated at a strain rate of 5×10^{-4} s^{-1}. Samples for tensile testing were prepared parallel to the rolling direction in case of cryorolled samples and along the plane perpendicular to the last forging pass in case of MAFed samples according to the ASTM E-8 sub standard size specimen of 25 mm gauge length shown in Figure 3.11. A set of four samples were tested and were averaged. Figure 3.12 shows the photograph of tensile S-Series, H25K-S materials testing machine for present work.

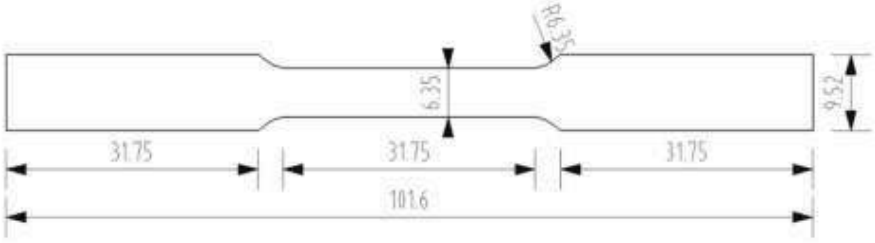

(All dimensions are in mm.)

Figure 3.11: Schematic diagram of a tensile specimen.

Figure 3.12: The photograph of the S-Series, H25K-S tensile testing machine.

3.5 Sample preparation

3.5.1 Mechanical grinding/polishing

The sample polishing was done first with the help of silicon carbide emery papers (320, 600, 800, 1200, 1500 & 2000 grit size) followed by cloth polishing (rough and fine).The magnesium oxide (heavy) was used during cloth polishing to remove very fine scratch from the sample.

3.5.2 Etching

The poultons reagent was used to etch the bulk and deformed alloy to obtain the microstructure through optical microscopy. The solution of reagent contained 50 ml poultons reagent, 25 ml HNO_3, 1 ml HF and 1ml H_2O. A few drop of reagent was applied on the polished surface for 30 seconds followed by washing with distilled water and drying with drier.

3.5.3 Electro polishing

Electropolishing was used for EBSD sample preparation. The samples after cloth polishing were electropolished to remove the stresses generated during mechanical polishing (paper & cloth). The etchant (20 % percholric + 80 % methanol) was used at -15˚C & 11 V for electro polishing. The stainless steel sample was used as cathode. Samples were polished for about 60 seconds and were then washed in distilled water followed by drying in air.

3.5.4 Twin jet electropolishing

Twin jet electropolishing was used for TEM samples preparation. Initially, the samples were reduced up to 0.1 micrometer thickness with emery papers of different grades (320, 600, 1200, 1500 & 2000) followed by twin jet polishing. The solution containing methanol and perchloric acid in the ratio of 80:20 by volume was used for twinjet polishing with 38 volt potential and for about 90- 120 seconds. To remove the etchant from sample surface sample was washed in methanol.

3.5.5 Differential Scanning Calorimetry (DSC)

The sample was first thinned to 0.7 mm thicknees with the help of emery papers than punch was used to take 5mm disk sample. Again this sample was thinned till weight of sample reduced upto 30 mg. The perkin Elmer's 8000 machine was used for DSC investigation. To produce the inert environment during heating in sample holder N_2 gass was used.

Chapter 4

Precipitation hardening behaviour of Al-Mg-Si alloy Processed by Cryorolling and Room temperature Rolling

4.1 Introduction

Aluminium alloys with high strength to weight ratio has gained enormous interest in recent literature due to continuous demand on increasing energy efficiency of the air craft's and automobiles through weight reduction of its structural components. The microstructural features such as grain size, dislocation density, nanosized precipitates etc. are vital factors to improve tensile and fracture resistance of Al alloys. Several strategies were adopted to develop materials with high strength through engineering of the above factors. Severe plastic deformation (SPD) technique is one of the popular thermomechanical processing techniques, is currently used to develop high strength materials, in the lab scale, for structural applications. The unique features of SPD processed metals and alloys are follows; microstructures with grain size less than a micrometer, high dislocation densities, and high volume fraction of grain boundaries. These materials are popularly known as ultrafine grained (UFG)/ nanostructured (NS) materials. Although UFG materials possess high strength, unfortunately, the ductility is poor. It is a challenge to achieve high strength of the SPD processed alloy without sacrificing ductility. In UFG metals, short time annealing is given to restore the ductility of SPD processed alloy. However, it is trade off with strength. Recently, several strategies were proposed to achieve high strength with ductility of light metals [109][162].Among them, introduction of nanosized precipitates has been found to be a suitable method for the materials processed through severe plastic deformation (SPD) [163][164]. It was achieved through precipitation during annealing/ageing treatments after SPD. However, hardening behaviour of the alloy during post ageing depends on the history of thermo mechanical treatments. Severe rolling at cryogenic temperature known as cryorolling (here after mentioned as CR) is found to be well suited for production of UFG in bulk materials [165][166]. The use of CR (near to the liquid nitrogen temperature) suppresses the dynamic recovery and hence accumulation of high density of dislocations in the material as compared to room temperature rolling (here after mentioned as RTR) [109][167][168].

Al 6061 alloy is a medium strength precipitation hardenable alloy. The widely used hardening strategy is through solid solution treatment followed by water quenching and subsequently to ageing at either room temperature or above room temperature. The precipitation sequence during ageing of Al 6061 alloy is complex and involves formation of several intermediate precipitates before forming equilibrium precipitates. The precipitation sequence of this particular alloy system involves [169][170]: super saturated solid solution (SSSS) → formation of clusters and co-clusters of Mg and Si atoms → small precipitates of unknown structure → β" precipitates → β' and β" precipitates → β Mg_2Si precipitates. The clusters that form at room temperature have gained greater attention as it affects hardening behaviour of the alloy during further hardening at high temperature [171][172]. Although there are several reports emphasizing the benefits of CR over RTR in Al alloys [173][174][175][176][177][178] a comparative study on the effect of ageing of CR and RTR Al-Mg-Si alloys is scarce in the literature. Hence, in the present work, Al 6061 alloy was subjected to RTR and CR up to true strain 2.3 to compare the improvements in mechanical properties obtained through both treatments. A detailed study of hardening behaviour of CR and RTR alloy during artificial ageing and natural ageing is investigated through DSC, TEM, and XRD. The differences in mechanical properties of CR and RTR materials are discussed based on their microstructural characteristics and heat effects associated with precipitation captured through DSC studies.

4.2 Experimental Procedure

The Al-Mg-Si alloy was procured in the form of extruded bars with 50X50 mm^2. The blocks with 40X30X10 mm^3 dimensions were machined and subjected to solid solution treatment at 530 °C for 3 hours and quenched in water at room temperature. The room temperature was 13 °C. Without any delay, the samples were subjected to room temperature rolling and cryorolling from 10 mm to 1 mm in several passes with about 4% reduction per pass. The process flow chart for CR and RTR conditions is shown in Figure 1. For rolling at liquid nitrogen temperature, the solutionized plates were dipped in liquid nitrogen for 15 min and after each pass, the plate was immersed in liquid nitrogen for 2 minutes before further reduction. Differential scanning calorimetry (DSC) was used to identify the precipitation sequence in the alloy. To study the age hardening behaviour, the CR and RTR rolled samples were subjected to ageing at 125^oC for varying times (1–80 h) in a muffle furnace. Vickers hardness was measured using 5 Kg load on rolled and aged samples. X-ray diffraction measurement was performed on CR, RTR samples using Rigaku system (Ultima IV) with a

Cu-Kα radiation of 1.5406 A°. Uni-axial tensile tests were conducted at room temperature with strain rate of $3 \times 10^{-3}\ s^{-1}$ on specimens that were machined as per ASTM E-8 sub-size specimen standards. Microstructural characterization was carried out in a FEI Technai 20 transmission electron microscope (TEM) operating at 200 kV and Scanning electron microscopy.

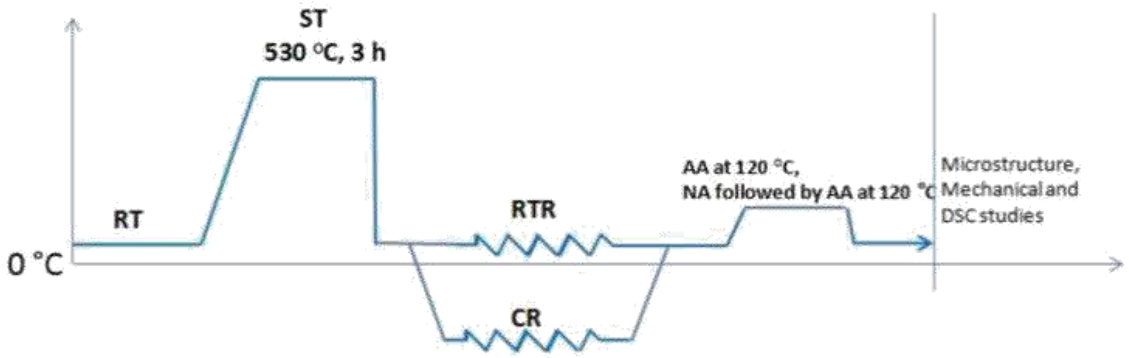

Figure 4.1: Process flow chart of CR and RTR conditions.

4.3 Results and Discussion

4.3.1 Effect of cold rolling

4.3.1.1 DSC studies

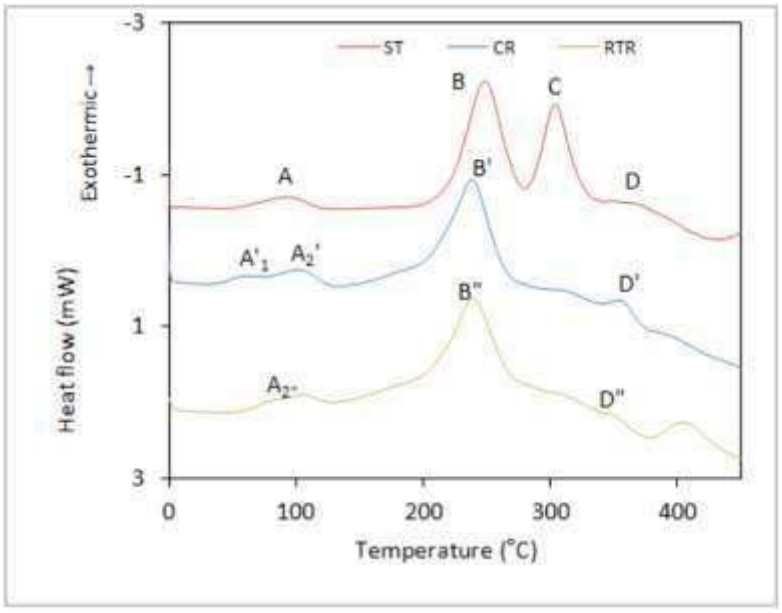

Figure 4.2: DSC thermograms of ST, CR and RTR alloy.

The DSC thermograms of ST, RTR and CR Al 6061 samples are shown in Figure 4. 2. A detailed study of DSC thermograms of ST material is discussed elsewhere [185]. Four main exothermic reactions labelled as A, B, C, D occurred at 90, 250, 290 and 360 °C correspond to formation of solute clusters, β", β' and β phase precipitates, respectively. It is evident from the DSC curves that significant changes have occurred during early stage precipitation (cluster formation) and medium stage precipitations (peak B'→β"/β' formation). Severe cold rolling has led to suppression/simultaneous formation of β' precipitates along with β" precipitates. It is also observed that the major exothermic peak corresponding to strengthening phase formation in rolled material has shifted to low temperature side. In Al-Mg-Si alloys, emphasis has been given to early stage precipitation due to its crucial role in the strengthening phase formation. According to Chang et al. [180], the earlier stage precipitation of ST material involves three clustering reactions, which occur in two stages. It was reported that the first two reactions are linked to each

other and completed within 1 hour after quenching. Whereas, the third reaction starts after 1 hr of quenching and it lasts for 2 weeks. The negative effect of clusters that forms at room temperature on artificial ageing is that it cannot serve as nuclei for further precipitation during artificial ageing.

In the present investigation, as the samples are immediately rolled at RT and cryogenic temperature, it is expected that no static ageing has occurred in the material after quenching. As a result of CR, clusters peak at around 90 °C in ST material appeared as a doublet (A'_1 and A'_2). This indicates effective suppression of clusters C0, C1 and C2 formation in the CR material. In the RTR material, a single broad peak (A_2") is observed at around 90 °C. It is possible that, the adiabatic heating of material during rolling might have accelerated the formation of C0 and C1 (peak A'_1). According to Chang et al., [180], the formation of clusters C0 and C1 affects hardening behaviour of the alloy during further artificial ageing.

Activation energy

Activation energy associated with the peaks A_2" and B" in the RTR material is calculated by applying Kissinger's method [181]. DSC scans performed with various heating rates 10, 15, 20 and 25 °C/min (Figure 4.3.a) were used for the calculation. The estimated activation energy are 78 and 143 kJ/mol of the reaction peaks A" and B" from the Kissinger plot (Figure 4.3.b) respectively. By comparing it with the activation energy value of cluster formation observed in the ST condition [179] of the alloy with same chemical composition, it can be seen that, RTR has decreased activation energy of the processed alloy from 88 to78 kJ/mol. With increasing deformation, reduction in activation energy has been reported in literature [11][182][183]. It is believed that, in deformed material, dislocations increase the diffusivity through high diffusivity paths [184][185]. However, for the peak B", the activation energy has increased (Table 2) as compared to peak B in the ST material.

The similar observation has been reported for the CR material [179]. The thermal behaviour of RTR materials is found to be similar to CR material. The reason for increase in activation energy values of major strengthening phase β"/β' (peak B' and B") in CR and RTR material could be overlapping or suppression of peak C in ST. The TEM micrograph of CR material [179] strengthens the possibility of simultaneous formation of β" and β' phases in CR and RTR material.

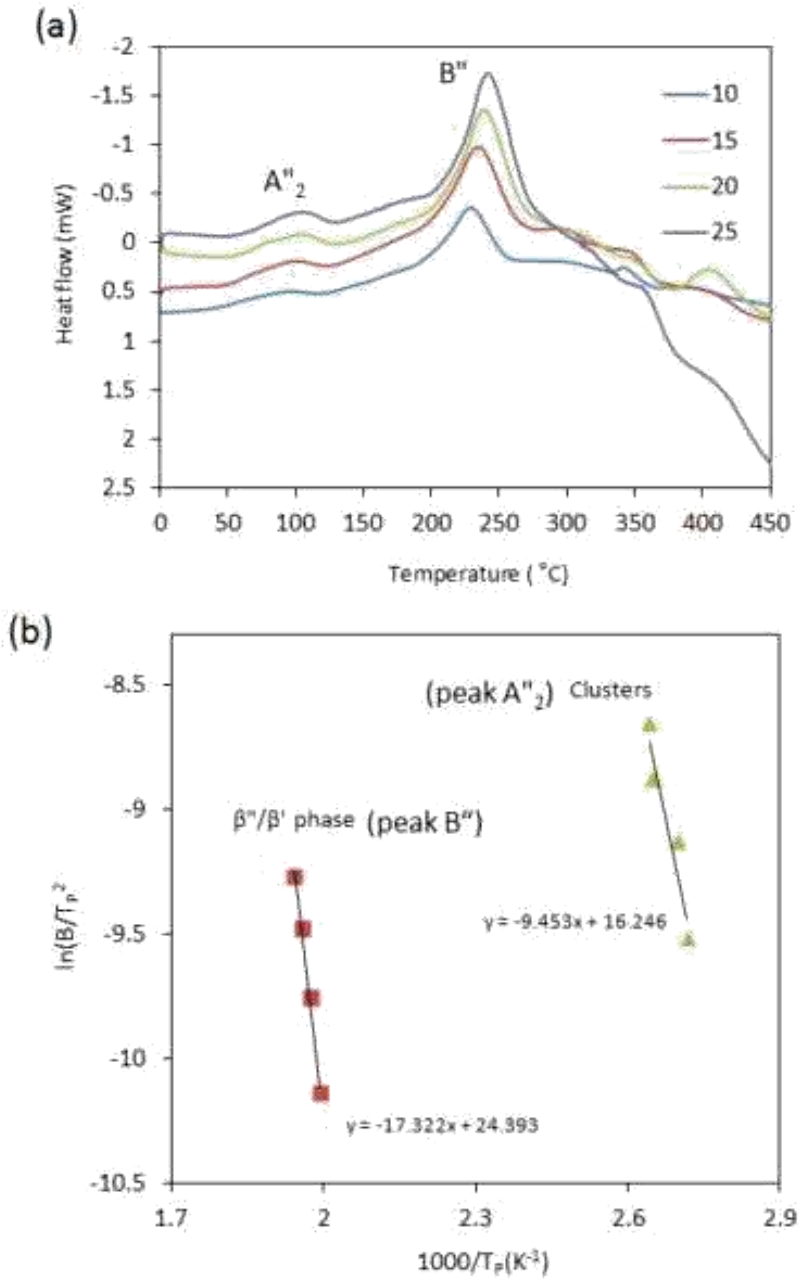

Figure 4.3: DSC thermograms with various heating rates (10, 15, 20, 25 °C/min) and Kissinger plots for various exothermic peaks in RTR alloy.

Hardness

Figure 4.4 shows the variation in hardness in CR and RTR material with increasing % of reduction in thickness. The difference in hardness between CR and RTR material at different

strain is negligible. It is attributed to dynamic precipitation of clusters (C0 & C1) during RTR.

Table 4.1: Activation energies of various exothermic reactions in ST, CR and RTR material

	ST[179]			CR[179]			RTR(present work)	
	Peak A (Clusters)	Peak B (β" phase)	Peak C (β' phase)	Peak A_1' (C1 type clusters)	Peak A'_2 (C2 type Clusters)	Peak B' (β"/β' phase)	Peak A" (Clusters)	Peak B" (β"/β' Phase)
Activation energy kJ/mol	88	114	124	56	87	136	78	143

It is likely that, these solute clusters also contribute to increasing dislocation density during rolling by acting as effective pinning agents [186]. This counteracts the softening effect by reduction in dislocation density through recovery. The similar behaviour has been reported for the Al-Cu alloy after CR and RTR [187] . The obtained hardness results are in tandem with the DSC plots of CR and RTR materials.

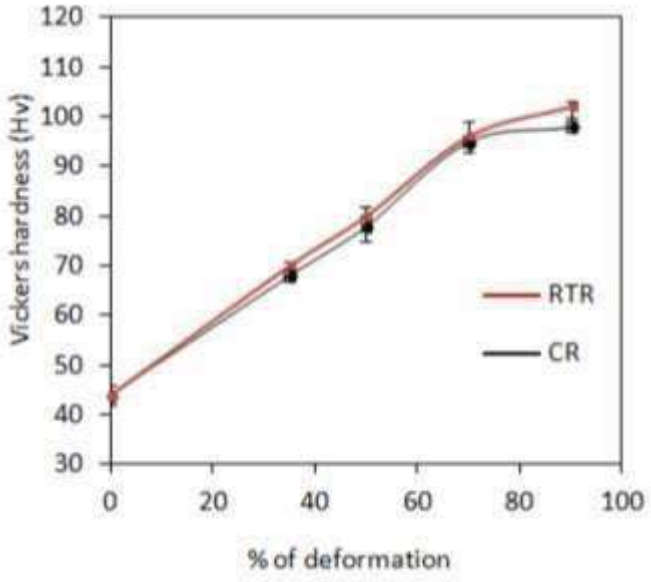

Figure 4.4: Variation in hardness in CR and RTR Al 6061 alloy with increasing % of thickness reduction.

XRD

The XRD patterns of Al 6061 alloy processed through CR and RTR is shown in Figure 4.5. Further, the structural characterization and peak shifts of Al alloy processed through CR and RTR is also shown in Table 4.2. Structural characterization using X-ray line broadening analysis can be used to characterize the SPD products in terms of crystallite size, microstrain, dislocation density, peak intensity and peak shifts. The crystallite size and microstrain were estimated by analyzing the broadening of XRD peaks using standard Williamson-Hall formula [188]. The intensity of Al (111), (200), (220), (311) planes were compared between RTR and CR material. The intensity of peaks corresponding to planes (111), (200) of CR material has decreased as compared to RTR material. This is attributed to higher strain in the CR material in the high atomic density planes. In addition, peak shift is observed in CR material. Whereas, the peaks representing the planes Al (220), (311), has decreased in RTR material but it is not much as compared to CR material. It is attributed to variation in activation energy of planes by varying deformation temperature.

It can be clearly observed from Figure 4.6 that peak broadening and reduction of peak intensity for cryorolled sample have occurred in (111) and (200) planes when compared to room temperature rolled sample. From Table 4.2, it is very clear that the RTR sample exhibited the lower value of crystallite size of 302 nm than 355 nm for CR material. Around 17% more reduction has occurred in RTR sample than CR sample. It was due to more deformation in Al lattice occurred during RTR which might produce more dislocation density. RTR has engendered dynamic precipitation of solute clusters. Even though faster kinetics of restoration through dynamic recovery manifests in RTR material, precipitation of solute atoms actively participates in the accumulation of dislocations by effective pinning. This was also observed in Table 4.2 that the dislocation density of RTR sample was 0.59015×10^{14} m^{-2}, whereas the dislocation density of CR sample was 0.51704×10^{14} m^{-2}. The dislocation density of RTR sample is 14% higher than that of the CR sample. Also, the corresponding microstrain of RTR sample was also higher than CR sample.

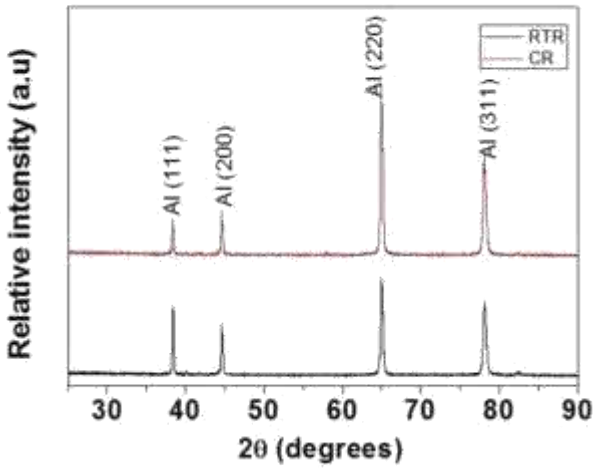

Figure 4.5: XRD plots of CR and RTR Al 6061 alloy.

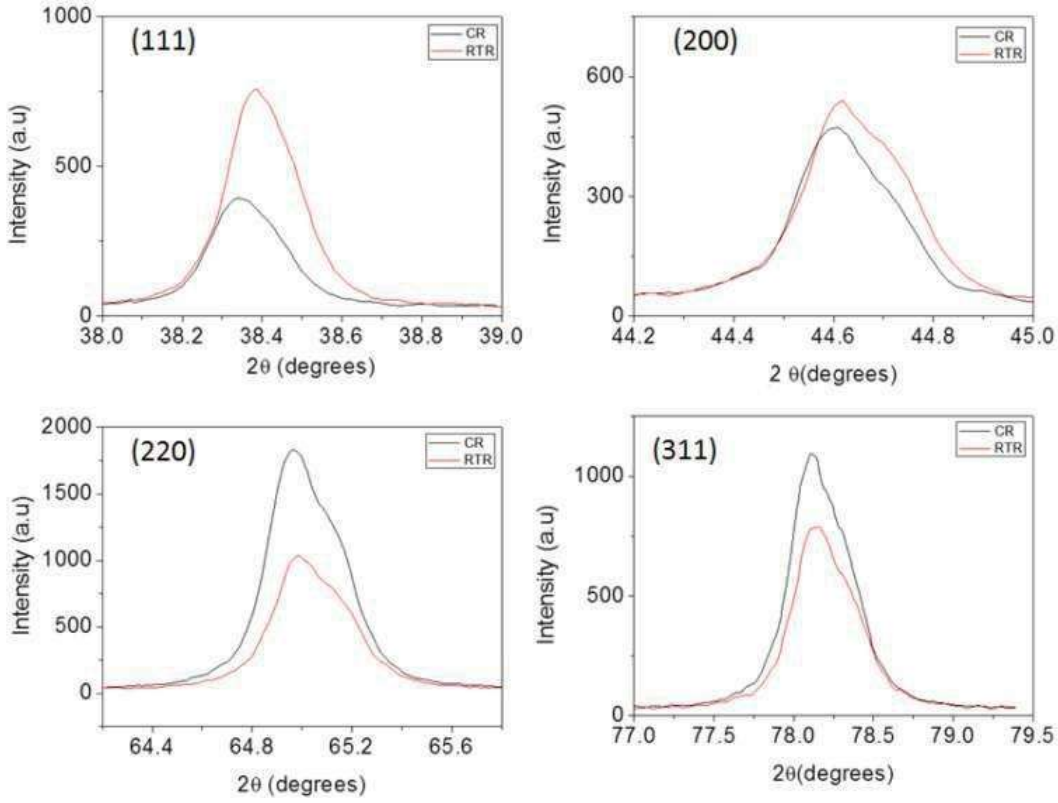

Figure 4.6: Comparative plots of peak broadening and intensity reduction in various planes (111), (200), (220) and (311) in CR and RTR Al 6061 alloy.

Table 4.2: Structural characterization and peak shifts of copper alloy processed through CR and RTR.

Sample condition	Crystallite size (t), Nm	Microstrain (ε), %	Dislocation density (ρ_D), m^{-2}	Peak intensity, a.u (Centre of angle, deg)			
				(1 1 1)	(2 0 0)	(2 2 0)	(3 1 1)
RTR	355±5	0.187	0.59014×10^{14}	689.55(38.40)	462.73(44.65)	919.94(65.00)	714.11(78.16)
CR	302±3	0.189	0.51705×10^{14}	348.8(38.36)	404.55(44.62)	1669.01(65.04)	987.52(78.19)

EBSD

Figure 4.7 shows the orientation image micrograph of CR and RTR alloy. Lines in black colour indicate low angle grain boundaries (1.5° < 15°) and lines in grey colour indicates high angle grain boundaries (> 15°). Black spots in the micrograph show unpartioned area. The role of stacking fault energy (SFE) in the deformation of FCC material is important. In high SFE metal, Al, the deformation at room temperature is primarily due to slip. During deformation at cryogenic temperature, the dislocation movement by slip is significantly restricted. Hence, the orientation difference in the microstructures of CR and RTR is expected through EBSD analysis. The analysis part is included in the revised thesis.

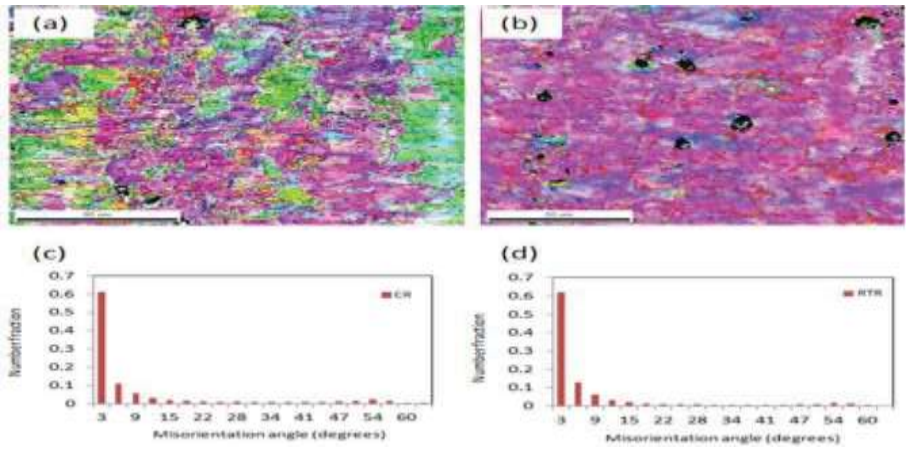

Figure 4.7: EBSD maps of CR and RTR material; (a) & (b) are inverse pole figure maps, (c) & (d) Misorientation distribution plots.

These spots are due to coarse impurity particles such as AlFeSi, Al_6Mn.etc. Figure 4.7 (c) and (d) represent misorientation profiles of the micrographs corresponding to Figure 4.7 (a) & (b). The misorientation distribution indicates that there is no significant change between CR and RTR material.

4.3.2 Effect of Ageing on Hardening of CR and RTR material

4.3.2.1 Artificial ageing

Microstructure

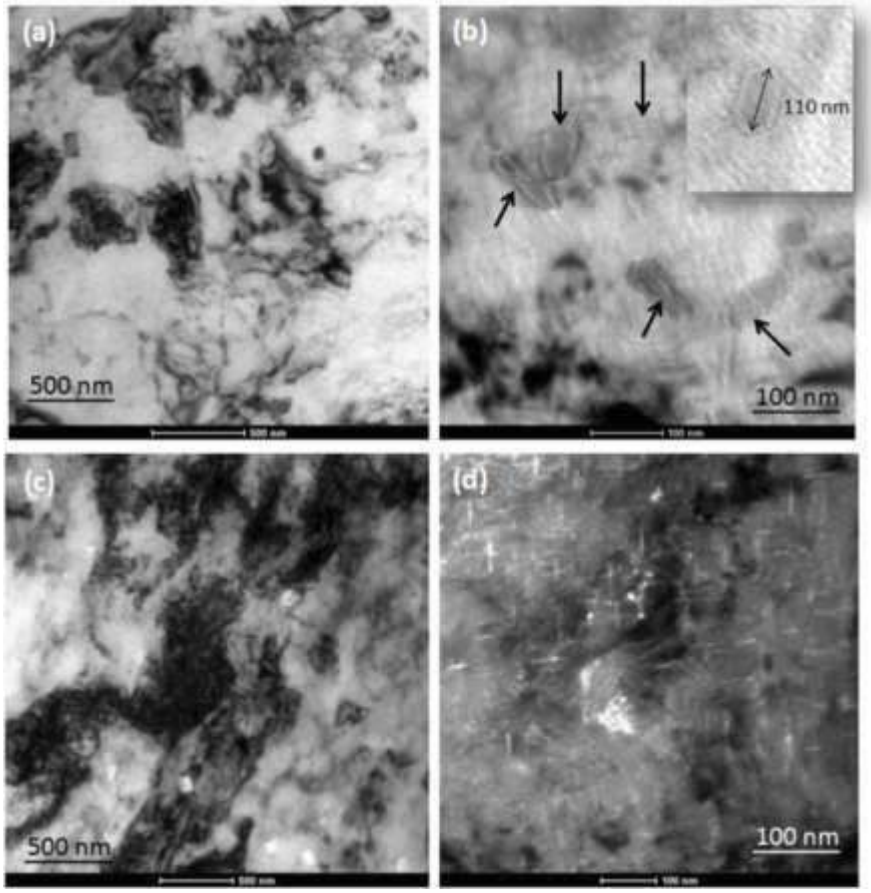

Figure 4.8: TEM micrographs of CR and RTR alloy after peak ageing treatment; a) bright field (BF) micrograph of CR +PA alloy representing ultrafine grains (UFG) structures, b) BF micrograph of CR +PA alloy representing nanosized precipitates, c) BF micrograph of RTR+PA alloy showing UFG along with dense dislocation tangled zones, d) Dark field micrograph of RTR+PA alloy showing nanosized precipitates.

Figure 4.8 shows the TEM micrographs of CR and RTR samples after artificial ageing at 125 °C for 68 hours. Our previous studies and available literature suggest that 125 ^{o}C is the optimum temperature to obtain maximum hardness in the rolled 6061 Al alloy. Artificial ageing has led to partial recovery in the severely deformed microstructure and formation UFGs with distinguishable sharp boundaries. Annihilation of dislocations through recovery during ageing promotes further accumulation of more dislocations, which imparts more % elongations to the aged alloys. The study of evolution of precipitates in the severely deformed material is more complex owing to simultaneous occurrence of precipitation and restoration of severely deformed structure. Figure 4.8b shows nanosized precipitates in CR peak aged material. The inset in Figure 4.8b shows the precipitates with length of 110 nm and diameter of 50 nm. Figure 4.8.d represents the dark field micrograph of RTR peak aged material. It is evident from the Figures 4.8b and4.8 d, that precipitates observed in RTR peak aged material are finer than CR peak aged material. Besides that, the number density of needle shaped precipitates is also observed to be more in RTR peak aged material. In Al 6XXX alloy, β" precipitates are considered to be primary strengthening phase to strengthen the Al matrix. However, the size, distribution and growth of the β" are depend on its precursors (clusters), which form at low temperature. Our investigations have revealed that room temperature rolling leads to the formation of clusters through dynamic ageing. Where as in the cryorolling process, cluster formation is restricted during rolling and therefore static ageing is used to introduce precipitates in the Al matrix. Our TEM observations indicate that dynamic ageing effect facilitates the formation of finer precipitates than static ageing. The positive affect through dynamic ageing can be attributed to the interaction of dislocations with precipitates. It is possible that, the dislocation movement (during dynamic ageing) cuts the precipitates in to finer size. Hence the size of nano-sized precipitates in RT rolled alloys are finer than CR materials.

Hardness

The hardness of the as-rolled CR and RTR samples are 98 and 101 HV5Kg, respectively. In the precipitation hardenable Al alloys, the hardening of the Al matrix depends on the nature, morphology, size, distribution and volume fraction of the precipitates. In Al 6061 alloy Mg and Si are the primary alloying elements, which forms precipitates to render strength to the matrix. The evolution of the precipitates involves, SSSS → formation of various types of clusters → β" →β′ → β (Mg_2Si) phase. The maximum strength is obtained from β" phase. Clusters, that form at low temperature act as precursors for β" phase precipitates, which forms at high temperature. It is well understood that, the type and distribution of the clusters plays critical role in deciding the strength contribution from the β" precipitates. The superior mechanical properties of RTR material over CR material indicates that,

the clusters that from at room temperature due to dynamic ageing affect are more favourable to form fine, coherent, well distributed nano-sized β" precipitates. It was observed from our earlier studies that 125 °C is the optimum temperature for low temperature ageing of rolled Al 6061 alloy. After rolling, with no delay, samples were subjected to ageing at 125 °C to observe the precipitation hardening behaviour. Figure 4.9 shows the hardness variation of the CR and RTR Al 6061 samples as a function of ageing time. In both CR and RTR material, the hardness has increased with ageing time.

This indicates hardening through precipitation is able to overcome the softening due to recovery in rolled material. This behaviour is not unusual, because similar behaviour has been observed in several precipitation hardenable Al alloys before [173][9][189]. The maximum hardness was obtained after 68hours of ageing in both the CR and RT samples. The unexpected behaviour observed in the ageing of RTR and CR material was; during early stage of ageing, the rate of increase in hardness in RTR material is more than CR material. The maximum hardness obtained in CR material after peak ageing treatment is nearly 10 HV lower than the RTR material. This peculiar behaviour of RTR material in the hardening can be understood by correlating with its DSC curves. As discussed in the previous section, RTR has promoted the formation of clusters C0 and C1.

In general, the clusters which form at room temperature will have negative effect on strengthening during further artificial ageing. Therefore, pre-ageing treatments are given to reduce the negative effect of natural ageing. It is found that, selection of pre-ageing temperature is very important to modify the clusters that form during natural ageing [190]. In the present investigation, the increase in hardness observed for RTR material is attributed to nature of the clusters that forms during RTR. It is possible that, due to dynamic ageing effect during RTR, the distribution and size of the solute clusters might get modified. In the CR material, the formation of clusters occurs after the deformation and it is possible that solute clustering and strengthening phase formation might take place within a heavily dislocated structure. Another possible reason for a lower hardness value observed in CR material during ageing could be faster restoration of heavily strained structure through recovery. Even though there is hardening effect through precipitation, but the softening effect through recovery would be more.

Whereas in RTR material, the presence of solute atoms may trap the dislocations and lead to low recovery rate. Sharma et al. [187] have investigated the precipitation behaviour in CR and RTR Al-Cu alloy. It was reported that RT rolled samples has shown lower hardening behaviour than CR material. This is contrast with the work reported by Weiss et al., [26] on strengthening and formability of CR and RTR Al 2024 alloy. RTR material has shown superior hardening behaviour than CR material. This indicates that the beneficial effect of the CR over RTR in precipitation hardenable alloys is yet to be established.

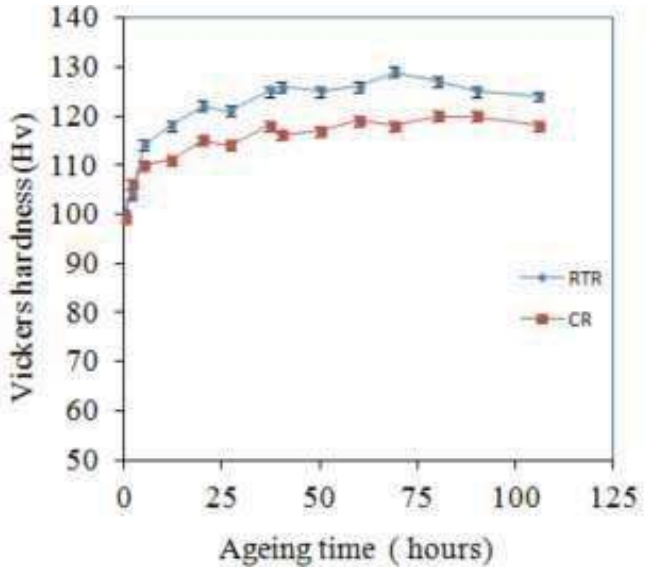

Figure 4.9: Variation in Vickers hardness behaviour of CR and RTR Al 6061 alloy during artificial ageing at 125 °C.

Tensile testing

Figure 4.10 shows the engineering stress - strain plots of ST, CR, RTR and their peak aged conditions of Al 6061 alloy. Rolling at cryogenic temperature and room temperature has resulted significant increase in the yield strength (YS) and ultimate strength of the starting material. The increases in YS in CR and RTR with respect to ST condition are 460% and 524% respectively. However, the increase in YS in CR and RTR material is followed with decrease in % elongation from 42% to 3.5%. The increase in YS of RTR material is slightly more than CR material;

however the % elongations are nearly same. The substantial increment in YS in CR and RTR material is attributed to presence of high dislocation density (Table 4.2) and decrease in grain size from several micrometers to sub-micrometer (Crystallite size; CR-355 nm, RTR-302 nm) range. The difference in YS between CR and RTR alloy is due to the fact that, dislocation strengthening is accompanied with precipitation hardening in the latter. In the CR process, it is believed that decrease in deformation temperature leads to increase in defect density through suppression of dynamic recovery, and as a consequence increase in YS is observed [35]. However, the dynamic recovery is not significantly suppressed for the materials with high stacking fault energy such as Al and its alloys [35]. In pure Al, we have observed that increase in YS of CR material is 6% more than RTR material (unpublished data). This slight increment (6%) will not viable for production from the commercial point of view. In precipitation hardenable alloys, starting material with ST condition is temperature sensitive. The higher strength of RTR over CR material observed in the present work proves that precipitation hardening during RTR plays a crucial role in increasing the YS of the material.

Artificial ageing at 125 °C for 68 hours has resulted simultaneous improvement in strength and ductility of both CR and RTR material. The YS and UTS of CR material are observed to be 355 and 370 MPa, respectively. Where as in the RTR material, YS and UTS are found to be 380 and 395 MPa, respectively, which is nearly 7% higher than CR material. This typical behaviour can be understood through TEM micrograph shown in Figure 4.8. In 6061 alloy, precipitation hardening is the primary strengthening mechanism. The hardening effect through precipitation depends on nature (type, size, volume fraction and distribution) of the major strengthening phase (β"/β' precipitates) present in the material. It is believed that the nature of the β"/β' precipitates depends on its precursors. However, investigation of clusters through TEM is a difficult task. From the DSC studies, it can be concluded that the RTR has altered the nature of clusters, whichis favourable to render maximum contribution from the β"/β' precipitates. The % elongation (~9%) is observed to be nearly same in both CR and RTR material. The increase in ductility upon ageing is attributed to decrease in dislocation density and increase in strain hardening effect by nano precipitates as evident from Figure 4.8.

.

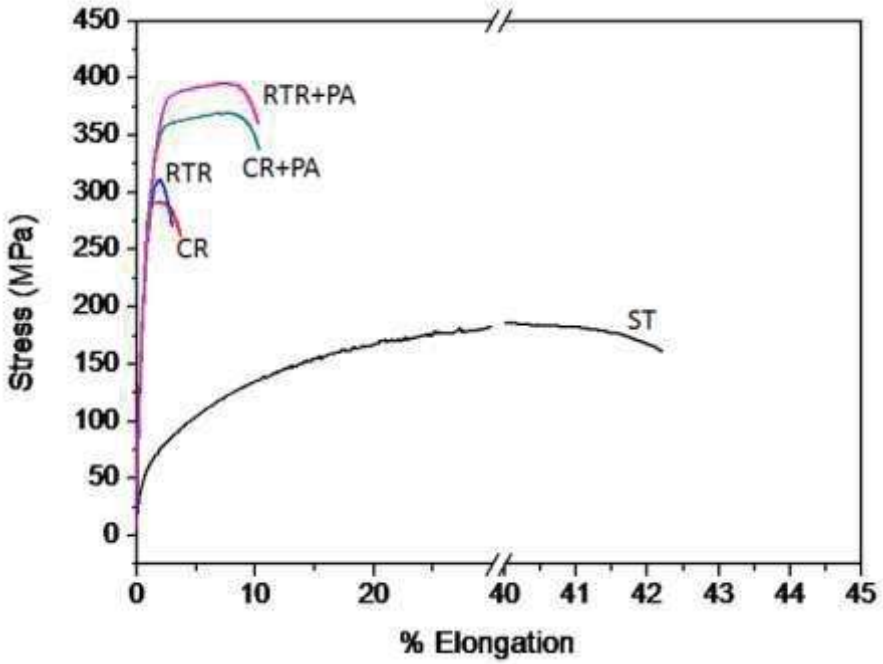

Figure 4.10: Engineering stress-strain plots of Al 6061 alloy processed under various conditions.

4.3.3 Natural ageing and its effects on artificial ageing

4.3.3.1 DSC

Figure 4.11 shows the precipitation behavior of RTR, CR and ST material while keeping at room temperature for 30 days. Notable changes have occurred in the low temperature peaks in all the samples.ST material shows a suppression of exothermic peak at 90 °C and the formation of deep endothermic peak corresponding to clusters dissolution. This phenomenon is as expected. In the CR and RTR material, the suppression of cluster peaks at low temperature is similar to the ST material. However, the endothermic peak corresponding to the dissolution of clusters is not significant. This indicates a complete formation of clusters during natural ageing whereas in RTR and CR, the effect of NA is very low.

In the precipitation hardenable Al alloys, the hardening of the Al matrix depends on the nature, morphology, size, distribution and volume fraction of the precipitates. In Al 6061 alloy Mg and Si are the primary alloying elements, which forms precipitates to render strength to the matrix. The evolution of the precipitates involves, SSSS → formation of various types of clusters → β" →β´ → β (Mg_2Si) phase. The maximum strength is obtained from β" phase. Clusters, that form at low temperature act as precursors for β" phase precipitates, which forms at high temperature. It is well understood that, the type and distribution of the clusters plays critical role in deciding the strength contribution from the β" precipitates. The superior mechanical properties of RTR material over CR material indicates that, the clusters that from at room temperature due to dynamic ageing affect are more favourable to form fine, coherent, well distributed nano-sized β" precipitate

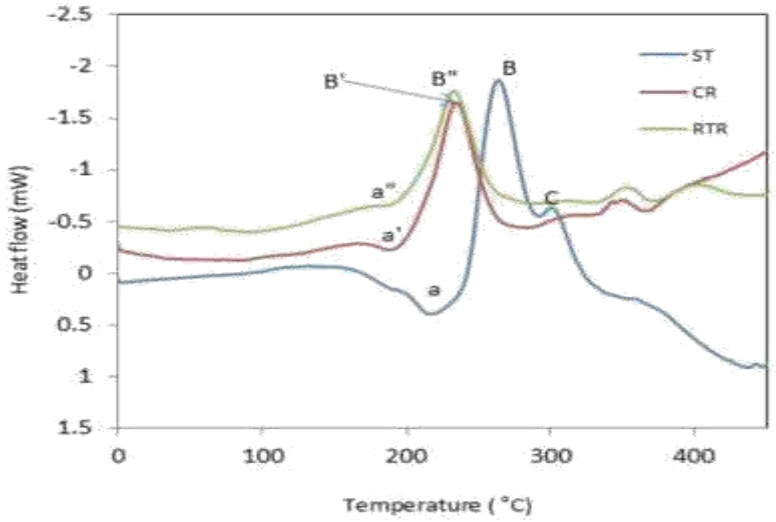

Figure 4.11: DSC thermo-grams of ST, CR and RTR material after natural ageing for 30 days.

4.3.3.2 Hardness

Figure 4.12(a) shows the hardness versus ageing time at room temperature and at 120 °C. After CR and RTR, the samples were kept at room temperature for 1 month to investigate the effect of natural ageing on hardening behaviour of CR and RTR material. It can be observed that, the first 36 hours of natural ageing has resulted increase in hardness from 98 and 100 Hv to 108 Hv in both CR and RTR samples.Rolling at cryogenic temperature suppresses the dynamic recovery, which leads to increase in dislocation density.

With further increase in ageing time to 720 hours, it has not shown much effect of hardening on the alloy. The quick rise in hardness during earlier hours is attributed to the formation of clusters of atoms. From our observation it was concluded that the cluster formation in rolled Al 6061 alloy has completed within 2 days of natural ageing (unpublished data). Natural ageing for one month results in reduction of the solute content in the matrix. Figure 4.12(b) shows the variation in hardness in natural aged CR and RTR material after artificial ageing at 125 °C. The maximum hardness (124 Hv) was achieved after 50 hours of ageing. The hardness

behaviour in both CR and RTR sample is same, which is attributed to similar rate of recovery and precipitation.

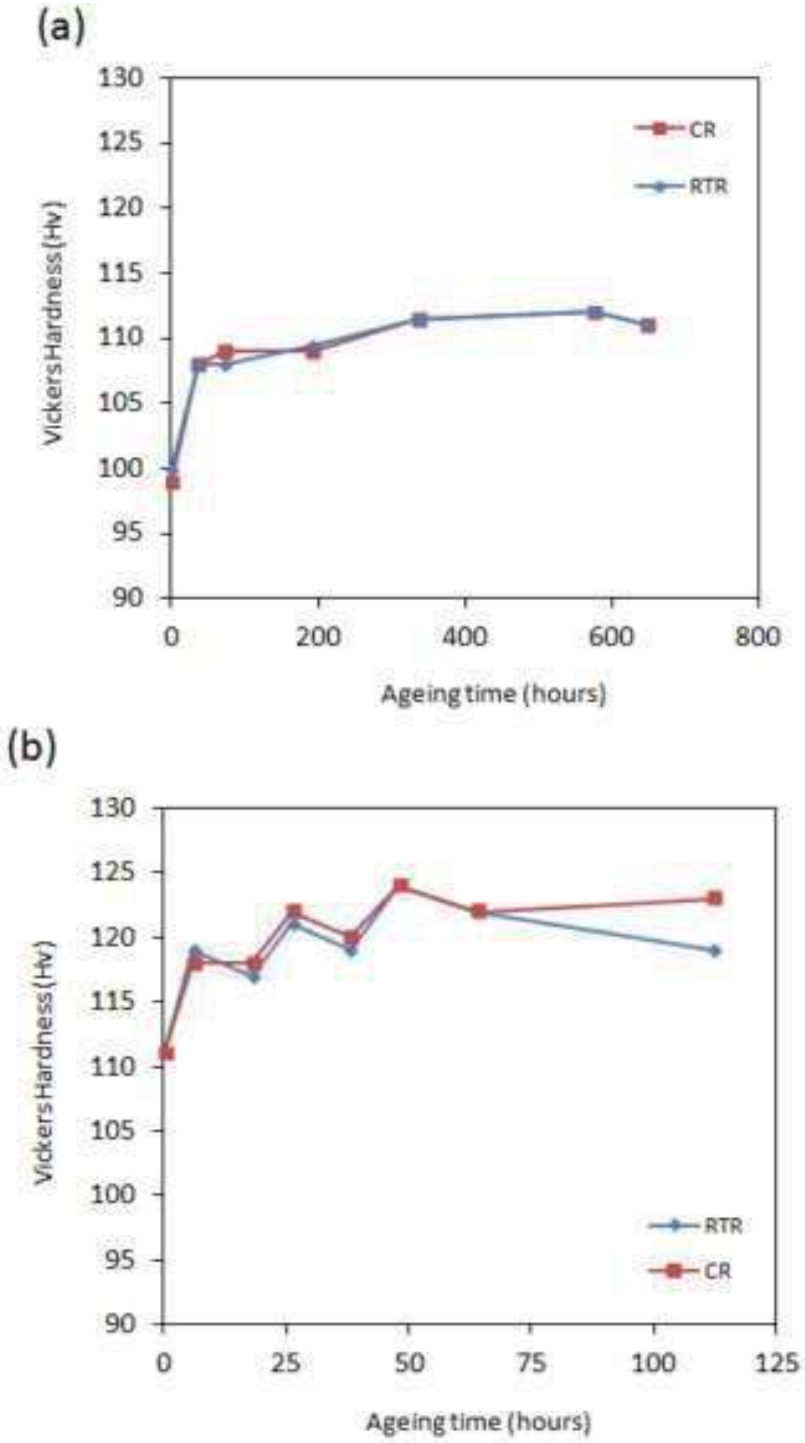

Figure 4.12: Variation in Vickers hardness behaviour of CR and RTR material; a) Natural ageing for 1 month, b) artificial ageing at 120 °C.

4.3.4 Annealing behavior

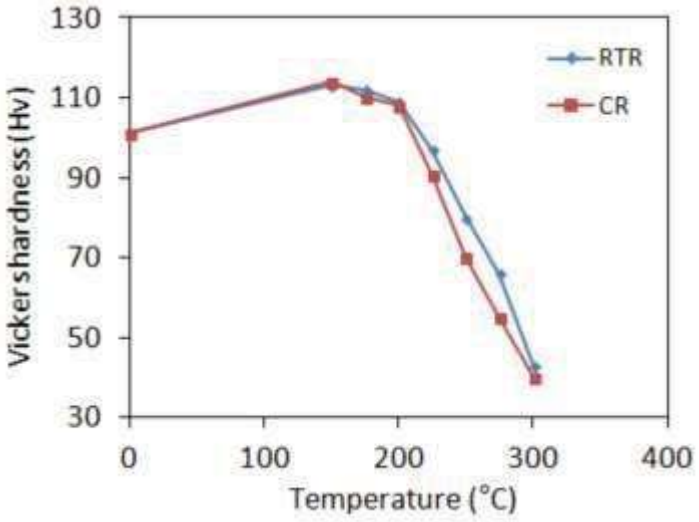

Figure 4.13: Variation in Vickers hardness behaviour of CR and RTR material during annealing at various temperatures from 150 to 300 °C.

Thermal stability of Al 6061 alloy after CR and RTR up to 90% reduction was analyzed by performing Vickers hardness test and tensile test at room temperature. Figure 4.13 illustrates the variation of Vickers hardness of CR and RTR samples after annealing at temperature range from 150 to 350 °C for 1 hour along with the variation in the fraction of recrystallization. After annealing at 150 °C for 1 hour, the Vickers hardness value of the both CR and RTR material has increased (Figure 4.13), which can be attributed to precipitation hardening effect. The Vickers hardness value started dropping gradually after annealing at 200 °C. After annealing at 250 °C, the hardness drops suddenly and the drop proceeds with the same rate up to 300 °C. There is no remarkable change observed in the annealing behaviour of CR and RTR material. .

4.4 Conclusions

The solutionized precipitation hardenable Al 6061 alloy has been rolled at room temperature (RTR) and liquid nitrogen temperature (CR). For each of the two conditions, the alloy has been aged in two different conditions: i) artificial ageing at 125 °C immediately after rolling; and ii) natural ageing for one month followed by artificial ageing at 125 °C immediately after rolling. The following conclusions are made based on the present study.

a) The increment in hardness after CR and RTR is nearly same as there is no significant difference between them. This behaviour in RTR material is attributed to dynamic ageing effect during rolling at room temperature.
b) Post ageing treatment at 125 °C of CR and RTR material has resulted significant improvement in hardness. However, the peak hardness observed in RTR material (129 Hv) is much higher than that in CR material (119 Hv). It can be attributed to the nature of the early stage precipitates that form during dynamic ageing.
c) Natural ageing prior to artificial ageing has resulted similar ageing behaviour in both CR and RTR material. Superior hardening behaviour in RTR material is vanished after natural ageing.
d) For the tensile testing performed for rolled and peak aged materials, the RTR material has shown higher values (YS- 380 MPa, UTS- 395 MPa) than CR material (YS- 355 MPa, UTS- 370 MPa) and with nearly same tensile ductility (10%) .
e) Hardness and DSC investigations have shown that the microstructural and thermal stability of the CR and RTR material is similar.

Chapter 5

Cryorolling followed by Warm rolling

This chapter mainly focuses about the effect of cryorolling followed by warm rolling at various temperatures (100 ℃, 145 ℃ and 175 ℃) with various % of thickness reductions (67%, 75% and 80%) on microstructure and mechanical properties in Al 6061 alloy. It also describes about the thermal behavior of above stated conditions through Differential scanning calorimetry studies (DSC). The mechanical properties were characterized by employing Vickers hardness and tensile testing machine. The microstructural features were characterized by adopting Electron back scattered diffraction (EBSD) and Transmission electron microscopy (TEM) techniques.

When the deformation is carried out above the room temperature and below the recrystallization temperature, the process is called warm rolling. It is suitable to get better mechanical properties in precipitation hardenable Al alloys through the phenomenon called dynamic ageing.

5.1 Introduction

Severe plastic deformation (SPD) techniques such as Equal channel angular pressing (ECAP), Twist extrusion (TE), Accumulative roll bonding (ARB), High pressure torsion (HPT), and Multi directional forging (MDF) are commonly used to produce UFG structure in the metals and alloys at room temperature or above room temperature. In precipitation hardenable Al alloys SPD at room temperature or above room temperature results complex phase transformations such as formation of second phase precipitates, their growth, fragmentation and dissolution[191][100][79] [192][107]. Microstructure developed through SPD is characterized by enhanced volume fraction of grain boundaries, enhanced dislocation and vacancy densities; consequently increased diffusion coefficient [193]. Uncontrolled precipitation during SPD leads to profound change in precipitate morphology. Sha et al.,[194] have reported, the dissolution of metastable precipitates in AA7136 alloy after ECAP processing at 200 °C. It is also reported that the precipitation evolution in ECAP processed alloy is 50 times faster than in conventional age hardening alloys. Gubicza et al.,[195] have reported similar observations in Al-Zn-Mg alloy. Faster rate of precipitation evolution in Al alloys, during SPD can by-pass the most effective strengthening phase. So it can be concluded that performing SPD of precipitation hardenable Al alloys at room temperature or above room temperature might lead to deterioration of mechanical properties. Selection of proper SPD process is essential to obtain optimum strengthening contribution from various strengthening mechanisms. In this regard, SPD at cryogenic temperature followed by low temperature artificial ageing can be an effective process which will not by-pass the effective strengthening phase unlike other SPD techniques. However it has been observed by several authors, that the kinetics of precipitation is accelerated during post deformation ageing [122] [196] [11], due to presence of high dislocation density. Post deformation ageing has resulted coarsening of precipitates due to high diffusion coefficients; simultaneous formation of semi coherent phase along with coherent phase precipitates [179]. Clusters that form at early stage of precipitation, has significant role in deciding the strengthening contribution from the later stage of precipitation. As it is evident from the Chapter 4, RTR has resulted better ageing hardening behavior than CR. The superior mechanical properties of the RTR peak aged material over CR peak aged material can be attributed to the nature of the early stage clusters that were formed during RTR.

It is also evident from the Chapter 4 that the precipitates formed during dynamic ageing have contributed to increase the dislocation density by acting as effective pinning agents.

. Kang et al. [197] have observed that cryorolling (CR) followed by warm rolling (WR) has significant effect on increase in strength of Al 5052 alloy. As well, they have also reported that post deformation annealing has resulted increase in ductility without losing its strength. Nageswara rao et al., have observed similar behavior in Al 6061 alloy by performing warm rolling at 145 ℃ after cryorolling. However there is no reported literature on detailed investigation of effect of warm rolling temperature and % of warm rolling reduction on the microstructure and mechanical properties of precipitation hardenable alloy (Al 6061). Therefore, the present section is mainly focused on effect of warm rolling temperature and warm rolling reduction after cryorolling on the mechanical and microstructural characteristics of Al 6061 alloy. We have also studied the effect of post deformation ageing at low temperature on strength and ductility of Al 6061 alloy.

5.2 Experimental Procedure

Al 6061 alloy samples were machined with 10x30x40 mm^3 from as received alloy plate and subjected to solid solution treatment at 530 ℃ for 3 hr followed by water quenching to room temperature. Cryorolling was performed to various percentages of reductions to 50%, 60%, 70% and 90%. The details of cryorolling process are discussed in the Chapter 3. Reduction per pass is 4% and total reduction is achieved through multiple numbers of passes. Cryorolled samples with various reductions (50%, 60% and 70%) were subsequently warm rolled at various temperatures (100 ℃, 145 ℃ and 175 ℃) to reductions of 67%, 75% and 80% respectively. Before each pass of warm rolling, samples were heated for 4 min in electric muffle furnace. In the present study, total thickness reduction final sample is maintained as 90%. Only the proportional percentage reductions of cryorolling and warm rolling are varied.

Mechanical properties were investigated by performing Vickers hardness test and Tensile testing at room temperature. For tensile testing, samples with dimensions according to ASTM E8 sub size specimens with gauge length 25 mm and thickness 1mm were used. Tensile samples were prepared along the plane parallel (RD-TD) to the rolling direction. Minimum three samples were tested to obtain average value.

Tinious Olsen machine was used with cross head speed as 1 mm/min. Minimum four samples were tested in each condition to obtain average value.

TEM investigation for the samples of CR and CR followed by WR with maximum percentage of reductions (CR 90%, CR+WR 80%) has been carried through by using FEI Technai 20 TEM operated at 200 KV. EBSD characterization was done for ST and CR+WR80% at various temperatures samples. Differential scanning calorimetry was used to investigate the thermal behavior of the above mentioned samples by using Perkin Elmer Paris Diamond DSC. Samples were tested under pure nitrogen atmosphere and heating rate applied was 10 °C/min. The staring temperature of the DSC scan was room temperature. Annealed pure aluminum was used as a reference sample.

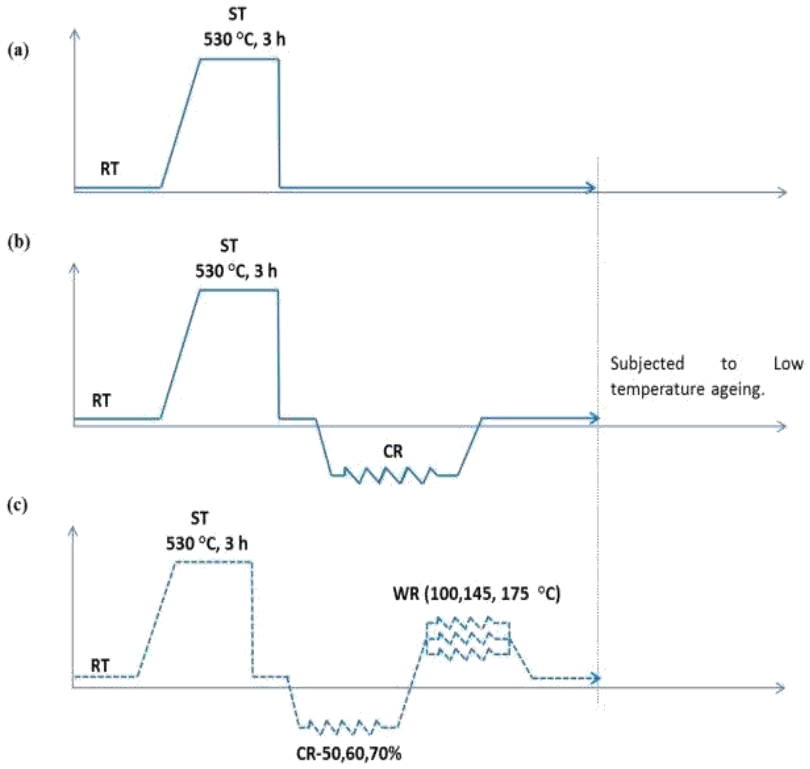

Figure 5.1 Process flow diagram
(a) ST
(b) CR
(c) CR+WR

5.3 Results

5.3.1 Effect of warm rolling

5.3.1.1 Mechanical properties

Figure 5.2 shows the variation in Vickers hardness of Al 6061 alloy processed with different combinations of cryorolling and warm rolling percentage reductions. The hardness of starting material after solid solution treatment followed by water quenching was 52 Hv. After cryorolling up to 90% thickness reduction, the hardness has increased from 52 Hv to 98 Hv (88 %). Cryorolling followed by warm rolling at 100 °C with 67% reduction have shown hardness 113 Hv. With increasing percentage of reduction up to 75% and 80% at the same temperature, the hardness has raised to 117 Hv, 121 Hv respectively. With increasing WR temperature from 100 °C to 145 °C, at the various percentage of reductions (67%, 75% and 80%), the observed hardness values are 121, 124, 125 Hv. For WR at 175 °C for various reductions, the observed hardness values are 124, 128, 129 Hv. With WR at 145 °C and 175°C beyond 75% reduction, the hardness scarcely improves whereas WR at 100 °C with increasing percentage of deformation, the improvement in hardness is linear. The improvement in hardness got nearly saturated after 75% reduction in 145 °C and 175 °C warm rolled samples.

To realize the effect of warm rolling on mechanical properties more clearly, uniaxial tensile testing has been performed for all conditions at room temperature and the test results are shown in Figure 5.3. As illustrated by the Figure 5.3(a), the CR sample with 90% thickness reduction has shown large improvement in YS (50 MPa to 280 MPa, 460%) and UTS (183 MPa to 296 MPa, 62%) compared with ST condition. However, the ductility of the CR material has dropped from 30% (ST material) to 4.5% (CR 90% material). Figure 5.3(b)-(d) illustrates the effect of WR in combination with CR on mechanical properties of Al alloys. The YS (352 MPa) and UTS (340 MPa) of WR 67% sample at 100 °C are significantly more than those of CR 90% sample (UTS-296 MPa, YS-280 MPa). With increasing % of deformation at WR temperature (100 °C) from 67% to 75%, YS and UTS of the material increased to 364 MPa and 376 MPa, respectively. With 80% WR deformation at 100 °C, the YS and UTS of the material have further increased to 375 MPa, 386 MPa, respectively. As compared to T6 condition (YS-278 MPa, UTS-306 MPa), samples subjected to cryorolling followed by warm rolling at even 100 °C earm rolling with 67%, 75% and 80% reductions have shown superior strength values.

Warm rolling at 175 °C (75% deformation) leads to increase in YS and UTS up to 392 MPa and 412 MPa. At 80% deformation, the YS and UTS are 401 MPa and 415 MPa, respectively with 6 % elongation to failure. With warm rolling up to 80% at 145 °C, 175 °C, there is no improvement in strength observed as compared to 75% reduction sample. This could be due to balance between hardening effect by work hardening and precipitation hardening and softening effect by dynamic recovery. This suggests that beyond 80% deformation at 175 °C may cause to drop in strength due to accelerated dynamic recovery. The obtained strength values at 175 °C with 80% deformation are significantly higher than CR, T6 and the rest warm rolled samples (WR at 100 °C, WR 145 °C). The reported UTS value of dynamically aged 6061 alloy in [198] processed through ECAP (UTS- 380 MPa) which is lower than the strength obtained in the present study. The values of % elongation to failure obtained for the WR samples (WR samples at 100 °C, WR samples at 145 °C) compared to CR 90% sample were nearly same. Whereas in WR samples at 175 °C (80% deformation) % elongation to failure has increased to 6%. This can attributed to dynamic recovery effect.

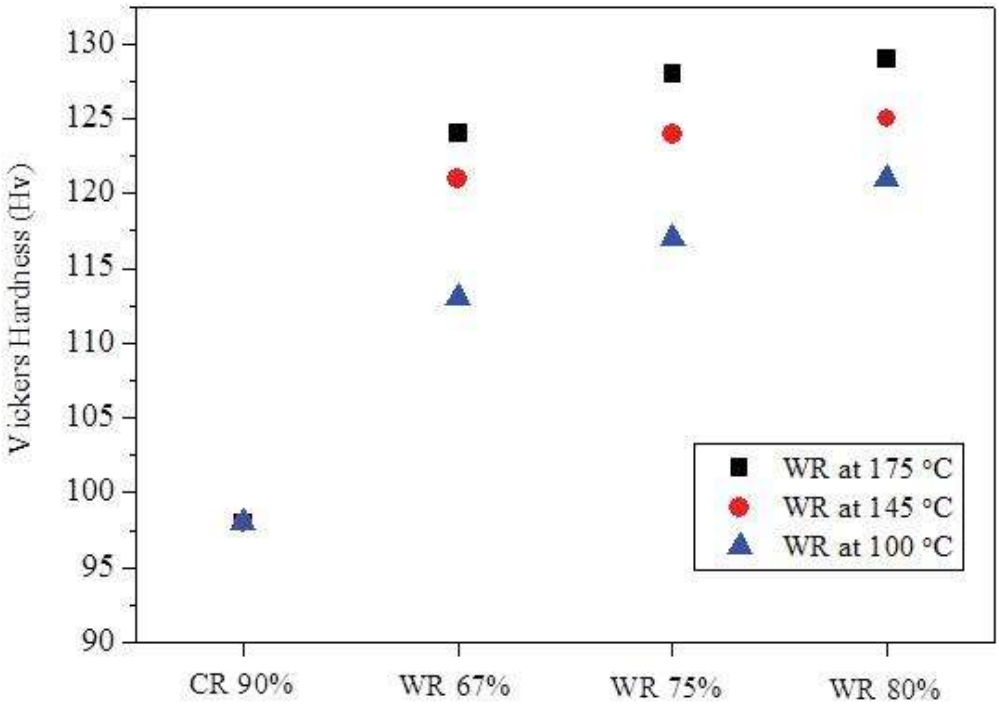

Figure 5.2: Variation in hardness with varying temperature and percentage of reduction of warm rolling after cryorolling.

(a)

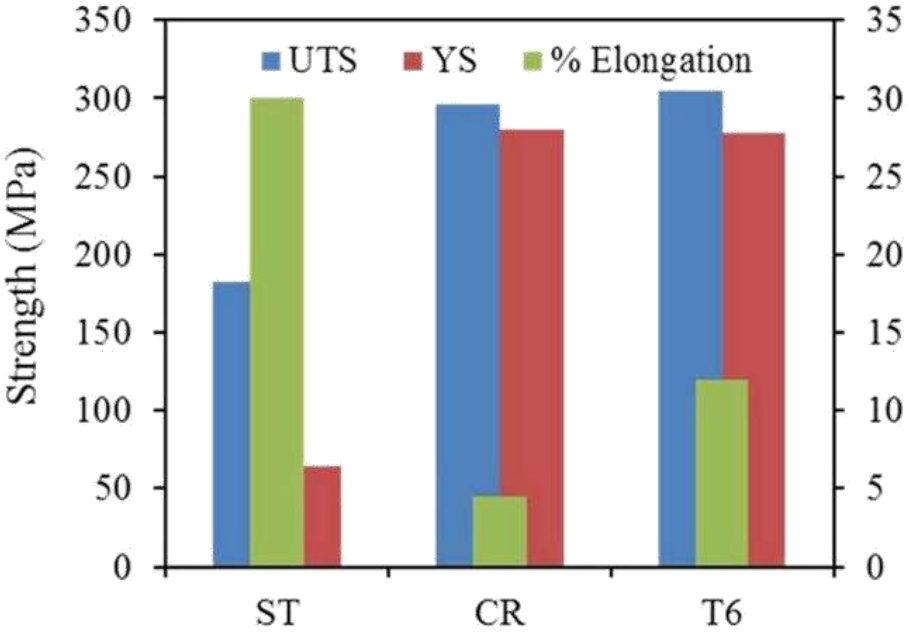
UTS
YS
% Elongation
Strength (MPa)
350
300
250
200
150
100
50
0
35
30
25
20
15
10
5
0
ST
CR
T6

(b)

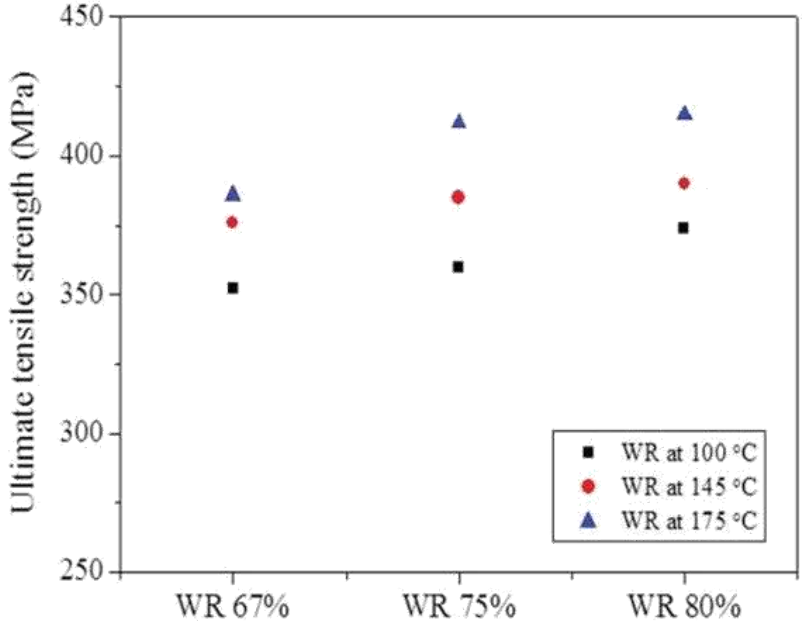
Ultimate tensile strength (MPa)
450
400
350
300
250
WR at 100 °C
WR at 145 °C
WR at 175 °C
WR 67%
WR 75%
WR 80%

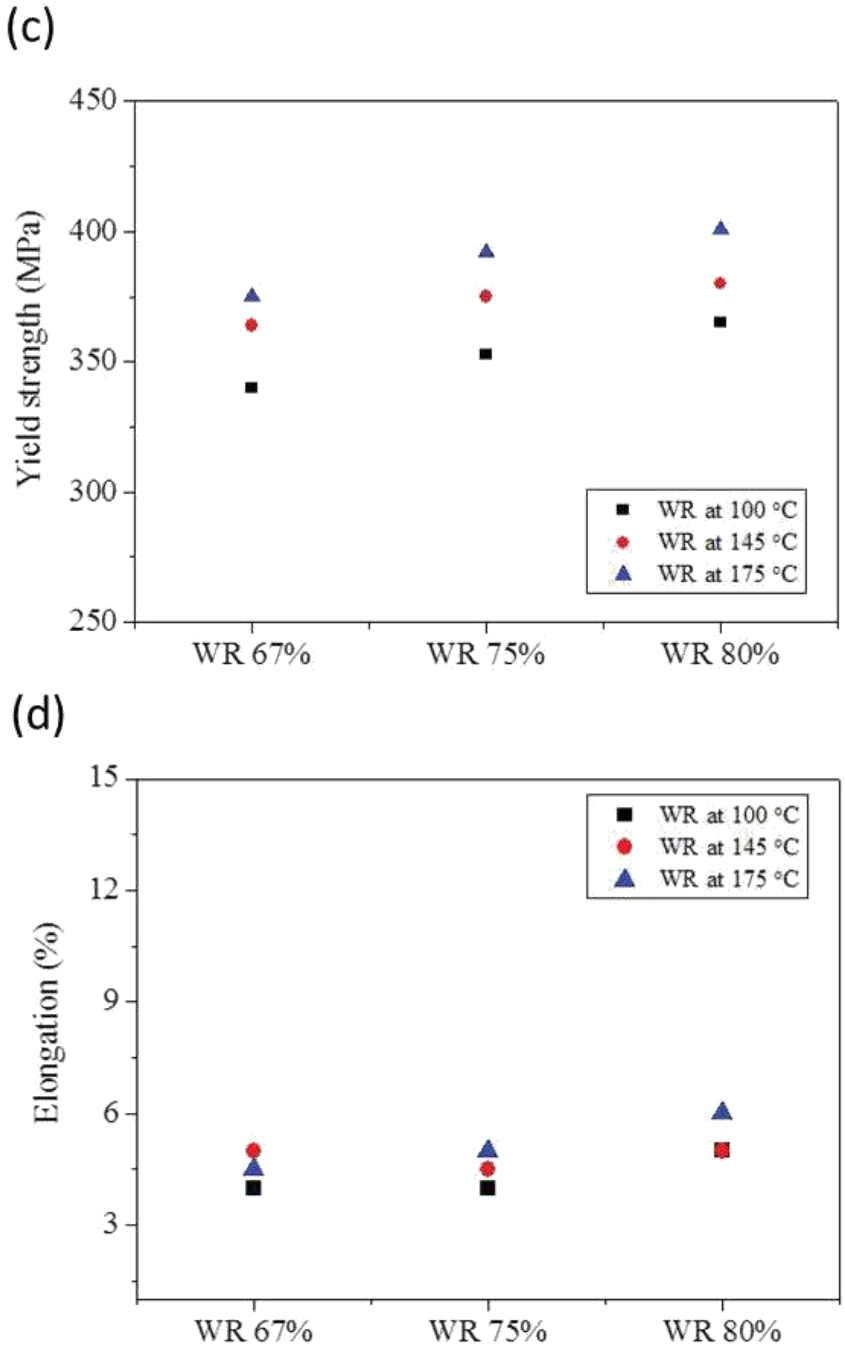

Figure 5.3: Mechanical properties of Al 6061 alloy after cryorolling and warm rolling; a) UTS,YS and % elongation of ST,T6 and CR material, b),c) and d) are variation in UTS,YS and percentage elongation of various warm rolled conditions, respectively.

5.3.1.2 DSC studies

ST and CR material

To investigate effect of CR and WR on the thermal behavior of Al 6061 alloy, DSC was performed with 10 °C/min scan rate under inert atmosphere. The starting temperature of the DSC scan was at room temperature. Figure 5.4 shows the typical DSC plots of ST, CR material. With heating rate of 10 °C/min, the peaks obtained for ST sample are identical with the precipitation sequence reported for Al 6061 alloy in the literature [169][199][200][201]. In the Figure 2.4, the DSC plot of ST sample shows five exothermic reaction peaks marked as 1 to 5 at temperatures around 80°C, 170°C, 242°C, 290°C, 350 °C, respectively and an endothermic peak at 190 °C is marked as 2'. The first two exothermic peaks at 80 °C and 170 °C were believed to be associated with the formation of clusters/co-clusters, and formation of G.P Zones of Mg/Si. The subsequent two major exothermic peaks 3 and 4 at temperatures 242 °C and 290 °C are corresponding to precipitation of β" phase and β' phase. The small hump observed at 350 °C (Peak 5) was in coincidence with the DSC data reported in the literature [202][203][11]. It is believed that the peak formed at high temperature (around 350 °C) (peak 5) corresponds to the precipitation of β-Mg_2Si or Si, which is not in agreement with the results reported in the literature [169][201]. An endothermic peak marked as 2' may correspond to the dissolution of GP Zones. After CR, the exothermic reaction peak which is ranging from 195 -260 °C, is believed to be the peak corresponding to β" has shifted to low temperature side as compared to that of ST sample.
However there is no change in the peaks corresponding to the G.P Zones and β phase precipitates of CR alloy.

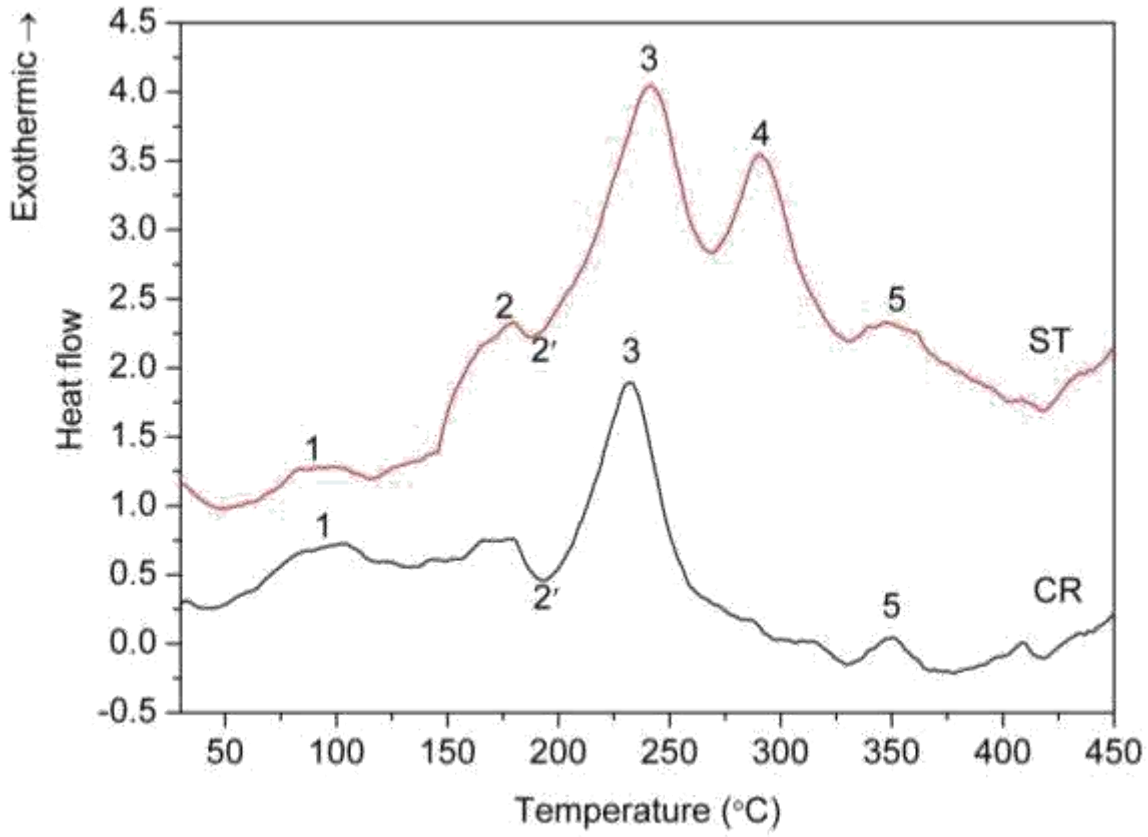

Figure 5.4: DSC heat flow curves of ST and CR Al 6061 alloy.

From the Figure 5.4 it is clear that, peak corresponding to β' formation (peak 4) is suppressed in the CR alloy. Instead a single peak with a little shift towards left is observed in CR sample due to the effect of deformation by cryorolling, which accelerates aging kinetics [11]. Appendino et al., Y. Birol, and Y.Song et.al.,[204][202][201] have also reported the similar behavior in the deformed monolithic and composites of Al 6061 alloy. It may be due to the simultaneous formation of β" and β' or formation and transformation of β" to β' without any sensible heat effect of transformation due to acceleration in ageing kinetics of precipitation by cryorolling.

(a)

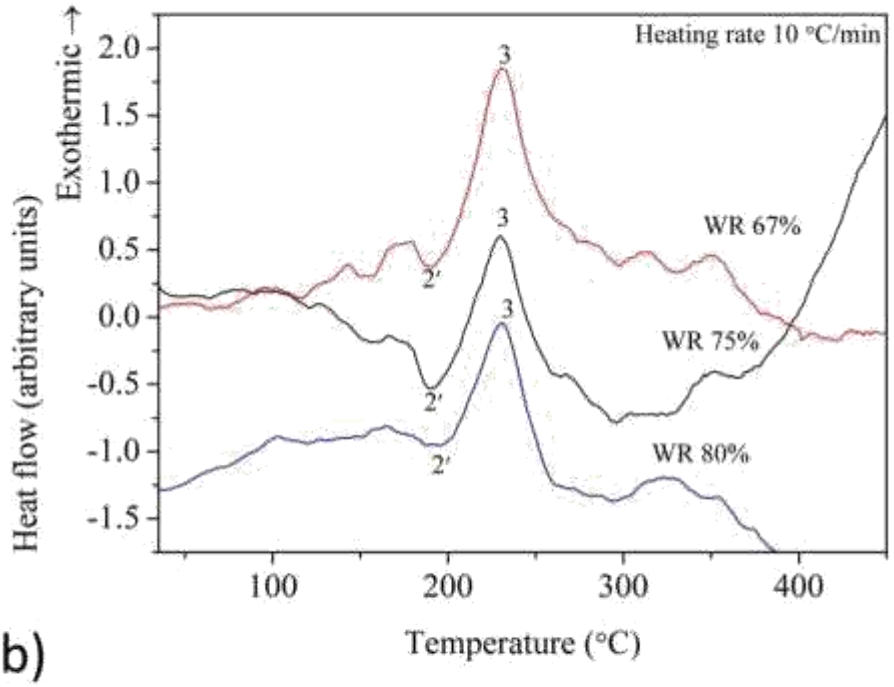
Heating rate 10 °C/min
Exothermic →
Heat flow (arbitrary units)
2.0
1.5
1.0
0.5
0.0
-0.5
-1.0
-1.5
100
200
300
400
Temperature (°C)
WR 67%
WR 75%
WR 80%
3
2'

(b)

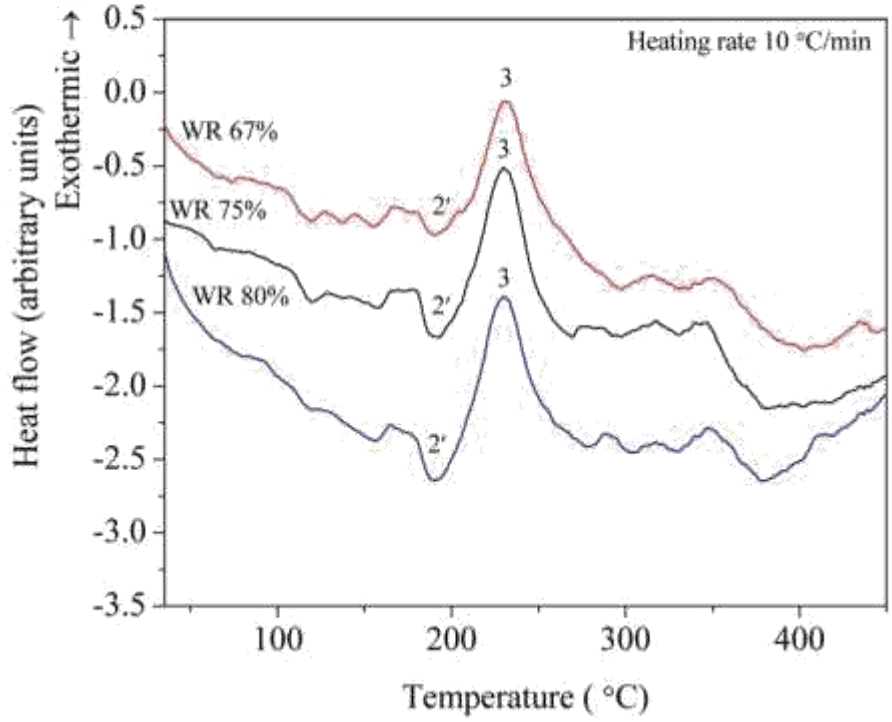
Heating rate 10 °C/min
Exothermic →
Heat flow (arbitrary units)
0.5
0.0
-0.5
-1.0
-1.5
-2.0
-2.5
-3.0
-3.5
100
200
300
400
Temperature (°C)
WR 67%
WR 75%
WR 80%
3
2'

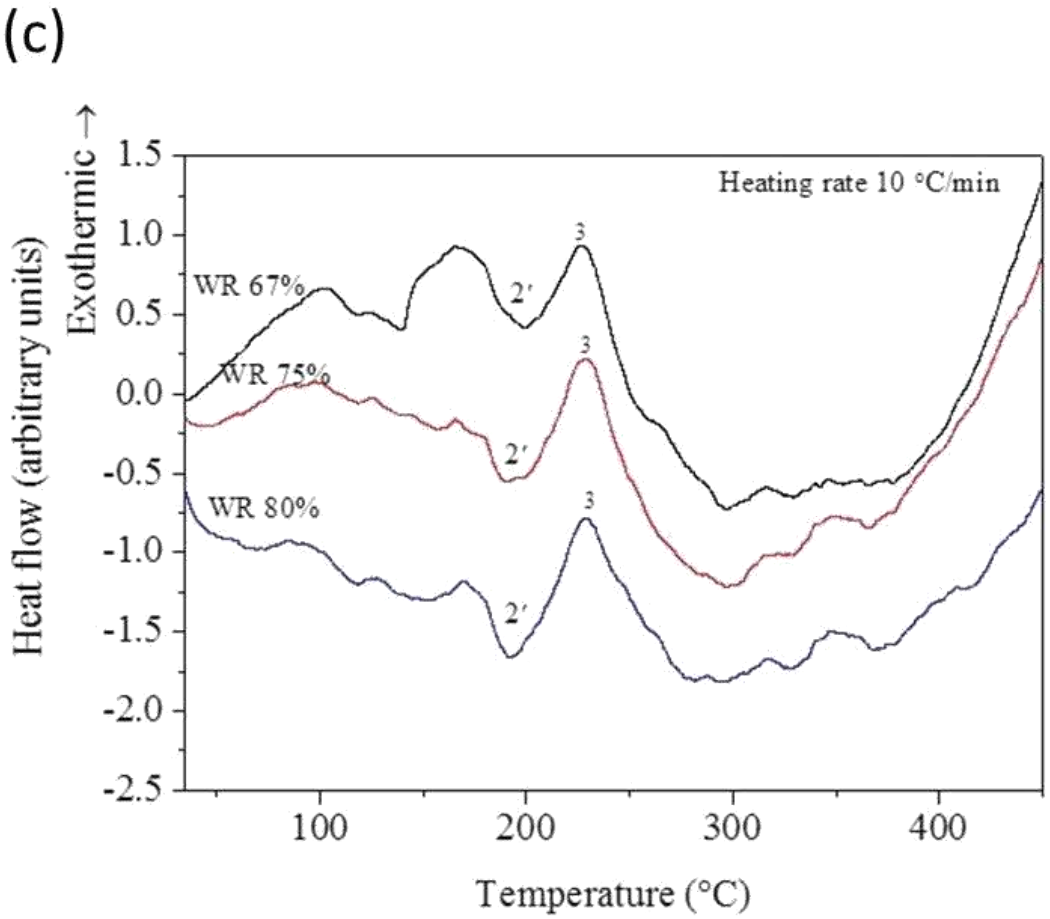

Figure 5.5: DSC heat flow curves of WR 66%, 75% and 80% at various temperatures; a) 100 °C, b) 145 °C, c) 175°C.

WR Material

DSC plots corresponding to various conditions of CR+WR samples are shown in Figure 5.5; the nature of the DSC plot of the samples with 67% warm rolling at 100 °C is appears to be similar to the CR sample with minor differences. The major exothermic peak (peak 3) position is similar to the peak of CR sample but with less peak intensity. Also, the peaks at low temperature corresponding to the formation of Mg/Si co-clusters and G.P Zones became flat compared to initial conditions. However, the peak position of β precipitates was identical in all three conditions (ST, CR, CR+WR). The reasons for flattening of low temperature peaks and decrease in intensity of peak 3 can be drawn from hardness plots of CR and CR+WR sample shown in

Figure5.3. With increasing temperature and % of deformation of warm rolling significant changes have occurred in the endothermic peak corresponding to cluster/GP zone dissolution and the subsequent exothermic peak corresponding to major strengthening phase (β"/β' precipitates) formation. The intensity of endothermic peak has increased, whereas the intensity of the β"/β' precipitates has reduced. The increase in hardness of CR+WR sample as compared to CR sample symbolizes that precipitation of G.P zones and β" might have occurred during warm rolling at high temperature (175 °C). The precipitation in CR+WR sample occurs because of enough driving force available for it through deformation strain and deformation temperature during warm rolling. The interesting behavior of CR+WR samples is that even at maximum temperature of warm rolling with maximum percentage of reduction (at 175 °C, 80% deformation) has shown the exothermic peak corresponding to β"/β' precipitates. However, the increment in hardness has become sluggish due to the dominant recovery effect.

5.3.1.3 Microstructure

a) EBSD

The electron back scattered diffraction (EBSD) micrographs of the ST material on RT-TD plane is shown in Figure 5.6.

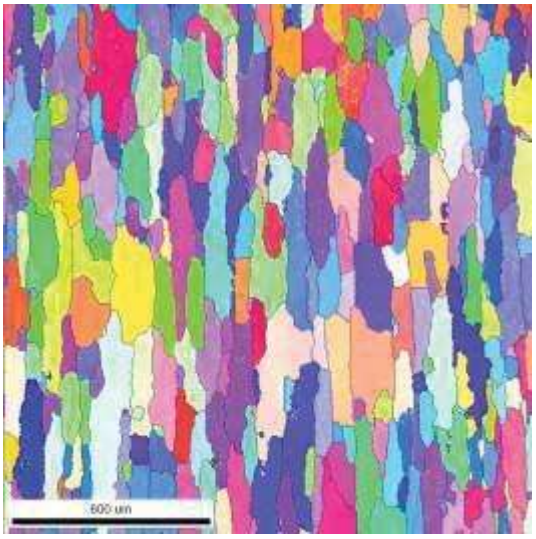

Figure 5.6: EBSD micrographs (inverse pole figure map) of ST material.

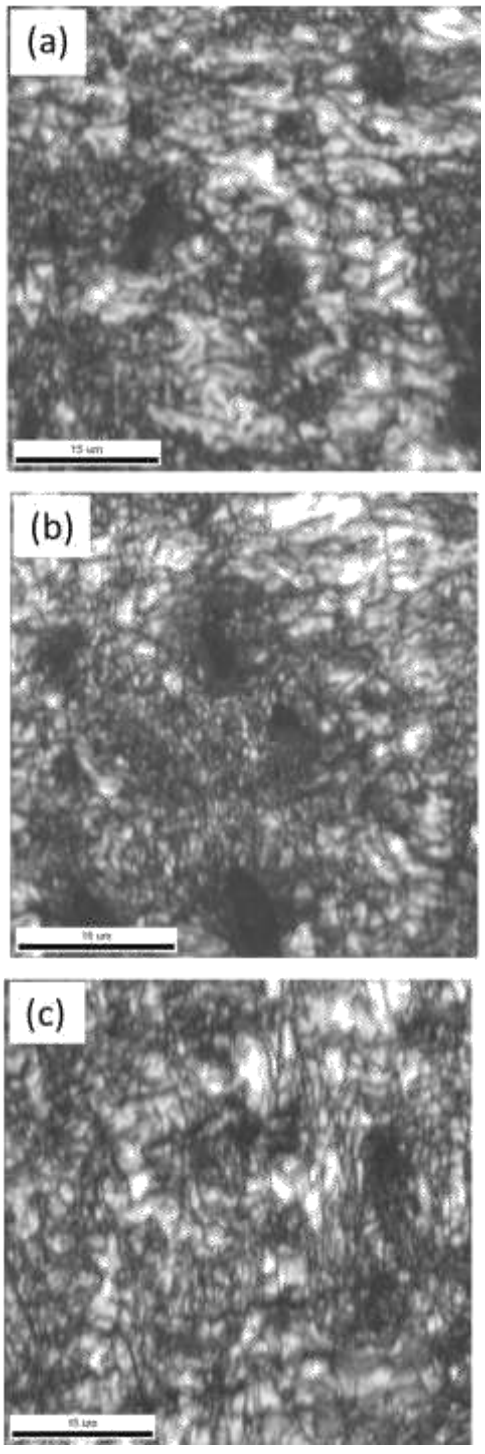

Figure 5.7: Image quality maps of cryorolled followed by warm rolled samples; a) 80% WR at 100 °C, b) 80% WR at 145 °C, c) 80% WR at 175 °C.

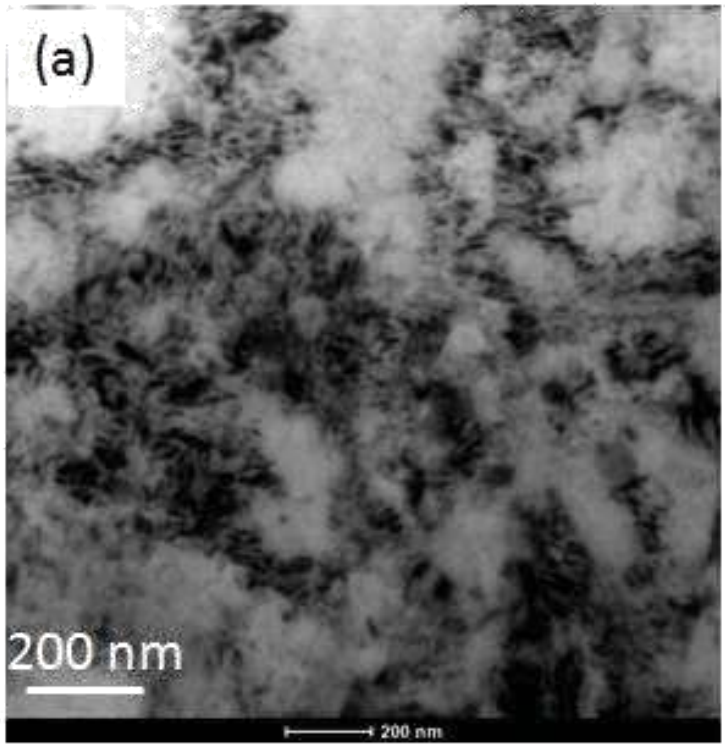
(a)
200 nm
200 nm

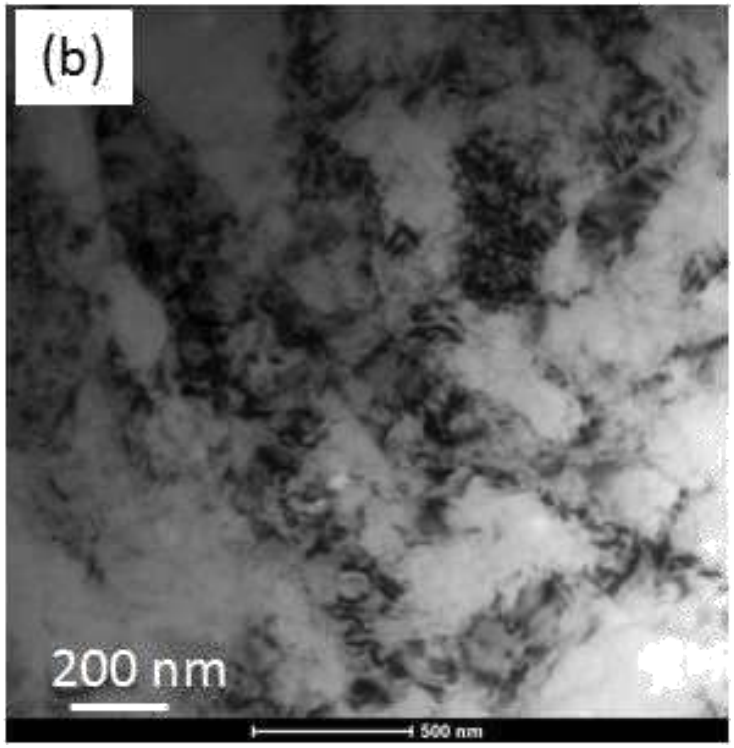
(b)
200 nm
500 nm

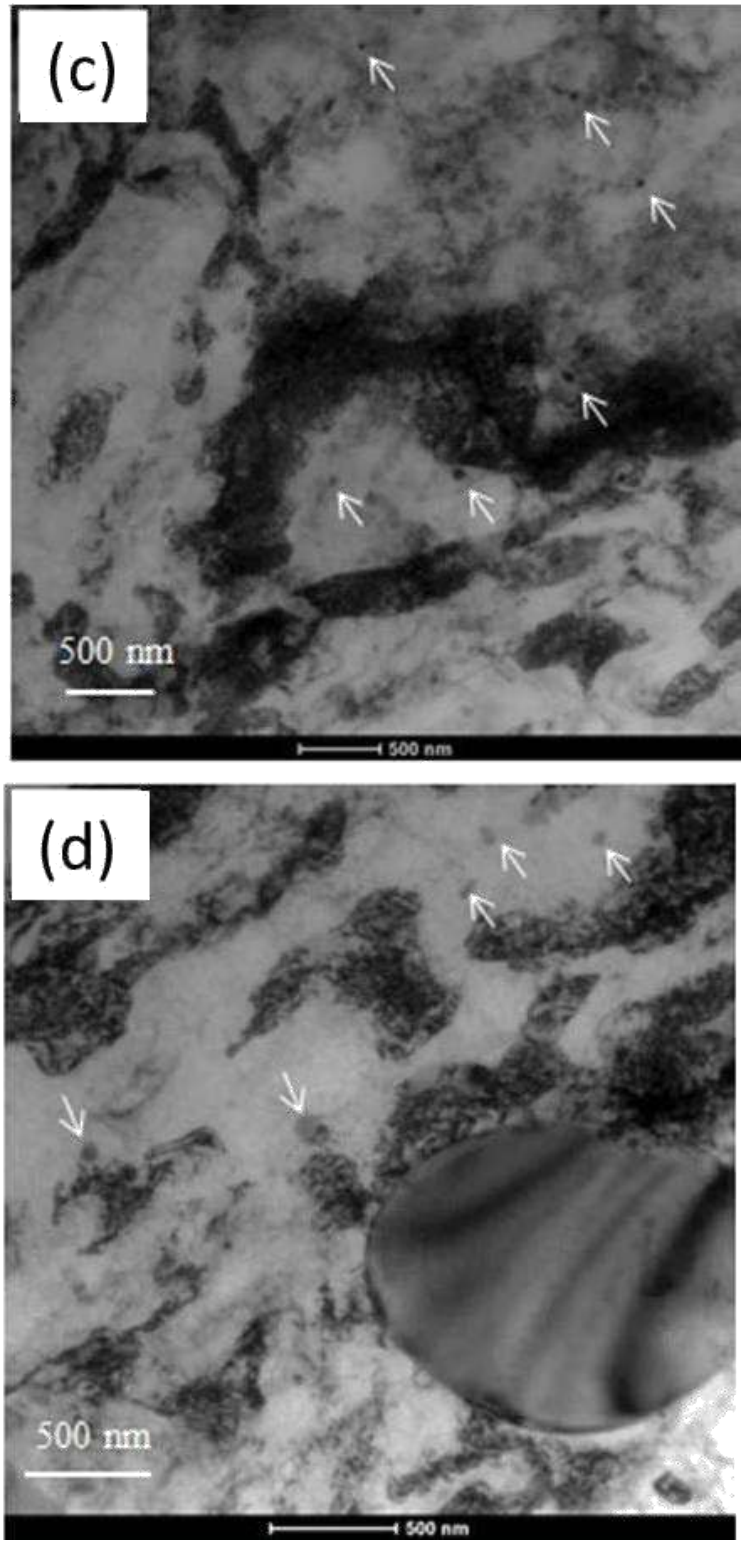

Figure 5.8 : TEM micrographs of Al 6061 alloy; c)WR 80% at 145 °C, d) WR 80% at 175 °C.

Since the as received material was in the rolled plate form, the microstructure possesses elongated grain structure along the rolling direction. In this study, the microstructural investigation of rolled samples was done on the RT- TD plane. In cryorolling followed by warm rolling conditions, EBSD is performed for the samples with maximum hardness in each warm rolling temperature. The respective image quality maps are shown in Figure 5.7. Upon closer inspection, it is reasonable to infer that with increasing warm rolling temperature, the area fraction of UFG structure has increased. Cryorolling followed by warm rolling promotes dynamic recovery, it facilitates to form UFG structure.

b) TEM

Further, a clear understanding of the effect of CR and WR on microstructure of Al alloy was examined through TEM along the plane parallel to rolling direction and their TEM micrographs are shown in Figure 5.8. The microstructure of the cryorolled sample (Figure 5.8 (a)) shows the presence of heavily deformed grains with high density of dislocations. Cell structures with unclear grain boundaries are seen from its micrograph. Whereas in case of CR+WR samples, with increasing warm rolling temperature, the fuzziness in the grain boundaries are decreased due to recovery effect. The subgrain boundaries are becoming clear. Also, the presence of fine precipitates are observed in all CR+WR samples as shown with arrow marks in Figure 5.8 (b)(c) and (d). The improvement in hardness with increasing warm rolling temperature is in accordance with the observed TEM results. The presence of precipitates observed in TEM micrographs of CR+WR samples supports the reduced intensities of the peaks corresponding to clusters/GP zones in the DSC plots.

5..3.2: Effect of ageing

As it was observed from the hardness results, among CR +WR conditions, material with 80% WR reduction at 175 °C has shown maximum hardness. DSC and TEM results suggest that, this material can be further age hardened. From the tensile test results, it is seen that even though this material has shown maximum UTS, the percentage elongation is very limited. With the objective to enhance the ductility, this material has been further artificially aged at low temperatures

(177°C, 145°C and 125 °C) and compared with pure CR material and bulk coarse grained material.

5.3.2.1 Mechanical properties

a) Hardness

Figure 5.9 (a) shows the variation in hardness of CR+WR material (80% WR at 175 °C) at various ageing temperatures, 125 °C, 145 °C and 177 °C. In coarse grained material, the recommended artificial ageing temperature and time are 177 °C for 8 hours. CR+WR material has shown improvement in hardness just after 1 hour ageing at 177 °C and it dropped immediately. On the other hand, for the samples subjected to ageing at 145 °C, the increasing trend of hardness has been observed up to 12 hours, beyond which it drops. By decreasing the artificial ageing temperature to 125 °C, the response in hardness has improved and the hardness values are quite stable for long hours of ageing time. It is believed that 125 °C is the suitable temperature for CR+WR material to obtained optimized properties. It can be seen from the hardness plot that maximum ageing response (Maximum hardness of 144 HV,) is observed at 125 °C after an ageing time of 45 hours. Ageing beyond 45 hours at the same temperature results in a slight decrease in hardness, but the drop in hardness is only 5 HV after 75 h. This drop in hardness 145 °C and 177 °C can be related to dominance of the recovery, structure coarsening, and depletion of solutes in the solid solution over precipitation hardening effect.

Figure 5.9 (b) shows the comparative study of hardness of ST, CR, CR+WR at an ageing temperature of 125 °C, which was found to be optimum for CR+WR samples. The improvement in strength after warm rolling can be attributed to formation of nanosized clusters/ β" precipitates through dynamic ageing. The DSC results indicate that, even after maximum reduction (80%) at 177 °C warm rolling, the material has the capability to undergo artificial ageing. By ageing treatment at 125 ^{o}C, the remnant solute atoms after warm rolling has led to the formation of fine nanosized precipitates. Hence, the strength of the material has increased further.In ST samples, the hardness increases from 54 HV to 98 HV for the ageing treatment of 72 hours. It is almost equal to the hardness of as received T651 Al 6061 alloy sample where its hardness was 101 HV. This increase in hardness in ST sample can be purely attributed to the formation of metastable precipitates from solid solution.

In case of CR sample after static ageing treatment at 125 °C for 53 hours of ageing time, the maximum value of hardness achieved was 117 HV. This shows an increment of 19% with respect to the hardness of cryorolled sample. The percentage rise in hardness after peak ageing treatment of CR sample was approximately two times than that of CR+WR sample where its percentage rise in hardness is 8% after peak ageing treatment at 125 °C for 45 h.

c) Tensile properties

Cryorolling followed by warm rolling (WR) has imparted superior mechanical properties to the alloy than cryorolling (CR) alone. In addition to dislocation strengthening and subgrain boundary strengthening effects by cryorolling, precipitation hardening comes from dynamic ageing during warm rolling. The CR strain in the material caused more nucleation sites for precipitation during subsequent WR, which in turn improves hardness and strength of the materials subjected to CR followed by WR.. During dynamic ageing, the nucleation of precipitates is dislocation assisted process. Warm rolling followed by low temperature ageing has resulted in simultaneous increase in strength and ductility. The ductility has improved by decrease in dislocation density through recovery process during artificial ageing treatment; it leads to create dislocation free rooms inside the grains, which enables to accumulate more dislocations. The increase in ductility can be attributed to the presence of high density of nano-sized precipitates in the grain interiors, owing to the fact that these nano-sized precipitates act as an effective sites for trapping and accumulation of dislocations while interacting or by-passing them. CR followed by low temperature ageing has led to less improvement in properties as compared toWR+PA.

Based on the hardness plots of various heat treated conditions of Al 6061 alloy, tensile testing was performed.

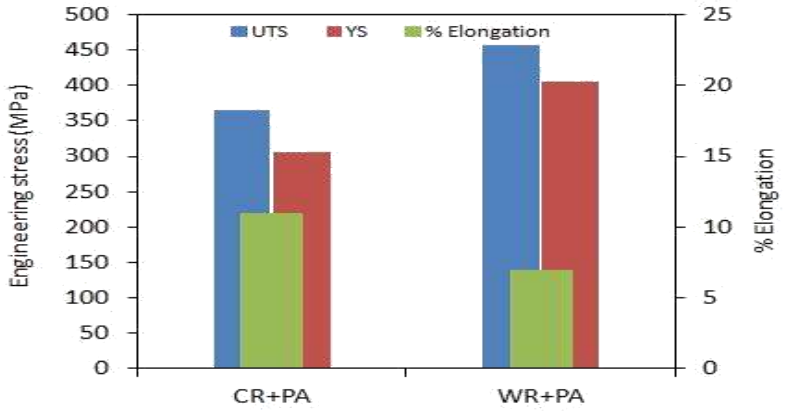

Figure 5.9: shows the tensile test results of CR + PA, and CR +WR + PA samples.

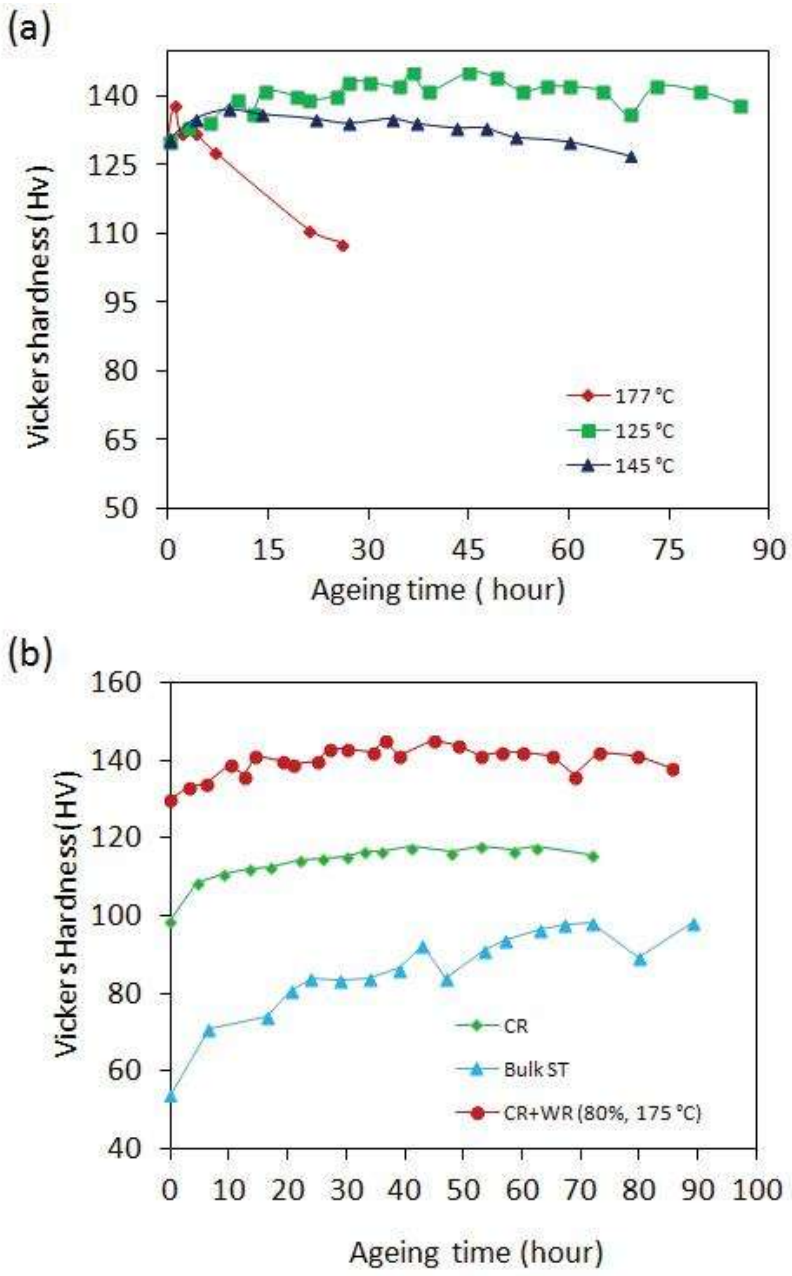

Figure 5.10: Vickers Hardness behavior of Al 6061 alloy; a) CR +WR sample after ageing at 125, 145 and 175 °C, b) ST, CR, CR +WR of Al 6061 alloy aged at 125 °C.

The UTS and YS, after artificial ageing, at 125 °C temperature for 53 and 45 h, of CR and CR + WR, respectively, have increased with no loss of ductility. CR +WR + PA sample shows a maximum strength of 445 MPa with 9% elongation at break. The ultimate tensile strength of T6 condition was 301 MPa with 12% elongation only. The ductility observed in CR + PA sample was 13%. This may be due to reduction in dislocation density in the material by recovery effect during ageing process is more in CR + PA sample than CR +WR + PA sample.

5.3.2.2 Microstructure

TEM

TEM micrographs of peak aged conditions of CR and CR+WR (80% at 175 °C) are shown in Figure 5.11. After peak ageing treatment, samples show well defined ultrafine grains with clear boundaries with mean size of 300 nm. In addition to this, there are some very fine crystallites with 100–150 nm size which are nucleated around to the second phase particle during ageing treatment. These dislocation free recrystallized grains contribute to increasing ductility during tensile testing. During ageing process, dislocation density has reduced in CR+PA and CR+WR+PA samples compared to CR and CR+WR samples due to annihilation of dislocations by recovery process. Figure 5.11(c) shows presence of high density of fine β" needle shaped precipitates observed in CR+WR+PA sample.

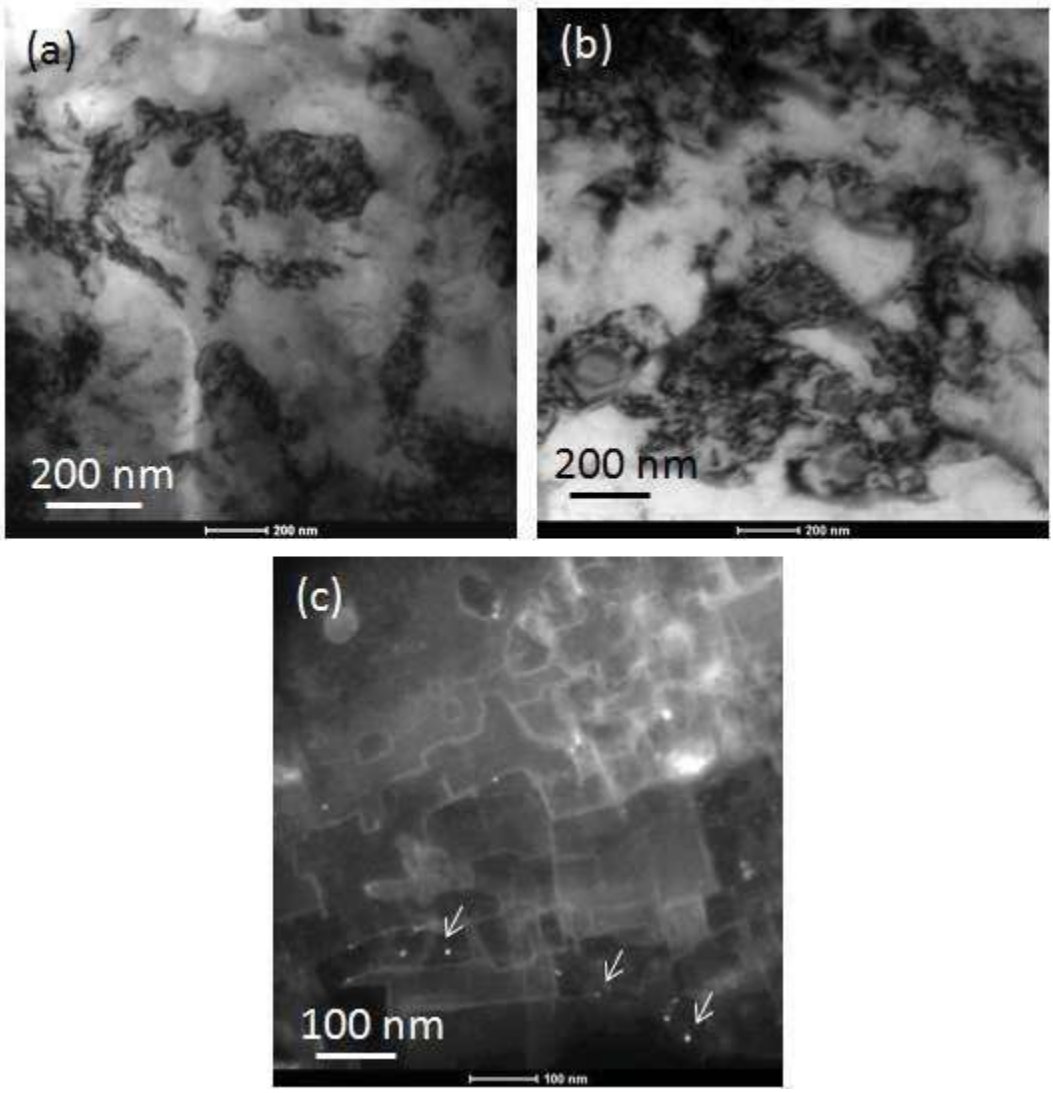

Figure 5.11 TEM micrographs of Al 6061 alloy (a) CR + PA, (b) CR +WR + PA, (c) Needle shaped precipitates of Mg2Si observed in CR +WR + PA

5.4 Discussions

Superior strength values (YS, UTS) has been observed in several metals and alloys by performing cryorolling as compared to room temperature rolling [109] [205] [206] [207] [208] [209] [168][210]. However as cryorolled materials possess poor percentage of elongations due to inability to accept adequate dislocations during tensile testing. Post cryorolling ageing turned out to be an effective method to enhance both strength and ductility in the alloy [207][211]. Plastic deformation at cryogenic temperature results enhanced dislocation densities in the material by suppression of annihilation of dislocations through dynamic recovery, which in result increased hardness and strength of the material [109]. In the present work the starting material is solid solution treated and water quenched. The increase in hardness and strength of the cryorolled material is mainly due to solid solution strengthening, sub grain boundary strengthening and dislocation strengthening. Cryorolling followed by warm rolling has resulted significant improvement in hardness and strength over CR material. In addition to dislocation strengthening and subgrain boundary strengthening effects by cryorolling, precipitation hardening is added by dynamic ageing during warm rolling. Due to CR strain in the material caused to more nucleation sites for precipitation by subsequent WR which in turn gives rise in hardness and strength in CR followed by WR material. It is reported that during dynamic ageing the nucleation of precipitates is dislocation assisted process [100].

With increasing WR strain at 100 °C the hardness and strength were also increased. During WR there are three possible phenomenon would occur simultaneously as follows; i) Softening effect by dynamic recovery due to cross slip and climb of dislocations, ii) work hardening effect due to plastic deformation, iii) precipitation hardening effect due to precipitation of second phase from the matrix. In the present case WR at 100 °C at all percentage of deformations (67%, 75%, 80%) hardening effect due to work hardening and precipitation strengthening dominates the softening effect due to dynamic recovery. It can be well understood the effect of warm rolling temperature on mechanical properties of the Al alloy by observing the data plotted for samples rolled at 145 °C and 175 °C in Figure 2.2 (b)-(d). There is an increase in YS and UTS up to 385 MPa and 375 MPa by warm rolling at 145 °C up to 75% deformation respectively. Further increase in deformation from 75% to 80% the improvement in strength is in scarce. The similar behaviour was observed in the material warm rolled at 175 °C. From the DSC result, it can be concluded that the improvement in mechanical properties of warm rolled

material is predominantly due to precipitation of nanoclusters/ G.P zones due to dynamic ageing effect during warm rolling and their active engagement in pinning and accumulation of dislocation during warm rolling. Upon ageing at low temperature has resulted improvement in hardness properties of warm rolled material.

The increase in hardness achieved for the samples during artificial ageing treatment at 125 °C might be due to the creation of non-shearable precipitates, which dominates over recovery, depletion of solutes from the solid solution, and the structure coarsening. The hardness behavior of precipitation hardenable alloys during ageing can be explained by the interaction of four competing factors such as; i) reduction in dislocation density by annihilation of dislocations by recovery process, ii) formation of non-shearable precipitates, iii) depletion of solutes in the solid solution, and iv) sub-structure coarsening as reported in the literature [212]. Warm rolling followed by low temperature ageing has resulted simultaneous increase in strength and ductility. The ductility has improved by decrease in dislocation density through recovery process during artificial ageing treatment; it leads to create dislocation free rooms inside the grains, which enables to accumulate more dislocations. The increase in ductility can be attributed to the presence of high density of nanosized precipitates in the grain interiors, owing to the fact that these nanosized precipitates act as an effective sites for trapping and accumulation of dislocations while interacting or by-passing them[79][213] [211].

5.5 Conclusions

In this section the effect of cryorolling (CR) followed warm rolling (WR) on microstructure and mechanical properties of Al 6061 alloy have been investigated. In addition the effect of artificial ageing on the strength and ductility of CR +WR samples has been investigated.

1) A significant enhancement in strength (415 MPa) and partial improvement in ductility (6%) was observed in CR +WR (80% at 175 °C) sample as compared to CR samples. After subsequent low temperature ageing treatments of CR +WR samples, the optimum ageing temperature to obtain maximum strength was found to be 125 °C.
2) The improvement in strength of CR +WR (80% at 175 °C) + PA sample as compared to starting condition solution treated condition (ST) was 128%.

3) From the EBSD and TEM investigation, it is evident that, the area fraction of UFG has increased with increasing warm rolling temperature. This may be due to increased dynamic recovery effect with increasing warm rolling temperature.
4) Dynamic ageing effect during warm rolling has resulted by the formation of nanosized precipitates (clusters) which is evident from the DSC thermograms. Remarkable improvement in hardness and strength of CR +WR sample is attributed to the combined effect of precipitation hardening, dislocation strengthening and partial solid solution strengthening. In CR + WR + PA sample, the improvement in strength and ductility can be attributed to ; i) the formation of β"/β' precipitates in the material after warm rolling followed by ageing at low temperature, ii) evolution of ultrafine grains with reduced dislocation density through recovery.

Chapter 6

Effect of pre-ageing on the ageing hardening response of cryorolled Al-Mg-Si alloy

The present chapter discuss about the effect of pre-ageing on hardening behavior of Al-Mg-Si alloys processed by cryorolling and its age hardening behavior. Two ageing conditions are examined. First, natural ageing for 2days, second pre-ageing at 100 ℃, 130℃ and 170 ℃ for 4 hours, 2 hours and 30 minutes respectively. The present investigation revealed that, the pre-ageing before cryorolling is useful to enhance the dislocation density during cryorolling. However artificial ageing of cryorolled samples is not influenced much with pre-ageing. It is observed that, maturing at room temperature of CR samples for 30 days has resulted better hardening response during artificial ageing.

6.1 Introduction

Al-Mg-Si alloys happen to be popular material for automobile body applications by virtue of its excellent combination of properties such as remarkable strength, high corrosion resistance and good formability [169] [214][215] . As it is evident from the reported literature, deformation at cryogenic temperature has led to increase in the dislocation densities in the material by suppression of dynamic recovery through cross slip. Consequently, the cryorolling process would require less strain to achieve UFG structure as compared with room temperature deformation process [205]. Unlike other SPD techniques, cryorolling has been used to enhance the strength and ductility both in precipitation hardenable alloys. Significant improvement in yield strength was reported the metal matrix composites, which were rolled at cryogenic temperature. Presence of second phase particles in the material would actively participate in hindering and accumulating the dislocations. Hence, increased dislocation density was observed. In the present work, pre-ageing technique is employed to induce nanosize precipitates in the aluminium matrix prior to cryorolling. The precipitation sequence, particularly at early stages in Al-Mg-Si alloy is found to be very complicated [169][199][216] [217]. In bulk alloys, "negative effect of natural ageing" is an important issue, which is being investigated by several authors [218][171][219]. Prolonged storage of solution treated Al-Mg-Si alloys at room temperature before artificial ageing is found to have adverse affect on hardening behavior. Formation of early stage precipitates at room temperature in the form of solute clusters led to less availability of solute atoms to form β" precipitates during artificial ageing. However this negative effect by clusters is found to be dependent of composition of Mg and Si and pre-ageing temperature. It is reported that materials with lower content of Mg and Si, natural ageing results positive effect on age hardening behavior during further artificial ageing [220]. Pre-ageing treatment immediately after solution treatment is found to be suitable strategy to suppress the formation of unwanted clusters. It is believed that clusters that form at pre-ageing temperature are more stable and acts as precursor for β" precipitates [180]. However, the effect of pre-ageing on the precipitation behavior of deformed Al alloys is scarcely reported in the literature. Hence, the present work is carried out to investigate the effect of natural ageing and pre-ageing on the precipitation evolution and hardening behavior of Al 6061 alloy.

6.2 Experimental details

Al 6061 alloy with sample size 10X30X40 mm^3 were machined from the as-received blocks and subjected to solid solution treatment at 530 °C for 3 hours. Prior to cryorolling the solutioninzed samples were subjected to pre-ageing treatment at room temperature and at above room temperature (100°C, 130°C and 170 °C) for 2days, 4 h, 2h and 30 min. Here after, samples aged at RT will be termed as natural aged samples (NA) and samples artificially aged at above room temperature prior to cryorolling will be termed as pre-aged samples (PA). The process flow diagram is shown in Figure 6.1. The detailed procedure of cryorolling is discussed in the Chapter 3. Cryorolled samples were subjected to artificial ageing at 125 °C with and without natural ageing. To study the effect of NA, PA and cryorolling on the precipitation behavior, Differential scanning calorimetry (DSC) measurements were done by using Perkin Elmer DSC 8000 under inert atmosphere. The measurement temperature range of the DSC scan was -5 °C to 450 °C. Vickers hardness testing and tensile testing was employed to characterize the mechanical properties of the alloy with various thermo mechanical treatments. Transmission electron microscopy (TEM) observations are made for optimized conditions.

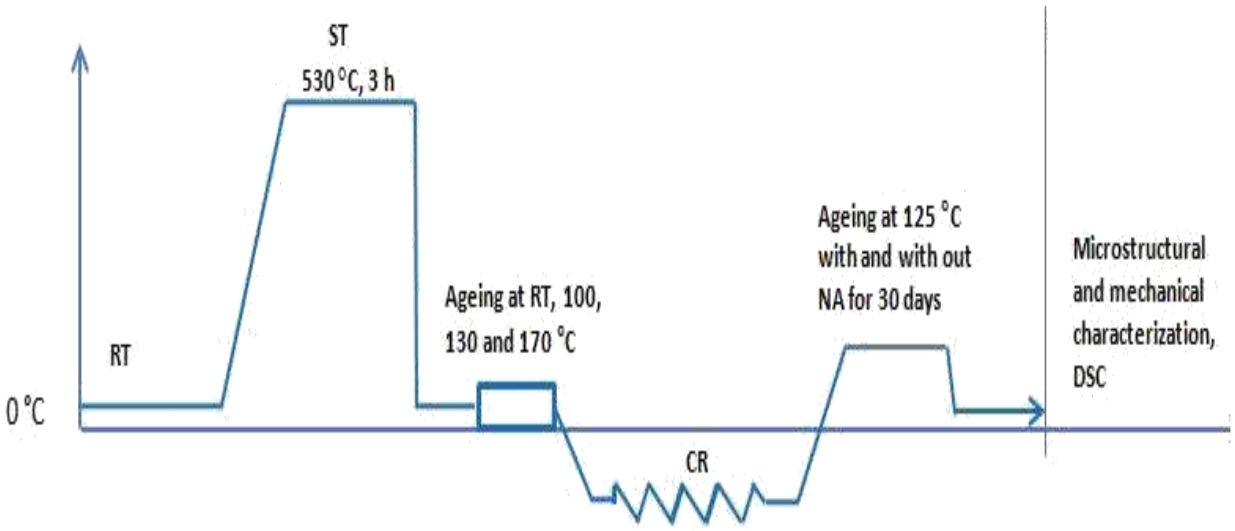

Figure 6.1: Heat treatment flow charts of various conditions investigated in the present chapter.

6.3 Results and discussion

6.3.1 Hardness

Figure 6.2 shows the variation in Vickers hardness of ST material after room temperature ageing for 2 days and pre-ageing at 100 °C, 130 °C and 170 °C for 4, 2 hours and 30 minutes respectively. Figure 6.2 also illustrates the effect of cryorolling on hardness behavior of various heat treated conditions as mentioned above. The hardness of the ST sample has increased from 42 HV to 66 HV after room ageing for 2 days, and rose up to 58, 60 and 61 HV after pre-ageing at 100 °C, 130 °C and 175 °C respectively. The error of each value is representing six individual hardness measurements. It is observed that, the error in NA and PA conditions are more as compared to the ST condition. The large error in NA and PA samples could be caused by the differences in the distribution and concentration of vacancy/solute complexes [220]. It is evident that natural ageing for 2 days has resulted maximum rise in hardness of the ST material. The intension of performing room temperature ageing and pre-ageing is to enhance the dislocation density of the material during cryorolling. To compare the benefit of NA ageing and pre-ageing before cryorolling, few samples have been cryorolled without any ageing treatment and this condition will be referred here onwards as "CR". From the Figure 6.2, it is evident that natural ageing and pre-ageing has significant effect on hardness behavior of cryorolled sample. The increase in hardness of CR material is attributed to solid solution strengthening and dislocation strengthening. Whereas in the materials subjected to natural ageing and pre-ageing before cryorolling, in addition to solid solution strengthening and dislocation strengthening, precipitation hardening will assist to enhance the hardness further. However natural ageing and pre-ageing will reduce the solid solution strengthening partially by reducing the solute content in the matrix.

The hardness curves of the samples with and without NA and PA, after artificial ageing at 125 °C is shown in Figure 6.3. From the above described heat treated conditions, it can be found that NA for 2 days + cryorolling+ NA for 30 days followed by artificial ageing at 125 °C for 48 hours has higher hardness as compared to the rest of the conditions. As discussed in the chapter introduction, unscheduled and unreasonable delays happen between solution treatment and further artificial ageing in commercial processing. In order to investigate the effect of natural

ageing on the cryorolled and pre-aged + cryorolled samples, samples were kept at room temperature for 30 days and then subjected to artificial ageing at 125 °C. Although there is slight increase in the initial hardness values of PA samples, there are no significant changes observed in the peak hardness values even after NA for 30 days. The behavior is similar to the samples without NA. Al-Mg-Si alloys with negative effect of natural ageing are treated with pre-ageing to improve the hardening behavior. It is believed that, precipitates that form at elevated temperature (above room temperature) are more stable at room temperature and will act as precursor for post precipitates during further artificial ageing [221]. In the PA samples, precipitates that formed after pre-ageing have contributed for increase in the dislocation densities by acting as dislocation pinning agents. However during NA of PA samples after CR, the precipitates remain stable. The slight rise in initial hardness of PA+CR samples after NA can be attributed to the precipitation of remnant super saturated solute atoms.

In CR material with NA the hardness has increased from 98 Hv to 111 Hv, subsequent artificial ageing has resulted rise in hardness up to 122 Hv. The NA has positive effect on the age hardening behavior of CR samples during artificial ageing. The peak hardness in the CR material is contributed by several factors, such as: dislocation strengthening, precipitation hardening, grain boundary strengthening and solid solution strengthening (partially). CR material is in supersaturated solid solution state. After CR, leaving material at room temperature for a long time results precipitation of solute atoms in the form of clusters/ G.P zones. CR material in the supersaturated solid solution state subjecting to artificial ageing results hardening through precipitation as well softening through annihilation of dislocation by recovery simultaneously. In order to retard the rate of recovery, usually CR samples were subjected to artificial ageing at lower temperatures than the usual temperatures (between 160 to 180 °C) applied for standard undeformed alloys. By keeping CR material at room temperature results precipitation hardening by formation of clusters without much affecting the dislocation densities present in the material. It is possible that these clusters might actively retard the annihilation of dislocations during further artificial ageing, consequently better hardening behavior in the CR+NA samples than CR samples. The similar behavior has been reported in the Chapter 4.

Room temperature ageing for extended hours of NA- 2 days samples after cryorolling has resulted into remarkable improvement in the hardening behavior of the alloy during artificial ageing.

The peak hardness (140 Hv) is achieved after ageing for 50 h. The similar behavior has been reported by Chang et al.,[220] in Al-Mg-Si alloy in undeformed state. In the present investigation NA for long time has influenced the mechanical properties of the alloy significantly. The significant hardening response of the alloy during artificial ageing after prolonged NA might be due to the presence of high density needle shaped precipitates along with small clusters [220].

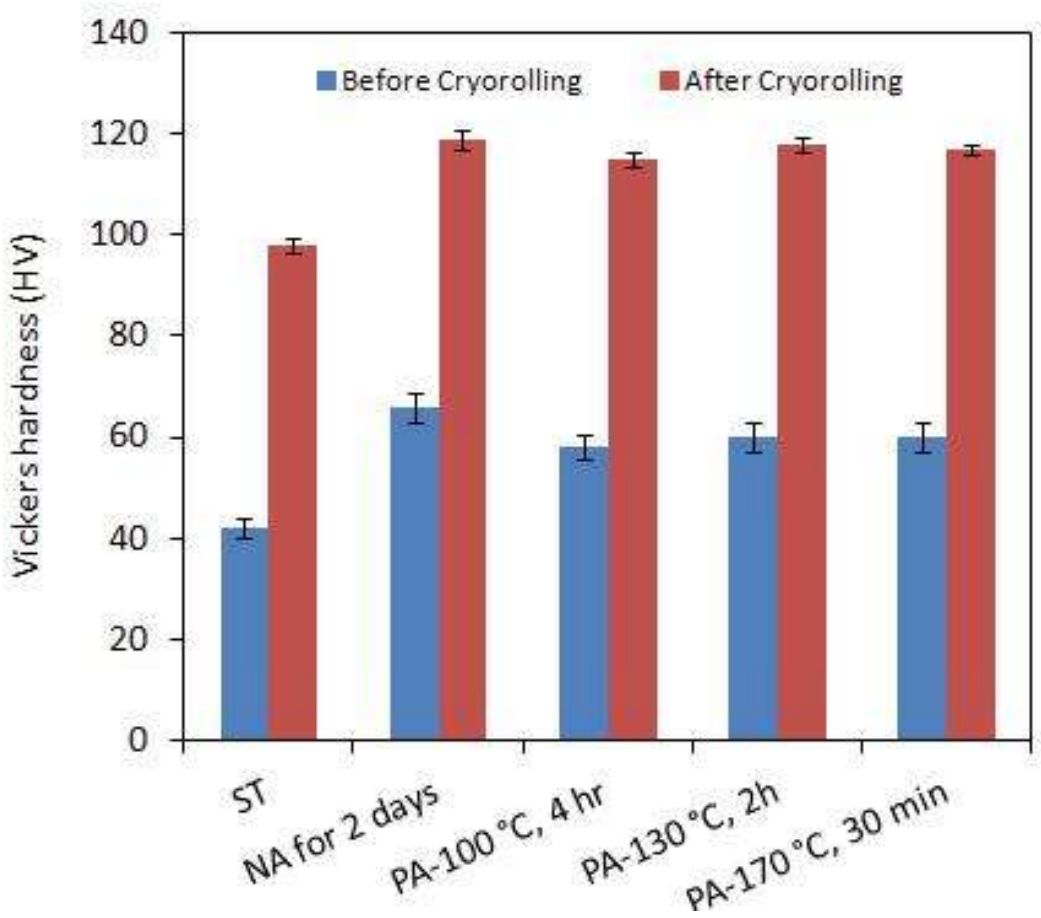

Figure 6.2: Variation in Vickers hardness of the samples after room temperature ageing and pre-ageing treatment followed by cryorolling.

(a)

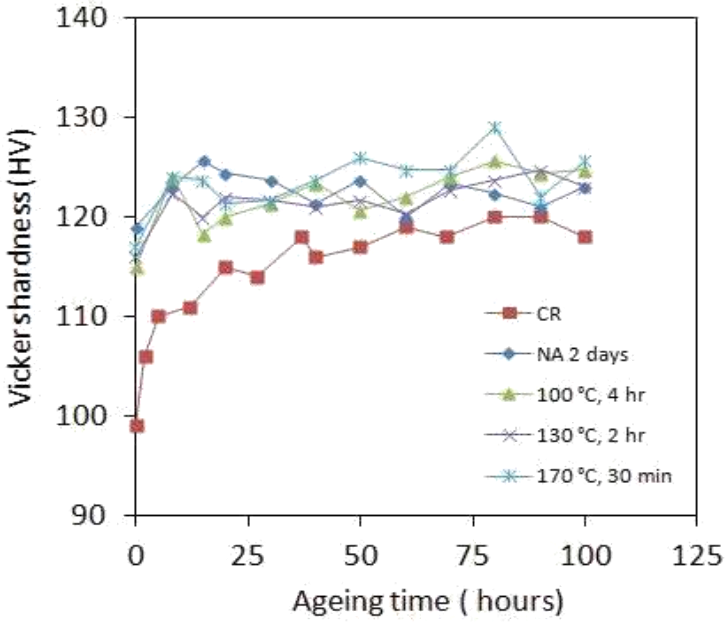

(b)

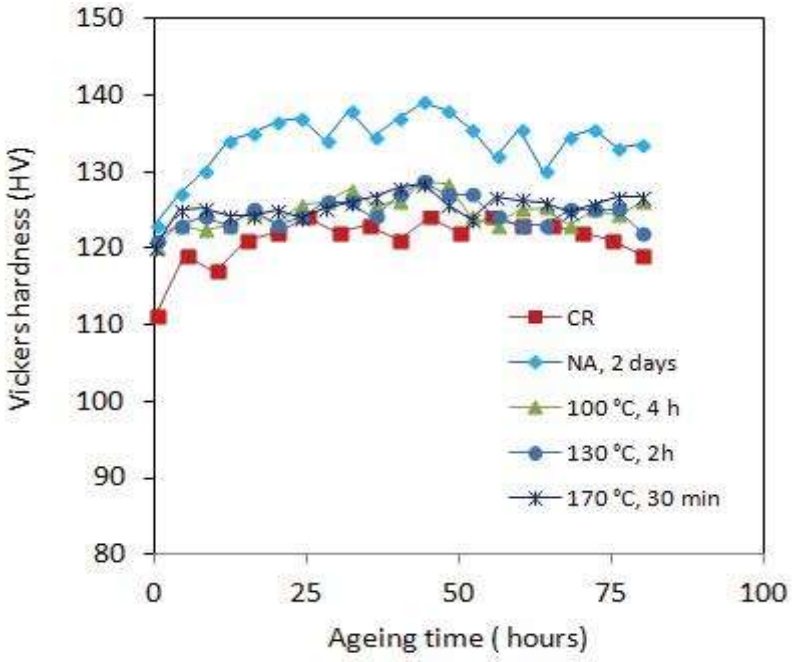

Figure 6.3: Artificial ageing (at 125 °C) behavior of cryorolled Al 6061 alloy with various heat treatments (ST, NA for 2 days, PA-100 °C for 4 h, PA-130 °C for 2 h, PA-170 °C for 30 min); (a) without natural ageing (NA-two months), (b) with natural ageing (NA- two months)

6.3.2 Differential Scanning Calorimetry (DSC):

DSC study supplements to the Vickers hardness data of various heat treated conditions. Figure 6.4 shows the DSC plots of ST and various pre-aged and natural ageing conditions. ST condition possesses four exothermic conditions corresponding to Cluster/ G.P zones, β", β' and β precipitates as discussed in the initial chapters. The position of precipitation reactions are in agreement with the reported literature [222]. ST material after NA for 2 days has resulted remarkable changes in the sequence of the precipitation. No exothermic peak, corresponding to formation of clusters/GP zones has appeared. Instead a pronounced endothermic peak is observed in the range of 180 ℃ to 240 ℃ which might be corresponding to dissolution of clusters/GP zones that were formed at room temperature. This indicates that the clusters that form at room temperature are not stable and dissolve during DSC. The rise in hardness after NA for 2 days is contributed to the formation solute clusters. Heating and sudden quenching of the alloy results creation of several vacancies at supersaturated state. The diffusion coefficient of the solute atoms is sufficient enough to drive the solute atoms to form clusters during natural ageing which in result increase in hardness[223][224][225]. The intensity of the exothermic peak corresponding to β" precipitates has increased and the intensity of the peak corresponding to β' has decreased [226]. Also the β' peak has shifted to high temperature side. However the β' peak position remains unchanged. After PA at 100, 130 and 170 °C no cluster peak exists before DSC. Low temperature (< 150 °C) peaks became flat which has reflected in the hardness evolution of PA samples. As well, there is no endothermic peak corresponding to cluster dissolution. This indicates PA result in formation of solute clusters which are stable and able to act as precursors for the β" precipitates. However the peak intensities of β" precipitates of all PA has reduced. The area under the reaction peak represents the volume fraction of the precipitate phase. This shows NA sample possess more volumes fraction of β" precipitates than that in the samples subjected to PA. Based on the intensity of β" peak and presence/absence of endothermic peak of clusters in the NA and pre-aged conditions, it can be concluded that, clusters that are formed in the NA samples are getting dissolved in the matrix and allowed to form higher volume fraction β" precipitates by providing more solute concentration. Whereas in the pre-aged samples, the clusters that are formed during PA are relatively stable and are acting as precursors for β" precipitates. The common opinion observed in the literature is that, the NA will have negative effect on the hardening behavior during artificial ageing of Al-Mg-Si alloys [221]. The reason was

given that the clusters of Mg and Si that forms at room temperature are highly stable at high temperature and neither they will act as precursor for β" precipitates nor get dissolved in the matrix. Consequently low volume fraction of maximum strengthening phase precipitates by depletion of solute concentration in the matrix. In contrast Chang et al., [220] have reported positive effect of natural pre-ageing on the mechanical properties of Al-Mg-Si alloys. It is reasoned that, the NA causes to produce a high density of clusters of Mg and Si, which controls the precipitation kinetics during further artificial ageing. These clusters either dissolve slowly or might act as precursors for the subsequent precipitation. Which in result formation of fine needle shaped precipitates in NA samples than in the samples artificially aged immediately after quenching[220]. In the present investigation, the nature of the DSC thermograms of NA and PA samples supports the argument that NA will have positive effect on mechanical properties of the alloy during further artificial ageing.

DSC thermograms of material subjected to Cryorolling after NA and PA are shown in Fig.6.6. Cryorolling has resulted clear separation of cluster peaks as C1 and C2 instead single peak observed in ST material. It has been reported that, pre-straining has resulted reduction in intensity of cluster peaks as compared to its ST condition [226] . It has been reasoned that, by introduction of dislocations through straining, the concentration of vacancies might have got lowered through annihilation [226]. However in the present study, the intensity of cluster peaks observed in the ST material after cryorolling is more than that in the material before cryorolling. The reasons are yet to be investigated. The onset temperature and peak temperature of the β" peak has shifted towards low temperature side in ST material after cryorolling. A single major exothermic peak was observed in the ST material after cryorolling. β' precipitate phase peak has been suppressed. This behavior is common in NA and PA samples after cryorolling. Nageswara rao et al.,[179] have investigated the effect of cryorolling on the precipitation sequence of Al-Mg-Si alloy through TEM and DSC studies. It has been reported that, high dislocation densities and large volume fraction of subgrain boundaries developed by cryorolling has accelerated the formation of β' along with β" phase [179]. The initial low temperature cluster peaks remain flat.
The intensity of β"/β" precipitates peak in NA 2 days samples is higher than the rest of PA samples. The onset and peak temperatures of cryorolled PA samples shifted towards low temperature side than the cryorolled NA sample.

Activation energy:

To estimate the reaction kinetics of precipitate formation and its dissolution, activation energy of various phase formation is calculated trough Kissinger's method. In fact several methods were used to calculate the activation energy in the literature [227] [228] . In the natural aged and pre-aged samples, more attention is paid for β" and β' peaks whereas in the cryorolled conditions of natural aged and pre-aged samples, more attention is given for single exothermic peak which was observed in the range of 180 to 260 °C (β"/β' peak). For this, series of measurements were carried out at various heating rates such as 10, 15, 20 and 25 °C/min in the range of 10 to 450 °C. Kissinger's method is based on the hypothesis that, with increasing temperature, the reaction passes by a maximum before decreasing [229][230]. With increasing heating rates reaction peaks are found to be shifted towards high temperature side. The activation energies are deduced from the slops of the linear relationship of the data plotted between ln (B^2/T) and ($1000/T_p$) where "T_p" is peak temperature for a given heating rate. "B" is the heating rate. The activation energies of various phases obtained from the plots (Figure 6.5, 6.6 and 6.7) are listed in the Table 6.1, 6.2 and 6.3.

Table 6.1: Peak temperatures and activation energies associated with β" precipitates in various heat treated conditions.

Heating rate (°C/min)	ST	NA 2 days	PA		
			100 °C, 4h	130 °C, 2 h	!70 °C, 30 min
10	237.5	228.6	237.7	236	231
15	243	234.3	247.5	244	238
20	249	240.3	258.37	253	248
25	254	240.6	258.64	257	256.6
Activation energy (kJ mol−1)	114	137	78.4	85	68

Table 6.2: Peak temperatures and activation energies associated with β' precipitates in various heat treated conditions.

Heating rate (°C/min)	ST	NA 2 days	PA		
			100 °C, 4h	130 °C, 2 h	!70 °C, 30 min
10	289.5	288	288.7	285	287.1
15	298	294	296.55	293.1	290
20	304	305	306.93	298.94	295
25	308	307	308.04	305	306.4
Activation energy (kJ mol−1)	124	106	105	114	105

Table 6.3: Peak temperatures and activation energies associated with β"/β' precipitates in various heat treated conditions after cryorolling.

Heating rate (°C/min)	ST	NA 2 days	PA		
			100 °C, 4h	130 °C, 2 h	170 °C, 30 min
10	228.2	228.6	227.9	227.9	228.5
15	234	234.3	234.8	235.11	234.3
20	238	240.3	237.7	236.44	238.4
25	242	240.6	241.1	241.08	240.9
Activation energy (kJ mol^{-1})	136	137	141	144	147.7

From the Table 6.1 it can be mentioned that the measured activation energy of β" in ST material is decreasing by increasing pre-ageing temperature whereas in NA material, it is increasing. For β' phase precipitates (Table 6.2), with NA and PA the activation energy values are decreasing. From the table 6.1 and 6.2 it can conclude that, the pre-ageing treatment has significant effect on formation of β" precipitates. Whereas in the case of β' formation it has little significance. After deformation through cryorolling of NA and PA material, the activation energy values have increased as compared undeformed material. As well as, there is no remarkable difference in the energy values of deformed samples.

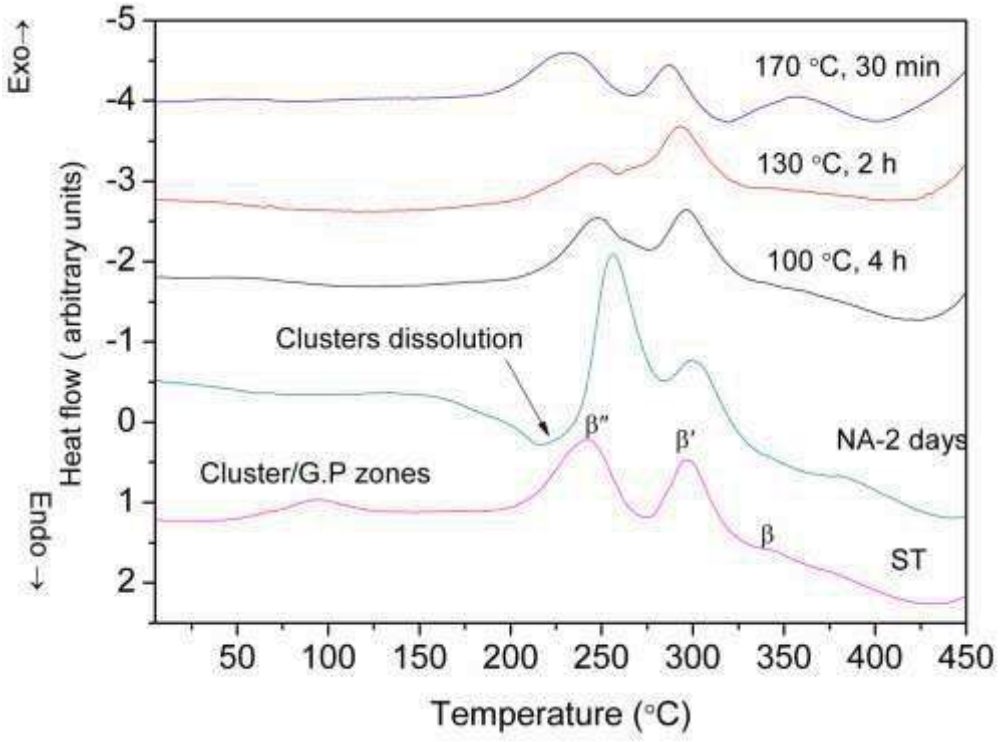

Figure 6.4: DSC thermograms of Al 6061 alloy with various heat treatments; ST, NA for 2 days, PA-100 °C for 4 h, PA-130 °C for 2 h, PA-170 °C for 30 min.

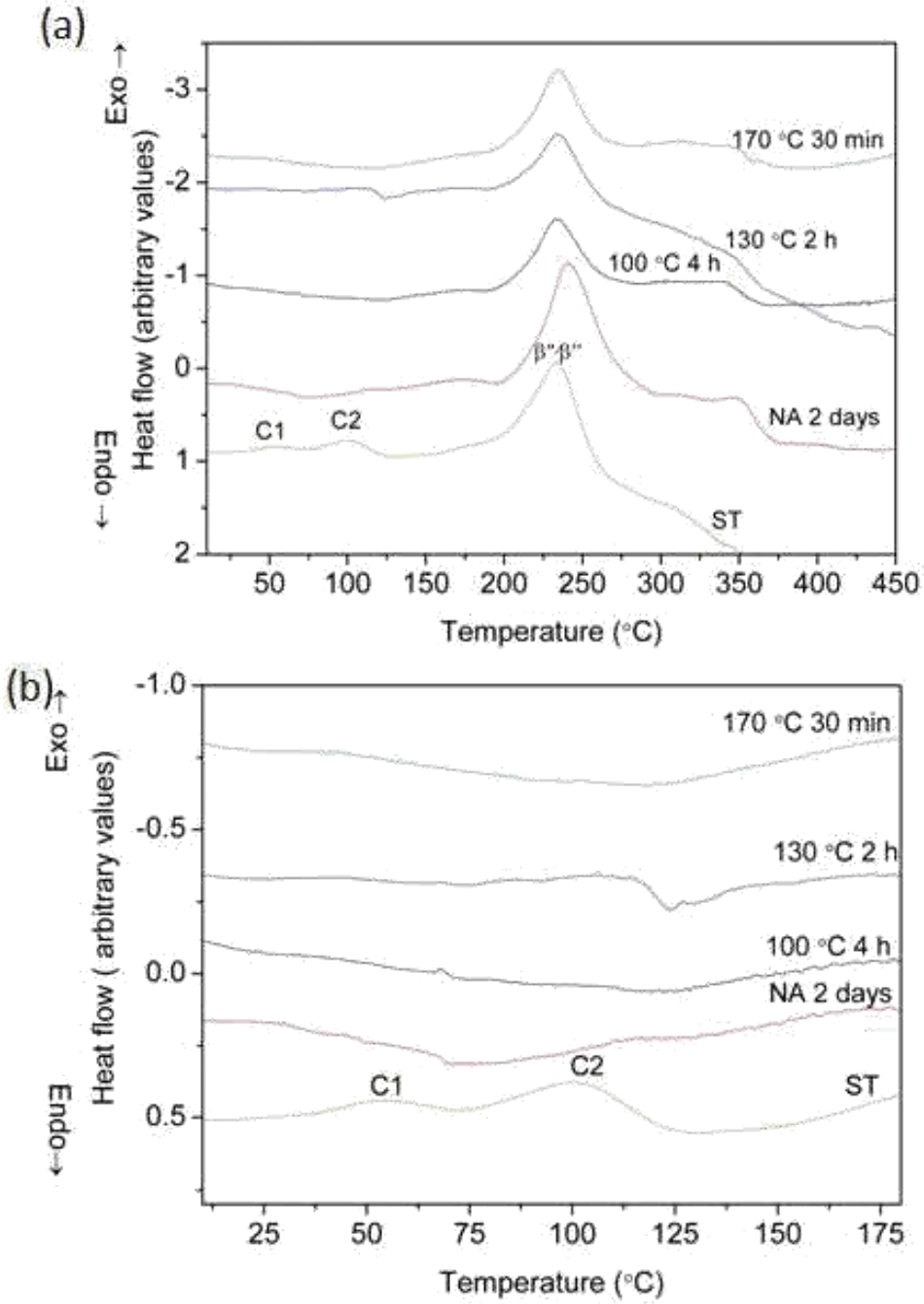

Figure 6.5: DSC thermograms of Al 6061 alloy with various heat treatments (ST, NA for 2 days, PA-100 ℃ for 4 h, PA-130 ℃ for 2 h, PA-170 ℃ for 30 min) after cryorolling; (a) representation of all peaks, (b) magnified view of low temperature peaks .

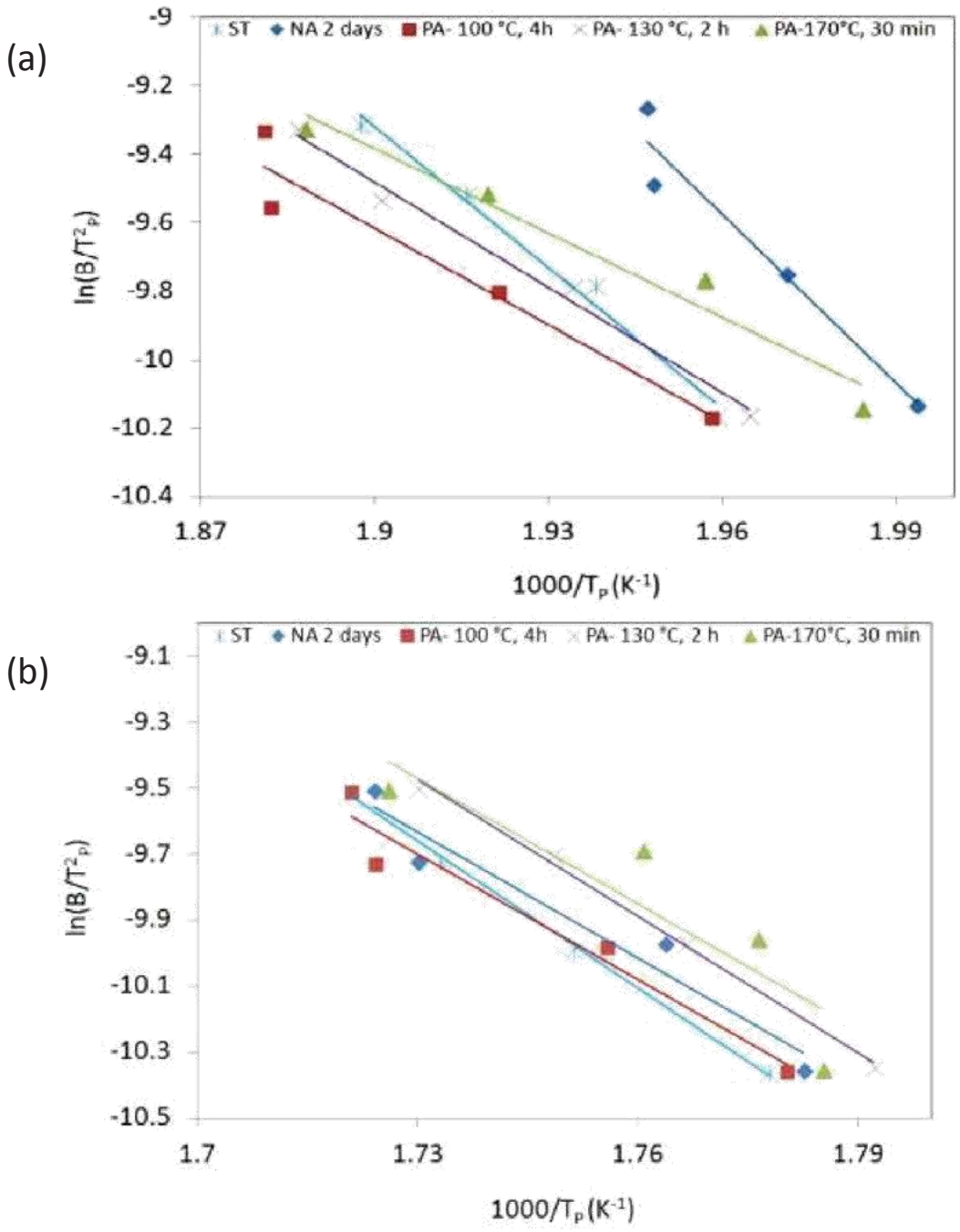

Figure 6.6: Kissinger plots for the various exothermic peaks in Al 6061 alloy processed through various heat treatments (ST, NA for 2 days, PA-100 °C for 4 h, PA-130 °C for 2 h, PA-170 °C for 30 min); (a) β" precipitates, (b) β' precipitates

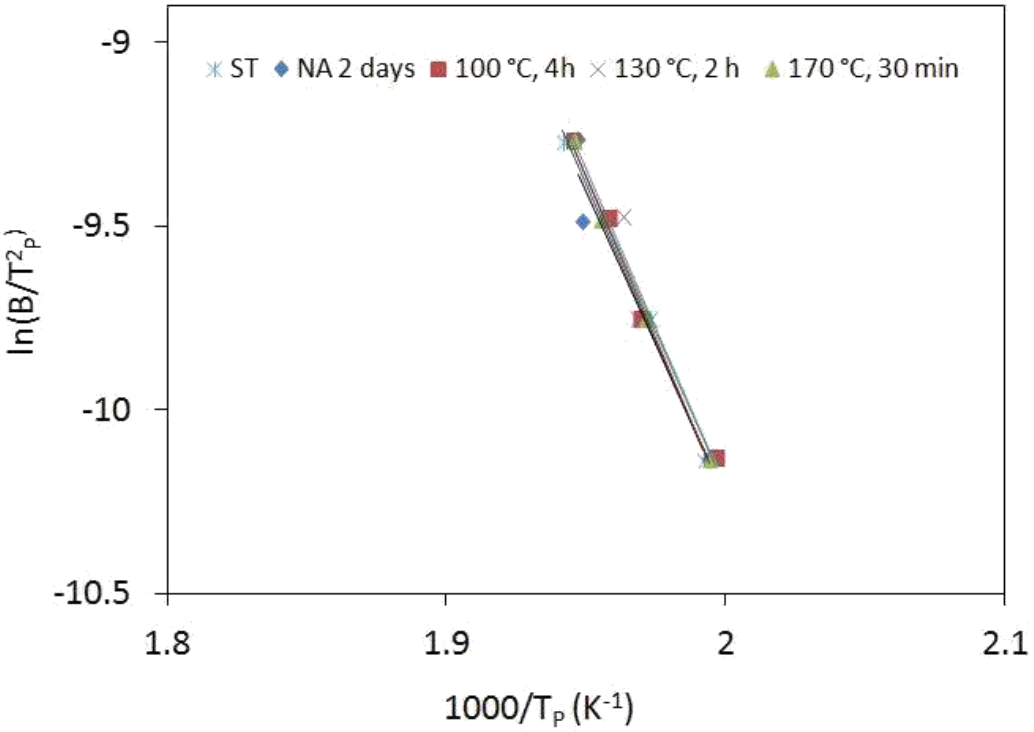

Figure 6.7: Kissinger plots for the exothermic peak (β"/β' precipitates) in Al 6061 alloy processed through various heat treatments (ST, NA for 2 days, PA-100 °C for 4 h, PA-130 °C for 2 h, PA-170 °C for 30 min) followed by cryorolling.

6.3.3 Microstructure

Microstructure investigation has been done through TEM for optimized conditions of PA and NA samples and the micrographs are shown in Figure 6.8. In PA conditions, since the behavior of all conditions are nearly same, only one condition (170 °C, for 30 min) has been investigated through TEM. Main focus is given for evolution of UFG structure and precipitate formation after subjecting to various thermo mechanical treatments. Precipitates are visualized through [001] zone axis of Al. The calculation of grain size is done by adopting linear intercept method. The grain size is observed to be in the range of 200 – 300 nm in both the conditions. Clear color contrast of the grains with matrix indicates formation of high angle grain boundaries [231][232]. However few grains are observed with retention of deformed microstructure filled with high dislocation density zones. Dislocation strengthening plays a important role in the strengthening of UFG alloys.

. Prolonged ageing at low temperature has resulted partial recovery of microstructure consequently UFGs with dislocation free interiors. Recovered grains play crucial role in increase in ductility and work hardenability of the material. PA and NA before cryorolling has resulted significant grain refinement as compared to the microstructure obtained through cryorolling alone (chapter 4).

Figure 6.9 shows the fine needle shaped precipitates obtained from optimized conditions of PA and NA conditions. These fine needles are believed to be β" precipitates which are aligned along <100> $_{Al}$ directions. The fine circular spots are believed to be the end sections of β" precipitates. Coarse circular spots are believed to be the G.P zones which were formed during NA. Clear observation of Figure 6.9 indicates β" needles observed in the optimized condition of the NA sample are much finer and with high aspect ratio than that in optimized condition of PA samples. Based on the DSC thermograms and TEM microstructures of PA and NA samples, the evolution of precipitates at various stages beginning from ST is illustrated in the Figure 6.10. The increase in the hardness of ST material after NA and PA is associated with the formation solute (Mg and Si) clusters that were confirmed by DSC studies. DSC thermograms indicate, clusters that form in the PA are more stable (shown in black color) which have not shown any sign of endothermic peak in the DSC. Whereas the clusters in NA are relatively unstable (shown in grey color), which will get dissolved before forming of post precipitates. It was reported that the clusters which neither dissolve nor grow will have negative effect of increase in hardness during artificial ageing [233]. The typical example is Si rich clusters that forms at room temperature [233] . NA alloy after cryorolling followed by NA and subsequent artificial ageing, possessing fine needle shaped precipitates along with spherical shaped precipitates which were formed at room temperature.

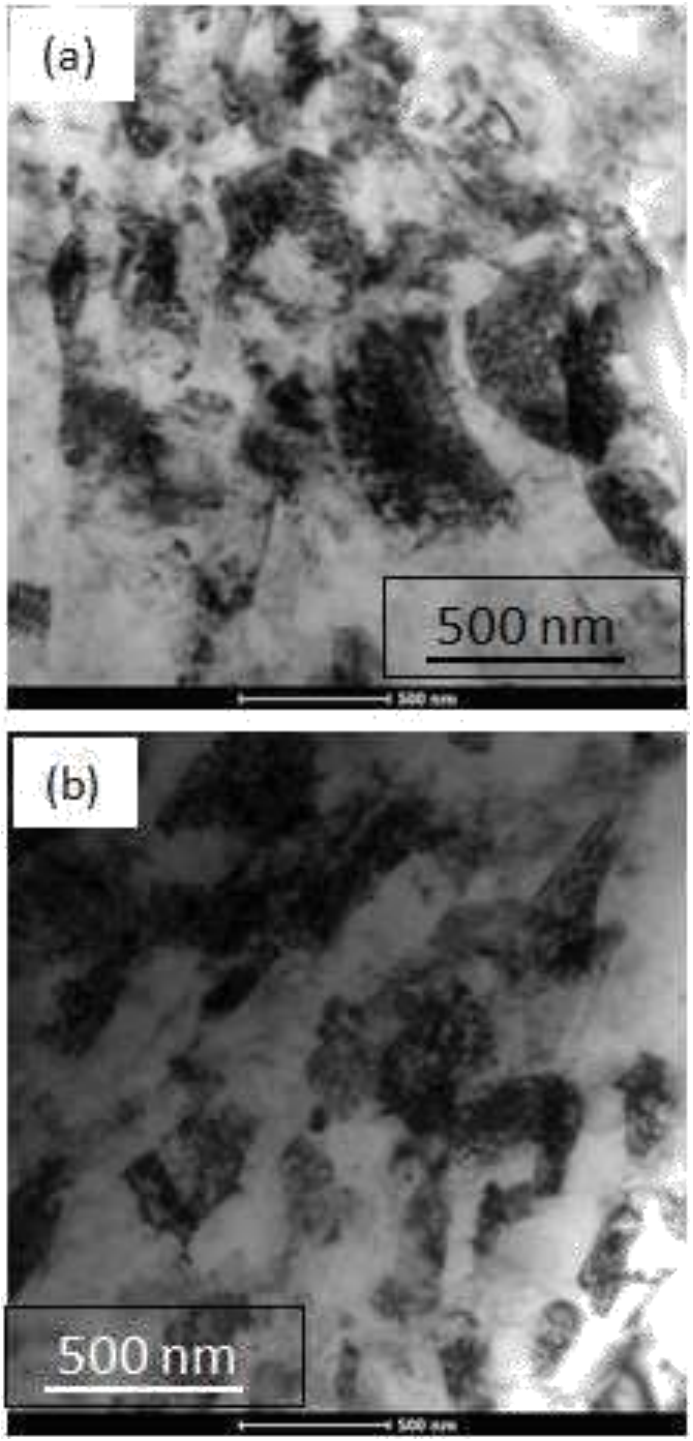

Figure 6.8: TEM micrographs of optimized conditions of PA and NA samples depicting UFG structure; a) PA, 170 °C for 30 min + cryorolled + NA for 30 days followed by artificial ageing at 125 °C, b) NA for 2 days + cryorolled+ NA for 30 days followed by artificially ageing at 125 °C.

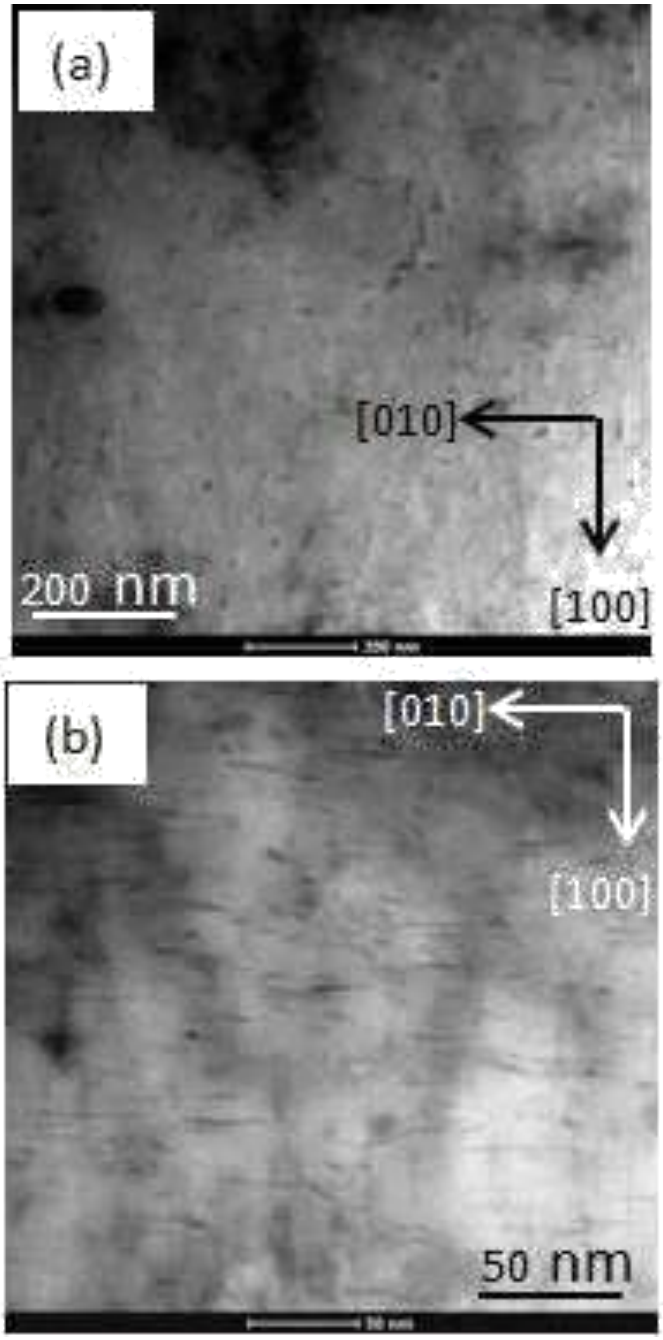

Figure 6.9: TEM micrographs of optimized conditions of PA and NA samples depicting fine needle shaped precipitate; a) PA, 170 ℃ for 30 min + cryorolled + NA for 30 days followed by artificial ageing at 125 ℃, b) NA for 2 days + cryorolled+ NA for 30 days followed by artificially ageing at 125 ℃.

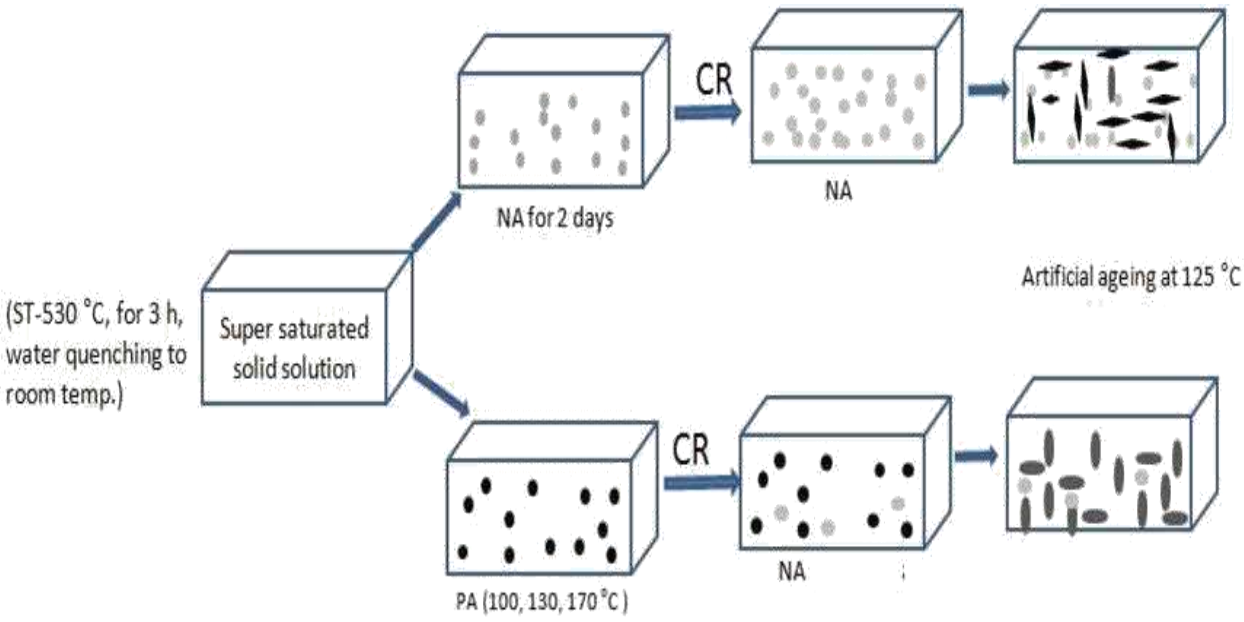

Figure 6.10: Schematic illustration of precipitate evolution in PA and NA material with various thermo mechanical t

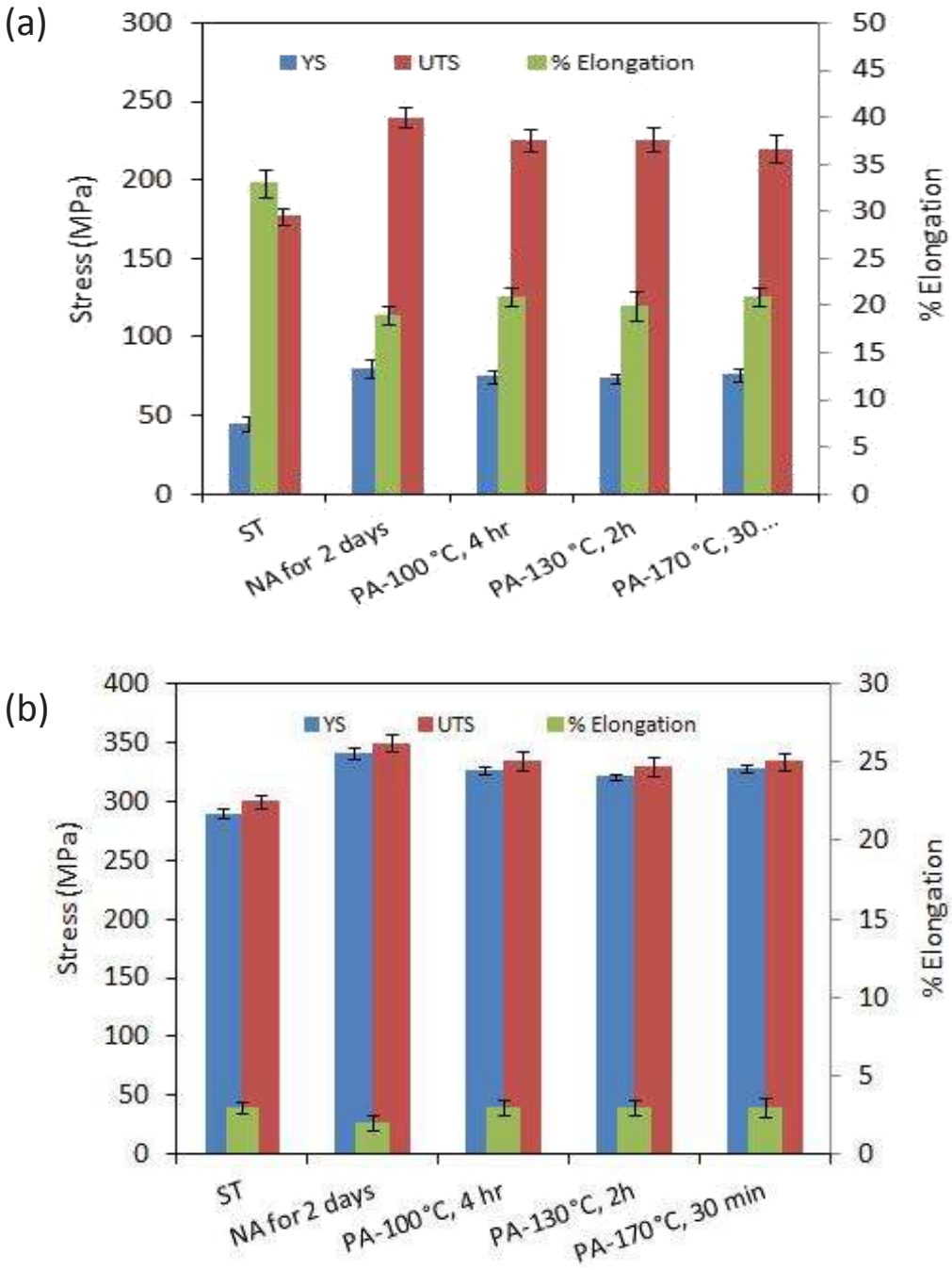

Figure 6.11: Variation in mechanical properties of Al 6061 alloy with various heat treatments; ST, NA for 2 days, PA-100 °C for 4 h, PA-130 °C for 2 h, PA-170 °C for 30 min;(a) before cryorolling,(b) after cryorolling

(a)

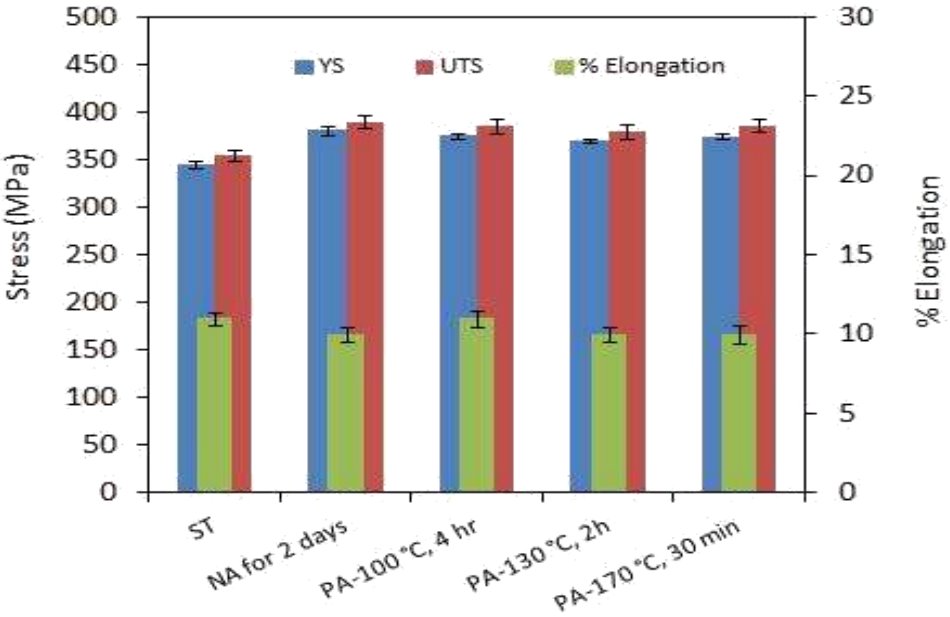

(b)

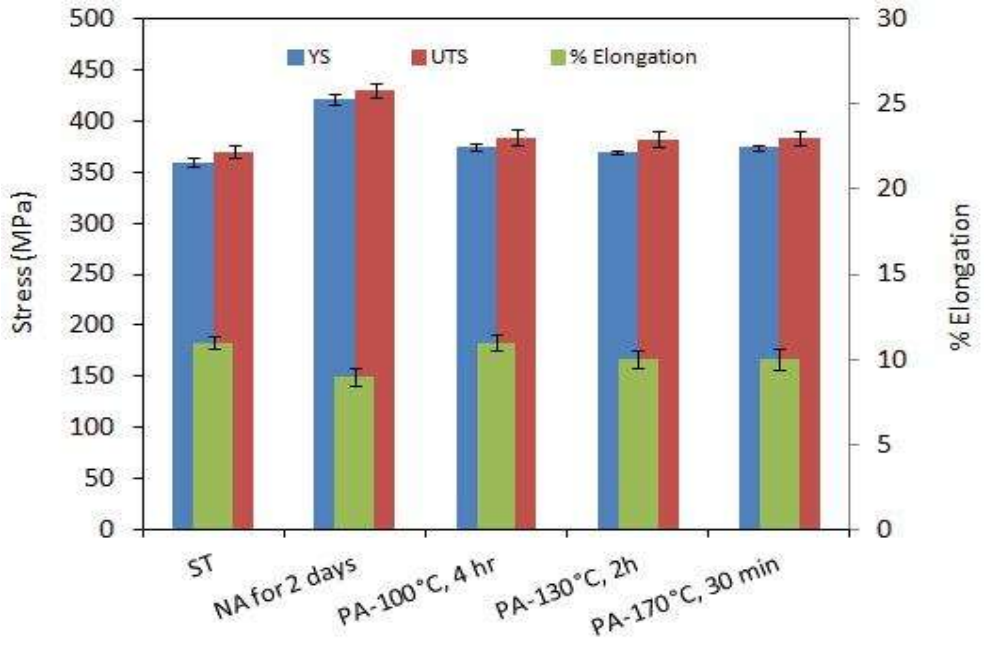

Figure 6.12: Variation in mechanical properties of Al 6061 alloy with various heat treatments (ST, NA for 2 days, PA-100 °C for 4 h, PA-130 °C for 2 h, PA-170 °C for 30 min) followed by cryorolling; (a) After artificial ageing at 125 °C, (b) NA for 1 months followed by artificial ageing

6.3.4 Tensile properties

The tensile properties of the Al 6061 alloy after different PA and NA treatments are presented in the Figure 6.11(a). In ST condition the alloy possess poor YS (48 MPa) and UTS (180 MPa) with large % elongation (33 %). With NA and PA at various temperatures (100 °C, 130 °C, 170 °C) the YS and UTS have increased. However the % elongation has been decreased. After NA for 2 days, the alloy posses highest UTS and YS as compared to the PA conditions. The increase in YS and UTS in NA and PA samples is attributed to the formation nano clusters followed by G.P zones which were confirmed through DSC studies. Figure 6.11 (b) represents the tensile properties of the ST, NA and PA conditions of Al 6061 alloy after cryorolling up to 90% thickness reduction. NA and PA has resulted significant improvement in the YS and UTS as compared to the ST condition. However the % elongation of the alloy after CR has dropped to 3 to 4%. With subsequent artificial ageing at 125 °C (Figure 6.12(a)) has resulted simultaneous increase in strength and ductility. Alloy with PA and NA has resulted superior mechanical properties over simple cryorolled material after solution treatment. The strengthening contribution from the precipitates is depends up on the morphology, size, distribution and volume fraction of the precipitates. In the present investigation, it is believed that NA has altered the size, distribution of the precipitates which favors for excellent mechanical properties.

6.5 Conclusions

1. Different ageing conditions influence the hardening behavior of cryorolled Al-Mg-Si alloy.
2. Room temperature ageing and pre-ageing before cryorolling is an effective approach to enhance the hardness of the Al-Mg-Si alloy. Partial ageing before cryorolling facilitates to enhance the dislocation density in the material by inducing solute clusters as trapping agents.
3. Pre-ageing temperature has not influenced the hardness behavior much during artificial ageing.
4. The affect of natural ageing on pre-aged cryorolled samples is not significant.

5. The optimum heat treatment condition could be chosen as “Natural ageing for 2 days + cryorolling 90% + Natural ageing for 30 days followed by artificial ageing at 125 ℃ for 48 hours.

Chapter 7

Effect of cryoforging followed by cryorolling on the microstructure and mechanical properties of Al-Mg-Si alloy

In the present investigation, ultrafine grained (UFG) Al alloy was produced from its bulk alloy by cryoforging followed by cryorolling. The bulk Al-Mg-Si alloy, with initial grain size 400 μm, was subjected to solid solution treatment (ST) followed by water quenching at room temperature. The ST treated alloy was subjected to ageing at 100 °C for 4 hours and 8 hours prior to cryoforging. The cryoforged alloy was subjected to cryorolling up to 2.4 true strain for producing long sheets. Finally, the deformed alloy was subjected to low temperature ageing at 120 °C to improve the tensile properties of the alloys. Microstructure and mechanical properties were evaluated through Vickers hardness testing, tensile testing and electron back scattered diffraction (EBSD). The results have shown that combined cryoforging + cryorolling followed by ageing led to remarkable improvement in strength (UTS- 452 MPa) and ductility (8%). The average grain size the alloy was found to be 240 nm, with increased fraction of high angle grain boundaries. Low temperature differential scanning calorimetry (DSC) was used to study thermal behavior of bulk and severely deformed alloy.

7.1 Introduction

The automobile industry is constantly demanding fuel efficient vehicles with pollution free technologies to reduce the energy consumption as well as to ensure a clean environment. The reduction in vehicle weight by 10% could result in improvement of 8–10% in fuel economy [234]. The unique properties of aluminium alloys, such as high specific strength, good formability, high corrosion resistance, and recycling potential, make them ideal for replacing the heavier alloys currently used in vehicles in the automotive industries. Al-Mg-Si alloys are used for automotive body structures due to their good formability, high corrosion resistance and better bake hardening response [234]. Among several Al alloys, more than 60% of them used in several structural and functional applications are based on 6xxx series [235]. Al-Mg-Si alloys are strengthened via dispersion of Mg_2Si nanosized precipitates through proper heat treatment. In order to meet the demand for materials with high strength to weight ratio, innovative processing techniques are being explored to enhance the strength of bulk alloys further. The common industrial practice is to reduce the grain size by adding grain refiners during the casting process [235][236]. However, the minimum grain size achievable through the conventional routes is limited to a few microns. Recently, severe plastic deformation techniques have been developed to reduce the grain size from micrometers to submicron or nanometer level by inducing severe strain in to the material[237][12][238][239] [210]. The size of samples that can be produced through severe plastic deformation (SPD) processes limits the use of ultrafine grained materials (UFG) materials in practical applications. Multi directional forging (MDF) is one potential technique used to produce UFG structures in the bulk materials. The samples size that can be produced through MDF is relatively large, which can be suitable for industrial applications [240]. It has been successfully used to produce UFG structures in brittle material at elevated temperature [241][242].

In addition to large plastic strains induced by the SPD processes, deformation temperature plays critical role to promote grain refinement down to nanocrystalline range [243]. Medium and high stacking fault energy materials has been successfully processed through forging and rolling at cryogenic temperature (cryoforging and cryorolling) to achieve better grain refinement[243] [244][245][109] .Cryorolling is one of the novel routes used to produce UFG structure in the bulk material with less induced plastic strain[210][109][246][206][247]. On the other hands hybriding of various SPD techniques could be exploited to produce UFG material in required shape with a

desired grain size. In the SPD processes, the development of UFG structure occurs through generation and accumulation of dislocations, formation of cell structure and its transformation to high angle grain boundaries through consumption of continuously generated dislocations [142][248][165]. Deforming at cryogenic temperature retards the dislocation mobility and hence reduces the rate of dynamic recovery, results accumulation of high density of dislocations than the material deformed at room temperature[243][109]. To date, there has been no systematic investigation on the development of UFG Al alloys through hybrid SPD processing techniques in the literature. Hence, the present work is focused on producing UFG microstructures in the bulk Al-Mg-Si alloy (slightly varied in Mg and Si composition as compared to Al 6061 alloy) through combined cryoforging and cryorolling and realize the substantial improvement in tensile properties of the alloys as compared to its bulk Al alloys. Detailed microstructural characterizations of the SPD-processed alloys were performed to ensure the formation of thermally stable UFG microstructures in the Al-Mg-Si alloys. The improvement in tensile properties of the alloys has been elucidated through strengthening mechanisms arising from the grain size effect, dislocation hardening, solid-solution strengthening, and precipitation hardening.

7.2 Experimental details

Commercially available Al-Mg-Si alloy was subjected to hybrid SPD for producing UFG microstructures in the alloy. Samples with dimension of 30.5×27×25 mm^3 were machined from the as received plate. They were subjected to solution treatment (ST) at 520 °C for 2 hours. The quenched blocks are pre-aged at 100 °C for 4 and 8 hours before subjecting them to multi directional forging (MDF) at cryogenic temperature. MDF was performed up to 4 cycles with a true strain of 2.4. These blocks were sectioned at center and further rolled at very low temperature by using liquid nitrogen (cryorolling) to achieve 1.5 mm thickness. A detailed procedure of MDF at cryogenic temperature and cryorolling is reported in Chapter 3. Rolling alone is insufficient to induce high strain in the material and pure MDF also poses a problem during processing due to deviation of its original shape at high strains. Six sets of conditions with different combination of strain and heat treatments as shown in Table 7.1 were used to process the bulk Al-Mg-Si alloy. Figure 1 depicts the detailed processing methodologies adopted in the present work.

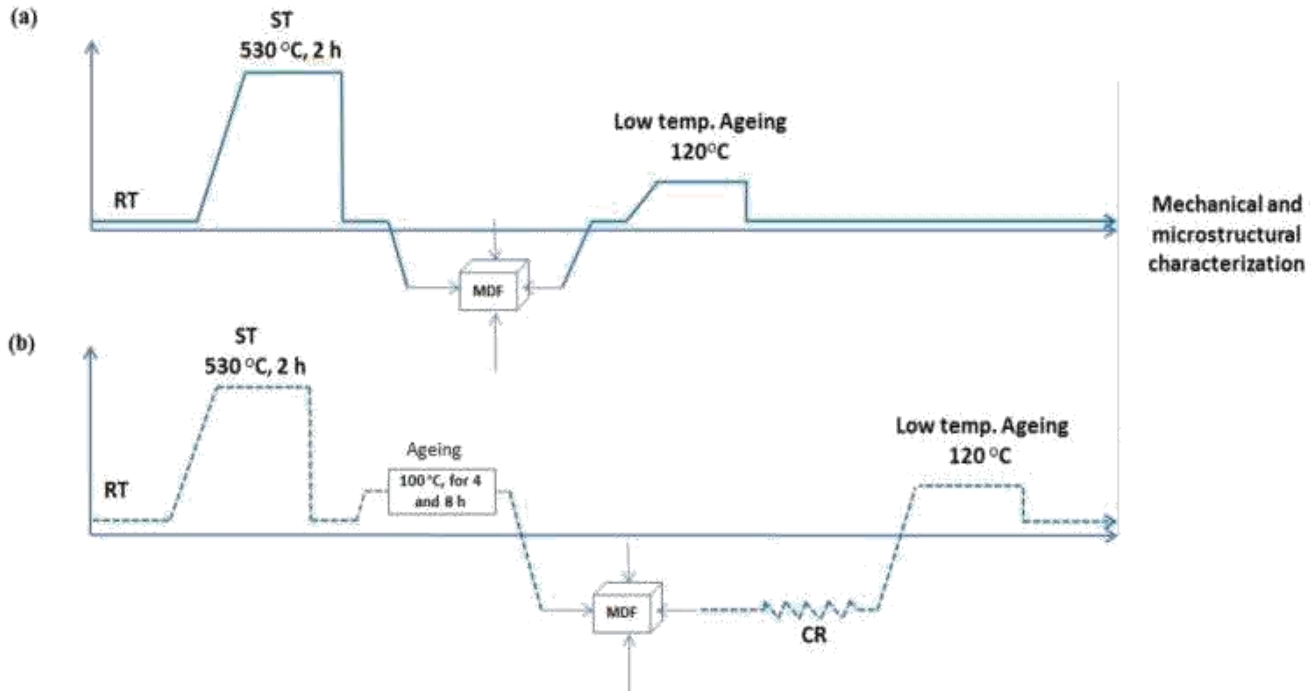

Figure 7.1: Flow chart of various processes adopted in the present investigation; a) MDF, b) MDF1 and MDF2.

Table 7.1: Sample designation and their respective processing condition

Designation	Processing condition
ST	Al-Mg-Si alloy solid solution treated at 520 °C for 2h followed by cold water Quenching
T6	ST material subjected to artificial ageing at 177 °C for 8 h
ST1	ST material subjected to ageing treatment at 100 °C for 4 h (Pre ageing)
ST2	ST material subjected to ageing treatment at 100 °C for 8 h (Pre ageing)
MDF	ST material subjected to Multi directional forging at liquid nitrogen temperature up to 2.4 true strains.
MDF+PA	MDF after peak ageing treatment
MDF1	ST1 material subjected to MDF followed by cryorolling up to 2.4 true strain
MDF1+PA	MDF1 after peak ageing treatment
MDF2	ST2 material subjected to MDF followed by cryorolling up to 2.4 true strain
MDF2+PA	MDF2 after peak ageing treatment

7.2.1 DSC Analysis

DSC analysis of deformed Al-Mg-Si alloys was performed by using low temperature differential scanning calorimetry under nitrogen atmosphere. Scans were performed with starting temperature of -5 °C, with heating rates of 10,15,20,25 °C/min, up to a final temperature of 450 °C. For starting material in the ST condition, samples of 5 mm diameter weighing 30 mg were solid solution treated and subsequently water quenched. They were immediately subjected to DSC measurements without any delay. The remaining conditions of samples were subjected to respective thermo mechanical treatments followed by punching to 5mm diameter sample with 30 mg weight. For all conditions, the surface finish of sample was maintained by grinding to 800 grit emery paper. Annealed pure Al was used as a reference sample. Base line correction was performed by subtracting the DSC heat flow curve of sample-reference with that of reference-reference.

7.2.2 Electron Back Scattered Diffraction (EBSD)

EBSD is used to investigate the microstructural evolution in different process conditions. Standard polishing procedures were adopted to polish the samples to a strain free mirror like surface. Etchant such as perchloric acid and methanol (20:80) with a voltage of 11V for 90 s at -20^{o} C is used for polishing the sample required for EBSD analysis using FEI Quanta 200 FEG-SEM/EBSD. A step size of 0.1µm was used for all EBSD scans.

7.2.3 Mechanical Characterization

Tensile testing was conducted with a strain rate of $9\times10^{-4}s^{-1}$ on non-standard sub-size specimens. For MDF condition, the samples with gauge length, width and thickness of 10mm, 3mm and 1.5 mm, respectively were used. For all other conditions, the sample dimensions were; gauge length-17mm, width-3mm, and thickness- 1.5mm. Hardness measurements were performed on Vickers hardness testing machine with 5Kg load, dwell time of 15 seconds.

7.3 Results and Discussion

Figure 7.2 shows the microstructure of the starting material after solution treatment. The average grain size is observed to be 400 µm. Figure 7.3 shows edge cracks developed in MDF1 and MDF2 samples due to severe strain. The thickness reduction per rolling pass is 0.4 mm. At initial passes of rolling, no edge cracks were observed, however when the sheet becomes relatively thin and the ratio of sheet thickness to reduction per pass decreased the edge cracks become severe. This indicates the limitation in the roll ability of the material further. Another reason could be reduced tensile ductility in the material due to pre-ageing affect. Pre-ageing is performed to form solute clusters, which helps in increasing the dislocation density in the material during rolling in the similar way what would be expected from a cryorolling process. It is also expected that these solute clusters suppresses the dynamic recovery through subgrain boundary pinning [186]. Detailed TEM investigations are required to establish the deformation characteristics of samples influenced by precipitation kinetics, grain refinements, and dislocation density during MAF+CR.

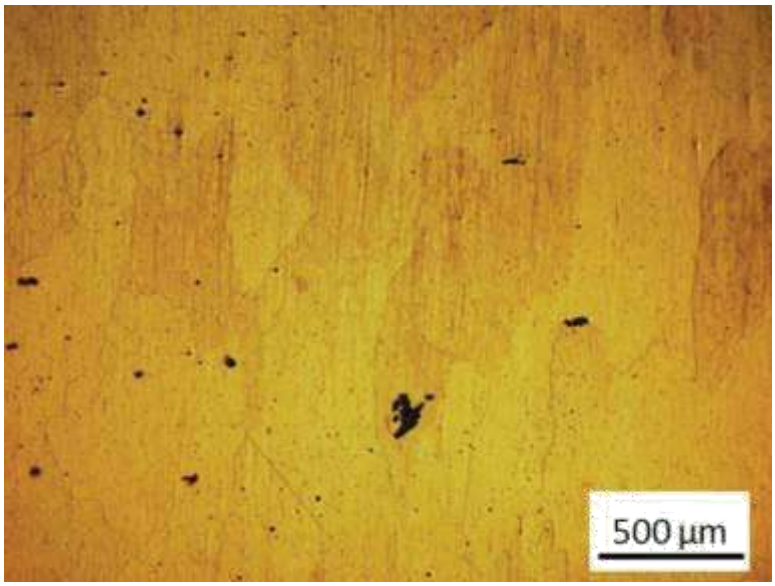

Figure 7.2: Microstructure of starting material after solid solution treatment at 520 °C for 2 h (Etchant used: Poltons reagent)

Figure 7.3: Photograph of UFG alloy sheets obtained through MDF1 and MDF2 routes.

7.3.1 Hardness

Vickers hardness value of the ST material is 40 Hv (Table 2). After MDF, a 125% increase in hardness (90 Hv) was observed. The initial hardness of sample subjected to ST1 and ST2 conditions were found to be 56 Hv and 62 Hv, respectively. The rise in hardness in ST1 with respect to ageing time is more significant than that in ST2. The starting hardness values of MDF1

and MDF2 are 130 and 138 Hv, respectively, which are about 132% and 122% more than the hardness value of starting material (ST1-56 Hv, ST2- 62 Hv). The increase in hardness after MDF1 and MDF2 with respect to ST are 225% and 245%, respectively. The deformed sample was subjected to low temperature ageing at 120 ℃ to improve its tensile properties due to precipitation hardening effect. As the strain induced in the material is very high, ageing temperature was selected as 120 ℃ for minimizing the recovery rate. Low temperature ageing has led to a slight drop in hardness in MDF1 and MDF2 at initial stages, followed by nearly stable behavior with increasing ageing time. On the other hand, in MDF and ST, an increase in hardness is observed from the beginning. Hardness plots are shown in Figure 4(a).

7.3.2 Tensile testing

Figure 4(b) shows the tensile plots of various conditions; test values are listed in Table 2. It is evident that the ST material possesses a large % elongation, low yield strength and remarkable work hardening behavior, which is typical of coarse grained annealed material. After T6 treatment, the % elongation has dropped from 30% to 12 % by increasing yield strength from 40 MPa to 290 MPa whereas MDF has resulted increase in yield strength of the ST material from 40 MPa to 265 MPa. The % of elongation at fracture is ~10%. However, the uniform elongation is limited to ~ 4% due to onset necking behaviour which is typical of UFG metals processed by SPD [249]. The limited uniform elongation is attributed to low dislocation storage capability which results non-uniform elongation. It is also reported that the sample size has significant effect on post necking elongation (non-uniform elongation)[249]. Samples with smaller gauge lengths tend to show higher elongations [249].

The YS of MDF1 and MDF2 have increased significantly to 420 and 455 MPa. The total true strain accumulated in the material through MDF followed by rolling at liquid nitrogen temperature is 4.8. In addition to the low temperature deformation effect, pre-ageing at 100 ℃ for 4 and 8 hours led to formation of clusters, which would actively participate in pinning and accumulation of dislocations. Thus, the dislocation densities can be increased further in the pre-aged material as compared to un-aged material. MDF1 and MDF2 material exhibit elongations of 5% and 4.5%, respectively. The reduction in % elongations is as expected but the interesting observation is that the elongation is of uniform in nature. The early stage of necking effect is comparable with MDF material.

Artificial ageing has resulted opposite trends in the tensile behaviour of bulk (ST) and UFG (MDF1 and MDF2) materials. With T6 treatment, % elongation has dropped but YS is increased compared to the ST material. On the other hand, UFG materials, upon ageing treatment, show a drop in YS (from 420 MPa to 400 MPa in MDF1 and 455 MPa to 440 MPa in MDF2) but increase in % elongation (MDF1-3%, MDF2-3.5%). In MDF material, the trend is similar to the ST material. The effect of ageing treatment on work hardening behavior is more significant than ductility in MDF material. The increase in uniform elongation after low temperature ageing treatment in UFG materials (MDF, MDF1 and MDF2) is attributed to reduction in dislocation density and precipitation of high density of nanosized precipitates[173]. It can be concluded from the tensile plots that MDF1 and MDF2 processing conditions have produced remarkable improvement in strength (MDF1- 415 MPa, MDF2- 452 MPa) with reasonable ductility (8%).

Table 7. 2: Mechanical properties of material subjected to various processing conditions

Processing condition	YS (MPa)	UTS(MPa)	% Elongation	Hardness Hv
ST	40	200	30	40
T6	290	325	12	110
MDF	265	286	10	90
MDF+PA	300	340	12	115
MDF1	420	426	5	138
MDF2	455	462	4.5	143
MDF1+PA	400	415	8	133
MDF2+PA	440	452	8	141

Microstructural features such as dislocations, grain boundaries and precipitates etc., play an important role in the mechanical properties of the precipitation hardenable Al alloys. However, presence of high dislocation density leads to heterogeneous and coarse precipitate formation in Al 6061 alloy. To achieve UFG structure with less dislocation density, high amount of strains are required. In the present work, a combination of cryoforging and cryorolling was used to achieve high amount of strain at super saturated solid solution state. Thus, the microstructure possesses UFG structure with reduced dislocation density. Further low temperature ageing has resulted fine and well distributed nanosized precipitates.

A combination of optimized micro/nano structural features has contributed to high strength and good ductility in the alloy.

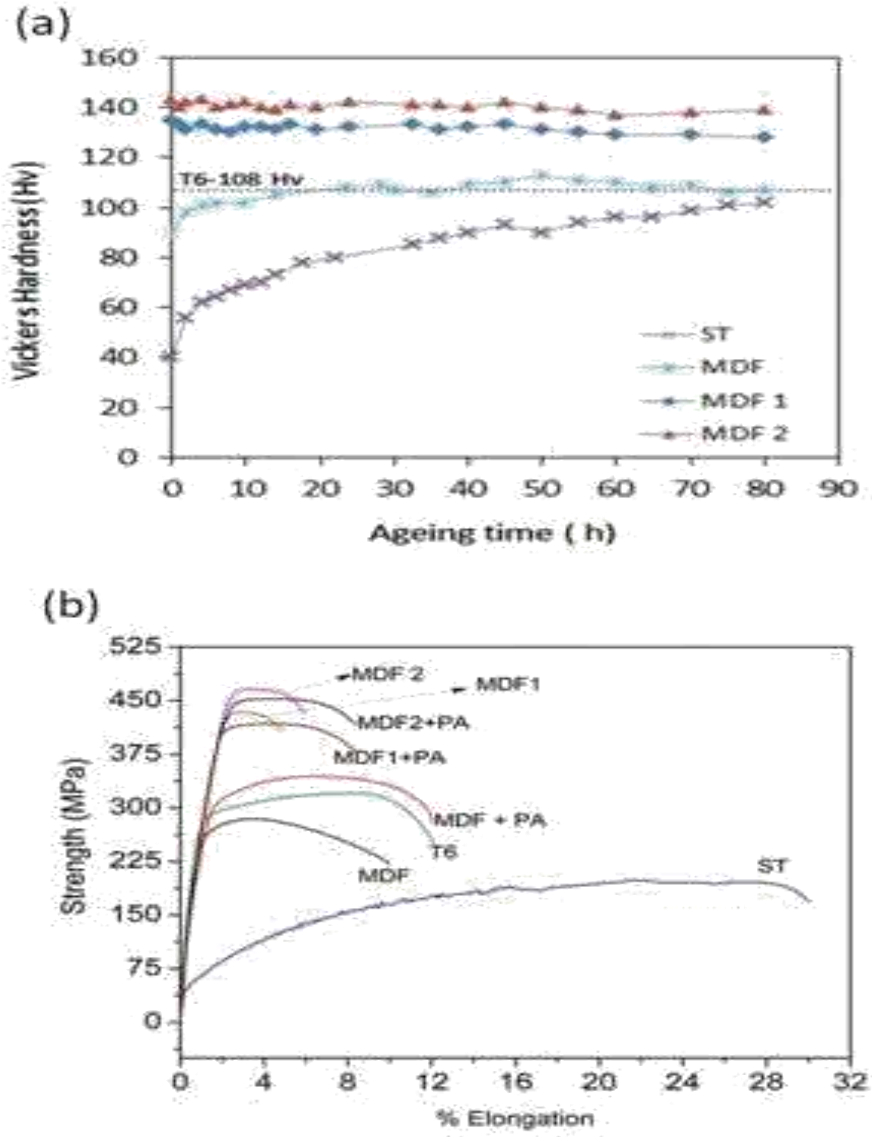

Figure 7.4: Mechanical behavior of an alloy processed through various conditions; a) Vickers hardness plots, b) Plots of engineering stress versus engineering strain

7.3.3 DSC

Figure 5 shows DSC heat flow curves obtained with a heating rate of 15 °C/min for various processed conditions of bulk and UFG material. ST material (Figure 5(a)) shows standard peaks that are observed commonly in Al-Mg-Si alloy. The widely accepted precipitation sequence in Al-Mg-Si alloys is Super saturated solid solution (SSSS) → Si–Mg–vacancy clusters → GP zones → β″→β'→β (Mg_2Si) [169][170] [250] [251] [252]. The initial broad low temperature exothermic peak followed by two sharp exothermic peaks correspond to cluster formation, β" phase formation (needle shaped, coherent with the matrix) and β' phase formation (rod shaped, semi coherent with the matrix) respectively. The exothermic peak that appears near 450 °C could be due to β phase (incoherent, stable phase Mg_2Si), which is not significant for strengthening. After MDF, significant changes have occurred in the exothermic peak intensities and positions. The effect of cryogenic deformation on DSC heat flow behavior of Al 6061 alloy was reported elsewhere [179]. The major difference observed in the present alloy, compared with common behavior of 6000 series alloys, is the behavior of β' phase. It is observed that deformation led to simultaneous formation of β' phase along with β" phase, which has reduced the strengthening contribution from precipitation hardening mechanism to overall strengthening of the matrix[179][185][201] . In the present investigation, the appearance of distinguished peaks of β" and β' signals showed a beneficial effect on strengthening. Comparing the position of the peaks in MDF material to ST material, the β" peak has moved towards a lower temperature and β' has moved towards a higher temperature. This indicates that MDF has led to accelerated formation of β" and delayed formation of β' phase. This phenomenon could cause the formation of stable β" phase thereby reducing the earlier transformation to β' phase.

Figure 5(b) shows DSC heat flow curves of ST1 and MDF1 materials. Ageing at 100 °C for 4 hours caused reduced intensities of cluster peaks and slight variations in the intensities and positions of β" and β' phase peak as compared to ST material. The behavior of heat flow curve of MDF1 material is slightly different from MDF material. There is shift in both β" and β' phase peaks towards lower temperature, but with clear separation between them. The hump that appears in between 150-200 °C indicated the formation of G.P zones [201][180][169] Conditions favorable to form G.P zones ought to be investigated in detail. After MDF1 samples were deliberately kept at room temperature to analyze the effect of small cluster peak that remained after ageing at 100 °C. A small endothermic peak (Figure 5(b), peak-C1/C2-D) that appeared

between 50 to 150 °C indicates, the remnant solute after ageing at 100 °C for 4 h, has formed clusters during natural ageing. These clusters dissolved during DSC heating. The main purpose of performing ageing at 100 °C is to develop stable clusters that which can grow further to β" phase as well as to enhance the accumulation of dislocations during deformation. In 6000 series alloys it was observed that the clusters that form at room temperature during natural ageing led to a delay in the formation of β″ particles and thereby lowers β″ volume fraction [253]. Ultimately this would influence the mechanical properties the alloy after final artificial ageing treatment. The proposed practice to get rid of natural ageing effect in 6000 series alloys is pre-ageing at above room temperatures immediately after solid solution treatment [221][254][255]. Clusters that forms during pre-ageing treatment are more stable and it will grow further to β" phase during a bake hardening process[221]. This practice enhances the bake hardening response. In the present investigation, the appearance of a residue cluster peak, even after 4 h of ageing at 100 °C, indicates the ageing time and/or temperatures ought to be increased further for complete formation of clusters. The ageing time has increased from 4 h to 8 h in the present study, which represented as ST2 condition.The pre-processing temperature was chosen based on the Differential Scanning Calorimetry (DSC) data. DSC data of Al 6061 alloy shows that the cluster formation in ST material is taking place at around 100 °C. Since the clusters are highly unstable, the preheat treatment was given immediately after ST. The reason for doing preheat treatment is to allow the solute atoms to form stable clusters which will act as precursors for β" precipitates formation. It also enhances the dislocation density by introducing solute clusters as pinning agents on dislocation movement during deformation.

Figure 5 (c) shows DSC heat flow curves of ST2 and MDF 2 material. The positions of the peaks are shifted further to lower temperatures as compared to former conditions. In addition to this, there is an additional small peak (indicated with arrow in Figure 5(c)) in between the β" and β' phase peaks. This has been checked with all heating rates and it has to be characterized in detail to determine the type of phase. At low temperatures, the cluster peaks are nearly suppressed. In MDF2 material, the behavior is similar to the MDF1 with very low intensity cluster dissolution peak.

Activation energies related to β" and β' phase formations in various conditions are calculated by using Kissinger analysis from the peak temperatures obtained at various heating rates (10, 15, 20, 25 °C/min). The values are listed in Table 3. Pre-ageing (ST1 and ST2) resulted in a slight increase in the activation energies with respect to ST material.

At the same time, the activation energy values associated with the formation of β" and β' phase in deformed materials (MDF,

MDF1 and MDF2) are also higher the ST material. Similar behavior has been reported in earlier work [179]. Quainoo and Yannacopoulos have reported that the decrease in activation energy of β" formation due to high strain energy induced in the material upon sever cold working[256].

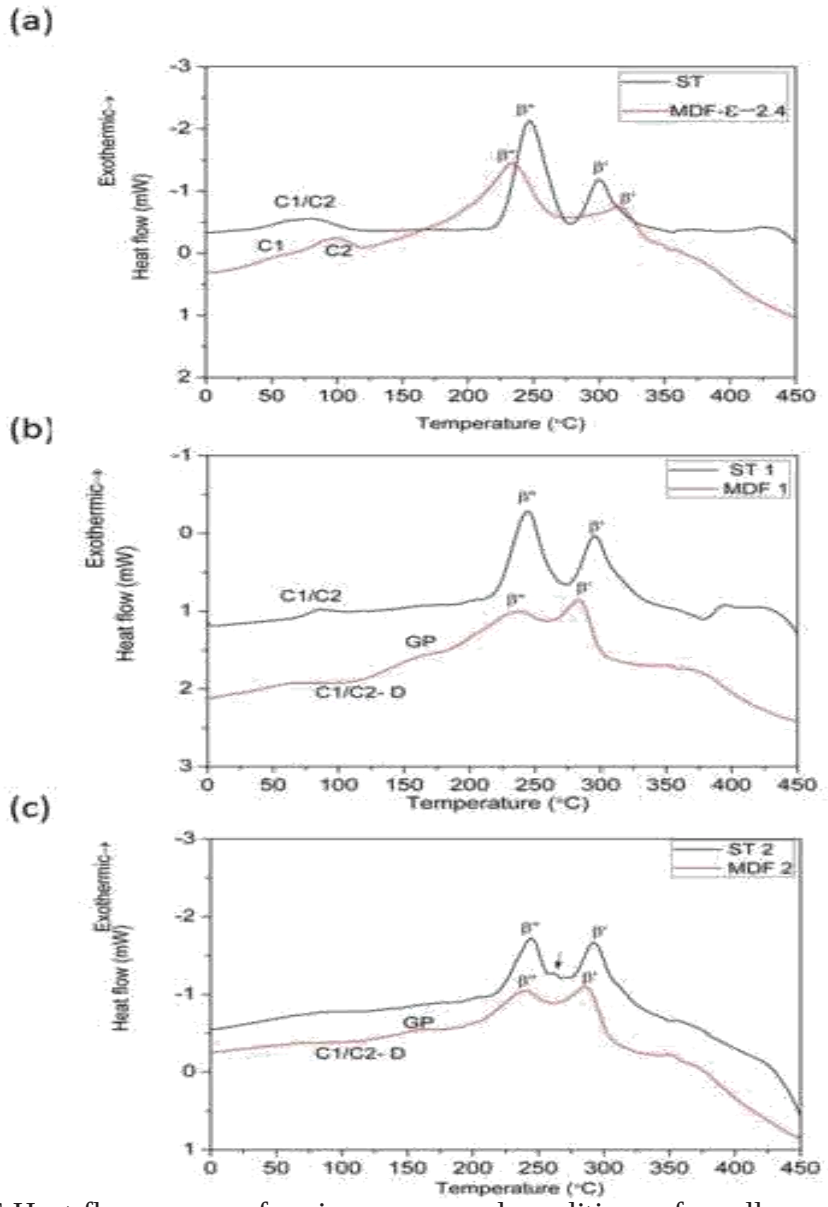

Figure 7.5: DSC Heat flow curves of various processed conditions of an alloy with heating rate 15 °C/min ; a) ST and MDF, b) ST1 and MDF1, c) ST2 and MDF2. (C1-Cluster 1 formation, C2-Cluster 2 formation, C1/C2-D- endothermic peak corresponding to clusters dissolution, GP- peak corresponding to GP zones formation, β", β' and β- peaks corresponding to various phases of Mg_2Si.

Table 3: Activation energies corresponding to β" and β' phase evolution under various processing conditions

Condition	Activation energy (E) (KJ/mol)	
	β"	β'
ST	82	103.4
MDF	130	148
ST1	99	113
ST2	104	115
MDF1	109	153
MDF2	115	147

The β" phase improves the strength of the alloy depending up on the percentage of cold work. The slight differences in the strength of the alloy observed in the present work could be due to the difference in severity of deformation strain induced into the material and its subsequent influence on microstructural features such as large volume fraction of subgrain boundaries and high dislocation densities.

7.3.4 Microstructure

Microstructure analysis was carried out using EBSD for MDF, MDF1, MDF2 samples as well as in their respective peak aged conditions. Inverse pole figure maps and misorientation of grain boundaries data obtained through EBSD is shown in Figure 6 and Figure 7 respectively. As a common representation, black lines indicates high angle grain boundaries (Misorientation > 15°) and grey lines indicates low angle grain boundaries (2° <Misorientation <15°). The location of EBSD scan for MDF material is at the center of the central plane of the sample block. The inverse pole figure map shows that the MDF material possesses predominantly low angle grain boundaries. High angle grain boundaries can be observed at shear band structures due to strain localization. In MDF1 and MDF2 materials, the fraction of high angle grain boundaries is more as compared to MDF material.

Another remarkable difference observed in MDF1 and MDF2 material is due to its decreased grain boundary spacing and increased dislocation density. The reduced recovery and enhanced dislocation pinning sites have led to accumulation of high density of dislocations in MDF1 and MDF2 materials.

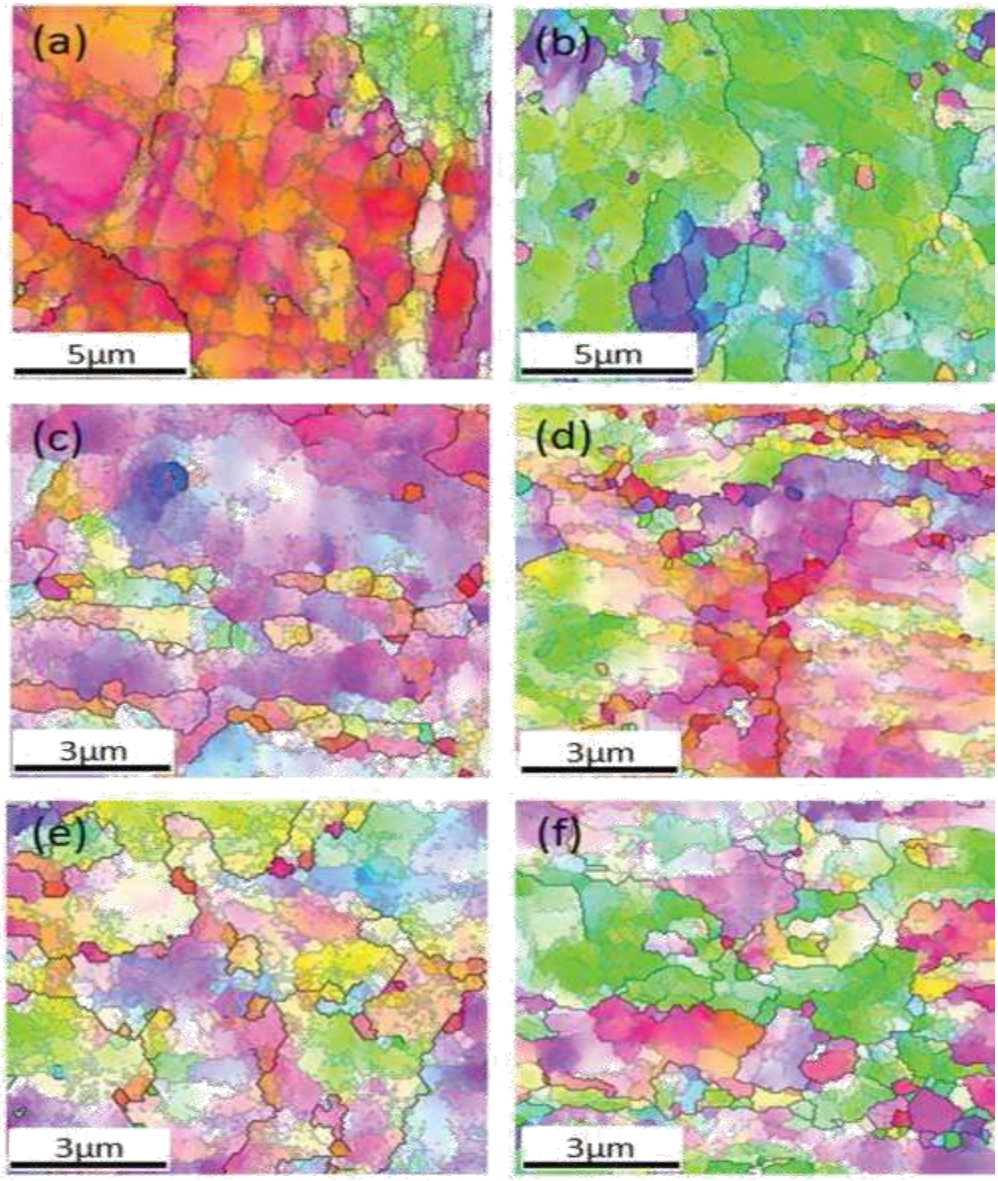

Figure 7.6: EBSD microstructures of an alloy processed through various conditions; a) MDF, b) MDF+PA, c) MDF1, d) MDF1+PA, e) MDF2, f) MDF2+PA.

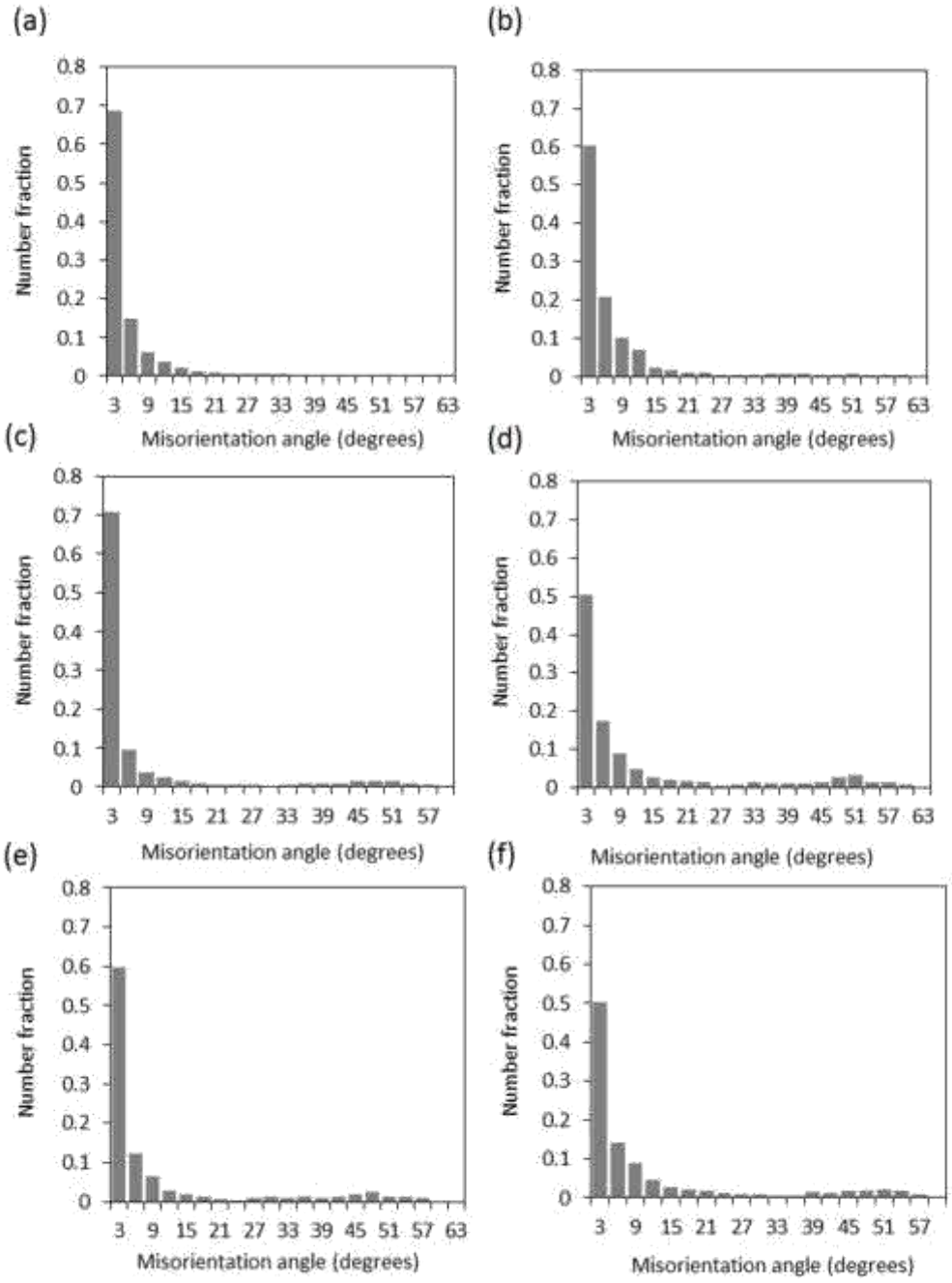

Figure 7.7: Grain boundary misorientation plots an alloy processed through various conditions; a) MDF, b) MDF+PA, c) MDF1, d) MDF1+PA, e) MDF2, f) MDF2+PA.

The prolonged ageing at low temperature has enabled rearrangement of dislocations into dislocation cell boundaries in MDF material with no significant effect on high angle grain boundaries. The fraction of high angle grain boundaries has increased in MDF1 and MDF2 materials. The grain size that observed in MDF1 and MDF2 materials are 270 and 240 nm, respectively. The grain size observed through EBSD is slightly higher than the actual size determined via through TEM due to the difference in spatial resolution.

7.4 Conclusions

In the present work the Al-Mg-Si alloy was subjected to hybrid SPD processing (Cryoforging + Cryorolling) to produce UFG microstructures with improved mechanical properties. The microstructural characteristics and tensile properties of the deformed and aged alloys were investigated in details and the following conclusions are made

1. Employing pre-ageing (100 °C for 4 h and 8h) has resulted significant improvement in strength and hardness in the MDF1 and MDF2 materials.
2. The material possesses a larger fraction of low angle grain boundaries even after deformation up to 4.8 true strain (in MDF1 & MDF2). This was attributed to suppression of dynamic recovery by rolling at very low temperature.
3. Low temperature ageing of severely deformed material has resulted in slight drop in hardness (from 138Hv to 133 Hv in MDF1 and from 143 Hv to 141 Hv in MDF2) at the beginning hours, later, the material possesses stable hardness. It indicates the balance between softening due to recovery and hardening due to precipitation. However, in lightly deformed material (MDF), the rise in hardness (from 90Hv to 113 Hv) with ageing time is observed. It can be attributed to dominant precipitation hardening over softening by recovery.
4. Cold deformation has not suppressed the post β" phase formation in ST, ST1 and ST2 materials but the peaks temperatures have varied.
5. Activation energy values of β" and β' phases are significantly higher in pre-aged and deformed materials as compared to ST material.
6. The above conclusions indicate that the combination cryoforging and cryorolling can be used as a simple and cost effective technique to produce high strength Al alloy sheets with UFG structure. Scheduling suitable heat treatments in precipitation hardenable alloys aids to achieve proper combination of properties.

Chapter 8: Results & Suggestions for Future work

The present work has summarized the effect of deformation temperature on microstructure evolution and mechanical properties of Al 6061alloy. Also the effect of nanosized precipitates on the hardening behavior of alloy has been enlightened.

- Hardness and DSC investigations have shown that the microstructural and thermal stability of the CR and RTR material is similar.
- From the EBSD and TEM investigation, it is evident that, the area fraction of UFG has increased with increasing warm rolling temperature. This may be due to increased dynamic recovery effect with increasing warm rolling temperature.
- Employing pre-ageing (100 °C for 4 h and 8h) has resulted significant improvement in strength and hardness in the MDF1 and MDF2 materials.
- Cold deformation has not suppressed the post β" phase formation in ST, ST1 and ST2 materials but the peaks temperatures have varied.
- Activation energy values of β" and β' phases are significantly higher in pre-aged and deformed materials as compared to ST material.

The following suggestions are proposed for future work as an extension of current work:

1.The present investigation suggests that, the nano-sized solute clusters that forms at early stage of precipitation have significant role in the deciding the final properties of the alloy. A thorough investigation is required through advanced characterization techniques such as Atom probe tomography (APT) to understand the evolution and kinetics of clusters.

2.A comprehensive study on the influence of asymmetric rolling at different temperatures can be performed to investigate the changes in microstructural features and its effect on mechanical properties.

3.Studies related to fatigue crack growth, fracture toughness, and wear characteristics of ultrafine grained 606 Al alloy produced under different thermo mechanical conditions can be investigated.

4.The influence of processed conditions on the corrosion characteristics of the material may be studied.

References

1. Light Alloys- Metallurgy of light metals, **I.J. Polmear,** Arnold, London, 1995.

2. Developments in the use of ECAP processing for grain refinement, **R.Z. Valiev, T.G. Langdon**, Reviews in Advanced Material Science,2006, Vol. 13, pp. 15-26.

3. Experimental parameters influencing grain refinement and microstructural evolution during high-pressure torsion, **A.P. Zhilyaev, G.V. Nurislamova, B.K. Kim, M.D. Baro, J.A. Szpunar, T.G. Langdon,** Acta Materialia ,2003, Vol. 51, pp. 753–765.

4.Microstructure evolution in pure Al processed with twist extrusion, **D.Orlov, Y. Beygelzimer, S.Synkov, V.Varyukhin, N.Tsuji, Z. Horita,** Materials Transactions,2009, Vol. 50, pp. 96-100.

5.Useful properties of twist extrusion, **Y. Beygelzimer, V. Varyukhin, S. Synkov, D. Orlov,** Materials Science and Engineering A , 2009, Vol. 503, pp. 14–17.

6.Ultra-fine grained bulk aluminum produced by accumulative roll-bonding (ARB) process, **Y. Saito, N. Tsuji, H. Utsunomiya , T. Sakai,R. Hong ,** Scripta Materialia,1998, Vol. 39, pp. 1221-1227.

7.Microstructures and Dislocation Configurations In Nanostructured Cu Processed By Repetitive Corrugation And Straightening ,**J.Y.Huang, Y.T. Zhu, H.G. Jiang, T.C. Lowe,** Acta Materialia,2001, Vol. 49, p. 1497-1505.

8.Friction stir welding and processing, **R.S. Mishra, Z.Y.Ma,** Material science and Engineering,2005, Vol. 50, pp. 1-78.

9.Simultaneous increasing the ductility and strength of nanostructured alloys, **Y.H. Zhao, X.Z. Liao, S. Cheng, E. Ma, Y.T. Zhu,** Advanced Matererials,2006, Vol. 18, pp. 2280–2283.

10. Effect of ageing on strength and ductility of ultrafine grained Al 6061 alloy,**S.K. Panigrahi, D. Devanand, R. Jayaganthan,** Advanced Matererials ,2010,Vol. 633-634, pp. 303-309.

11.A DSC study on the precipitation kinetics of cryorolled Al 6063 alloy, **S.K. Panigrahi, R. Jayaganthan, V. Pancholi, M. Gupta,** Materials Chemistry and Physics,2010, Vol. 122 , pp. 188–193.

12.Using high-pressure torsion for metal processing: Fundamentals and applications, **A. Zhilyaev, T. Langdon,** , Progress in Material Science, 2008, Vol. 53(6), pp. 893–979.

13. Simultaneously increasing the ductility and strength of nanostructured alloys , **Y.H. Zhao, X.Z. Liao, S. Cheng, E. Ma, Y.T. Zhu**, Advanced Materials,2006, Vol. 18, pp. 2280–2285.

14. Nanostructuring of metals by severe plastic deformation for advanced properties, **V. Ruslan, Nature materials.** 2004, Vol. 38, pp. 511-516.

15. Nanocrystalline materials, **H. Gleiter,** Progress in materials science, 1989,vol. 33, pp .223-315 .

16. Materials processing by simple shear, **V. M. Segal,** Materials Science and Engineering: A,1995, vol. 197, pp. 157-164**.**

17. New methods for severe plastic deformation processing,**D.J Alexander,** Journal of materials engineering and performance,2007. Vol. 16, pp. 360-374 .

18. Shearing phenomena at high pressures, particularly in inorganic compounds**,Bridgman,** Poceedings of the American Academy of Arts and Sciences, American Academy of Arts and Sciences.

19. Producing bulk ultrafine-grained materials by severe plastic deformation,**Z.R. Valiev, E.Yuri, Z.Horita,L.G Michael, J.Zechetbauer , T.Y.,Zhu.T.Yuntian,** 2006, vol. 58, pp. 33-39.

20. A new technique for preparing bulk ultrafine-grained materials through twist extrusion ,**Xiao-xi, Xue Ke-min Wang, L. I. Ping**, Journal of Plasticity Engineering, 2009,vol.27,pp.23-34.

21. Ultra-fine grained bulk aluminum produced by accumulative roll-bonding (ARB) process, Y. **Saito, N. Tsuji, H. Utsunomiya, T.Sakai,R.G. Hong.** Scripta materialia,1998, vol. 39,pp. 1221-1227.

22. Plastic flow, structure and mechanical properties in pure Al deformed by twist extrusion, **Orlov, Dmitry, B. Yan,S Sergey,V. Vitkor,T. Nobuhiro,H. Zenji,** Materials Science and Engineering A,2009, vol. 519,pp. 105-111.

23. Properties of ultrafine-grained steel by repeated shear deformation of side extrusion process, **A. Akira, K. Aoki,** Materials Science and Engineering A, 2002,vol. 33(7), pp.45-49.

24. Severe plastic deformation by the cone-cone method, potential for producing ultrafine grained sheet material, **B. Olivier, Y. Estrin, H.S. Kim,** Revue de Métallurgie,2007,vol. 104 ,pp. 318-322.

25. High tensile ductility in a nanostructured metal, **W. Yinmin, C. Mingwei, Z. Fenghua. Maen,** Nature, 2002,vol. 419, pp. 912-915.

26. Influence of transverse rolling , **J.B.Clark ,R.K. Garrett ,T.L. Jungling , R.L. Asfahani ,** Metallurgical Transactions A,1992, vol. 23,pp. 2183-2191.

27. Grain refinement of high purity aluminium by asymmetric rolling, **Q. Cui, K. Ohori,** Materials Science and Technology, 2000, vol. 16, pp.1095-1101.

28. Microstructure and high tensile ductility of ZK60 magnesium alloy processed by cyclic extrusion and compression, **Lin Jinbao, Wang Qudong, Peng Liming,Roven.J.Hans ,** Journal of Alloys and Compounds, 2009, vol. 47,pp. 441-445.

29. Microstructure and mechanical properties of AZ31 magnesium alloy processed by cyclic closed-die forging, **Jou Guo Wei,Wang Qudong,Ye Bing, Zhou Hao,**Journal of Alloys and Compounds, 2013, Vol. 558, pp. 164-171.

30. Hydrostatic extrusion as a method of grain refinement in metallic materials, **Kurzydłowski, J. Krzysztof**, Materials Science Forum, 2006, Vol. 503.

31. Grain Refinement of C-Mn Steel to 1. MU. m by Rapid Cooling and Short Interval Multi-pass Hot Rolling in Stable Austenite Region, **Tomida Toshiro, Imai Norio,Miyata Kaori,Okada Yasutaka,** , ISIJ international, 2008, vol. 48,pp. 1148-1157.

32. The principles, Processes and Machines of Helical Rolling, and Cross Wedge Rolling, **Z. H. Hu, X. H. Xiu, D. Y. Sa,** Metall. Ind. Press, Beijing, 1985.

33. Large straining behavior and microstructure refinement of several metals by torsion extrusion process, **Mizunuma Susumu,** Materials Science Forum, 2006 , Vol. 503,pp.185-192.

34. Different processing routes for deformation via simple shear extrusion (SSE), **N. Pardis, R. Ebrahimi,** Materials Science and Engineering A, 2010, vol .23, pp. 6153-6156..

35. A novel single pass severe plastic deformation technique: Vortex extrusion,**M. Shahbaz , N. Pardis, R. Ebrahimi, B. Talebanpour,** Materials Science and Engineering A,2011,vol.530 ,pp. 469-472.

36. Principles of equal-channel angular pressing as a processing tool for grain refinement, **Ruslan, Z. Valiev, G. Terence Langdon,** Progress in Materials Science, 2006,vol .51.pp. 881-981.

37. Continuous frictional angular extrusion and its application in the production of ultrafine-grained sheet metals, **Y. Huang, P. B. Prangnel,** Scripta materialia, 2007,vol. 56,pp. 333-336..

38. Friction stir welding and processing, **S. Rajiv Mishra, Z. Y. Ma** , Materials Science and Engineering A, 2005,vol. 50,pp. 1-78.

39. Development of severe torsion straining process for rapid continuous grain refinement, **Nakamura Katsuaki, Neish Koji,Kaneko, Kenji,Horita Zenji,** Materials transactions , 2004, vol 45.pp. 3338-3342..

40. Severe plastic deformation of metals by high-pressure tube twisting, **L. S.Toth, M.Arzaghi, J.J Fundenberger, B. Beausir, O. Bouaziz, R. Arruffat-Massion** , Scripta Materialia, 2009,vol. 60,pp. 175-177.

41. Cyclic expansion-extrusion (CEE) A modified counterpart of cyclic extrusion-compression (CEC),**N. Pardis , B. Talebanpour ,R. Ebrahimi , S. Zomorodian ,** Materials Science and Engineering A,2011 ,vol. 528, pp. 7537-7540.

42. Development of high-pressure sliding process for microstructural refinement of rectangular metallic sheets, **Fujioka Tadayoshi, Zenji Horita,** . Materials transactions, 2009, Vol. 50,pp.930-933.

43. Microtexture and microstructure evolution during processing of pure aluminum by repetitive ECAP, **A. P .Zhilyaev, D.L Swisher, K. Oh-ishi , G.T Langdon,. R.T McNelley,** Materials Science and Engineering: A, **200**6, vol. 429, pp. 137-148.

44. Deformation Behavior of 6061 Aluminum Alloy Through Tube Channel Pressing: Severe Plastic Deformation, **Mohammad Hassan Farshidi, M. Kazeminezhad,** Journal of materials engineering and performance, 2012, vol. 21, Pp. 2099-2105.

45. Theoretical and practical aspects of the production of thin-walled tubes by the KOBO method, **Bochniak Włodzimierz, Krzysztof Marszowski, Andrzej Korbel.** Journal of Materials Processing Technology, 2005, vol.169,pp. 44-53.

46. Improvement of mechanical properties of magnesium alloy ZK60 by integrated extrusion and equal channel angular pressing, **Orlov Dmitry, G. Raab, T.T Lamark,, M Popov, Y. Estrin**, Acta Materialia, 2011, vol. 59,pp.375-385.

47. Plastic flow at equal channel angular processing in parallel channels, **G. I Raab,** Materials Science and Engineering A,2005, vol. 410, pp. 230-233.

48. Microstructures and dislocation configurations in nanostructured Cu processed by repetitive corrugation and straightening, **J. Y Huang, Y.T Zhu, H Jiang, C.T. Lowe**, Acta Materialia, 2001, vol. 49,pp.1497-1505.

49. Enhanced Superplasticity in a Magnesium Alloy Processed by Equal-Channel Angular Pressing with a Back-Pressure, **Lapovok Rimma, Y. Estrin , V.M. Popov, G.T Langdon,**Advanced Engineering Materials, 2008,vol .5, pp. 429-433.

50. Continuous high-pressure torsion, **Edalati Kaveh, Zenji Horita,** Journal of materials science, 2010, 45,vol.17,pp. 4578-4582..

51. Continuous ECAP process design for manufacturing a microstructure-refined bolt, **Jin Young Gwan, M.H Hyun Moo Baek, T.Y Im,** Materials Science and Engineering A, 2011, vol .530, pp 462-468.

51. Observations and issues on mechanisms of grain refinement during ECAP process, **Zhu Yuntian Theodore, Terry C Lowe,** Materials Science and Engineering A,2000 ,vol. 291,pp. 46-53.
.

53. Principles of equal-channel angular pressing as a processing tool for grain refinement, **Valiev Ruslan Z, Terence G. Langdon,** Progress in Materials Science, 2006 , vol. 51,pp 881-981.

54. On the use of accumulative roll bonding process to develop nanostructured aluminum alloy 5083 **Toroghinejad, Mohammad Reza, Fakhreddin Ashrafizadeh, Roohollah Jamaat,** Materials Science and Engineering A, 2013,vol. 561, pp. 145-151.

55. Role of shear strain in ultragrain refinement by accumulative roll-bonding (ARB) process, **S. H.Lee, Y. Saito ,Z. Tsuji ,H. Utsunomiya , T. Sakai ,** Scripta Materialia, 2002, vol. 46,pp. 281-285.

56. ARB (accumulative roll-bonding) and other new techniques to produce bulk ultrafine grained materials, **Tsuji Nobuhiro,** Advanced Engineering Materials, 2003,vol. 5.5,pp. 338-344.

57 Dynamic processes for nanostructure development in Cu after severe cryogenic rolling deformation, **Wang Yinmin, Tong Jiao, En Ma,** Materials Transactions, 2003 .vol. 44,pp. 1926-1934.

58. Bulk nanostructured materials from severe plastic deformation,**Valiev Ruslan Zafarovich, Rinat K. Islamgaliev, Igor V. Alexandrov,** Progress in materials science, 2000,vol. 45, pp103-189.

59. Extreme grain refinement by severe plastic deformation a wealth of challenging science, **Estrin Yuri, Alexei Vinogradov,** Acta materialia, 2013,vol.61,pp. 782-817.

60. Microstructure evolution and mechanical properties of nanocrystalline zirconium processed by surface circulation rolling treatment, **Yuan Chao,** Materials Science and Engineering A, 2013,vol. 565 ,pp. 27-32.

61. Effect of cryo-rolling and annealing on microstructure and properties of commercially pure Aluminium,**Rangaraju Nikhil,** Materials Science and Engineering A, 2005,vol .398, pp.246-251..

62. Formation of nanostructures in commercial-purity titanium via cryorolling, **S. V. Zherebtsov,** Acta Materialia, 2013,vol. 61, pp.1167-1178.

63. Microstructures and mechanical properties of ultrafine grained 7075 Al alloy processed by ECAP and their evolutions during annealing, **Y.H Zhao, X. Z. Liao, Z Jin, R.Z Valiev, Y.T Zhu,** Acta Materialia, 2001, Vol. 52, pp 4589-4599.

64. Mechanical behaviour and microstructure of a thermally stable bulk nanostructured Al alloy, **V.L Tellkamp, A. Melmed, E.J. Lavernia ,**Metallurgical and Materials Transactions A, 2001, Vol. 32, Pp.2335-2343**.**

65. Nanocrystalline Al-Mg alloy with ultrahigh strength and good ductility, **K.M Youssef, R.O. Scattergood, K.L Murty, C.C.Koch,** Scripta Materialia, 2006, Vol. 54,pp 251-256.

66. Microstructures and mechanical properties of ultrafine grained 7075 Al alloy processed by ECAP and their evolutions during annealing, **Y. H.Zhao,** Acta Materialia **,**2004, Vol. 52,pp. 4589-4599.

67. On the origin of the extremely high strength of ultrafine-grained Al alloys produced by severe plastic deformation, **R. Z. Valiev,** Scripta Materialia, 2010, Vol. 63,pp. 949-952.

68. Effect of annealing temperature on microstructures and mechanical properties of a 5083 Al alloy deformed at cryogenic temperature, **Lee Young Bum,** Scripta materialia, 2004, Vol. 51, Pp.355-359 .

69. Microstructures and mechanical properties of 6061 aluminum alloy processed by accumulative roll-bonding, **S. H. Lee,** Materials Science and Engineering A, 2002, Vol. 325, Pp**.**228-235.

70. Fatigue life of fine-grain Al–Mg–Sc alloys produced by equal-channel angular pressing, **Vinogradov,** Materials Science and Engineering A ,2003, Vol. 349,pp. 318-326.

71. Strengthening mechanisms in an Al-Mg alloy, **E.L. Huskins.,B. Cao,K.T. Ramesh ,** Materials Science and Engineering A,2010 , Vol. 527,pp. 1292-1298.

72. Materials science and engineering: an introduction, **D.William Callister, ,David G. Rethwisch, New York Wiley,** 2007, Vol. 7.

73. Improvement in the r-value of aluminum strip by a continuous shear deformation process, **Y Saito, H Utsunomiya, H .Suzuki, T .Sakai**, Scripta Materiala,1139, 2000, Vol. 42.

74. Properties & Selection: Nonferrous Alloys and Special Purpose Materials, **A. S. M Handbook, ASM International**, Materials Park, OH, 1990, Vol. 2.

75. Industrial development of non heat treatable aluminum alloys, **Jr. R. E**. **Sanders, P. A. Hollinshead, E. A .Simielli, ,**Materials Forum,2004, Vol. 28,pp.53-64.

76. Kinetics of flow and strain hardening. **H. Mecking, U.F. Kocks,** Acta Materialia, 1981, Vol. 29 ,pp.1865-1875.

77. Physical modeling of materials problem, **M.F. Ashby,** Material science and Technology**,** 1992, Vol.8, pp. 102-111.

78. Symposium on internal stresses, **E. Orowan**, Institution of Metals, London**,**1948, Vol. 415.

79. Nanostructured aluminium alloys produced by severe plastic deformation New horizons in development, **I. Sabirov, M.Yu. Murashkin, R.Z. Valiev**, Materials Science & Engineering A, 2013, Vol. 560, pp. 1-24.

80. Modelling grain boundary strengthening in ultra-fine grained aluminum alloys, **E. Nesa, B. Holmedal, E. Evangelista, K. Marthinsen**, Materials Science and Engineering A,2005, Vols. 410–411, pp. 178–182.

81. The deformation and ageing of mild steel III Discussion of results, **E.O. Hall,** Proceedings of the Physical Society, Section B,951, Vol. 64 , pP. 747.

82. **N.J Petch,** J. Iron Steel Inst., 1953, Vol. 174,pp. 25.

83. On the origin of the extremely high strength of ultrafine-grained Al alloys produced by severe plastic deformation, **R.Z. Valiev, N.A. Enikeev, M.Yu. Murashkin, V.U. Kazykhanov, X. Sauvage**, Scripta Materialia , 2010, Vol. 63, pp. 949–952.

84. Hall–Petch relation and boundary strengthening, **Niels Hansen** 8, Scripta Materialia, 2004, Vol. 51, pp. 801–806.

85. Mechanical behavior of nanocrystalline metals and alloys, **K.S Kumar, H. Van Swygenhoven, S. Suresh,** 19, Acta Materialia, 2003, Vol. 51, pp. 5743–5774.

86. Strengthening Mechanisms in Solid Solution Aluminum Alloys, **Oyvind Ryen, Oscar Nijs,** E**mma Sjolander, Bjørn Holmedal, Hans-ErikEekstrom, Erik Nes**, **M**etallurgical and Materials Transactions A, 2006,Vol. 37A, pp. 1999.

87. Nanostructure and related mechanical properties of an Al–Mg–Si alloy processed by severe plastic deformation, **Gulnaz Nurislamova, Xavier Sauvage, Maxim Murashkin, Rinat Islamgaliev,Ruslan Valiev**, Philosophical Magazine Letters, 2008, Vol. 88, pp. 459–466.

88. Nanostructural hierarchy increases the strength of aluminium alloys, **P.V. Liddicoat, X.Z. Liao, Y.H. Zhao, Y.T. Zhu, M.Y. Murashkin, E.J. Lavernia, R.Z. Valiev, S.P. Ringer**, Nature Communications, 2010, Vol. 1, pp. 63.

89. Grain boundary segregation in UFG alloys processed by severe plastic deformation, **X. Sauvage, A. Ganeev, Y. Ivanisenko, N. Enikeev, M. Murashkin, R. Valiev**, Advanced Engineering Materials , 2012.

90. Influence of equal-channel angular pressing on precipitation in an Al–Zn–Mg–Cu alloy, **G. Sha, S.P. Ringer, Z.C. Duan, T.G. Langdon**, Int. J. Mater. Res. , 2009,Vol. 100, pp. 1674–1678.

91. Superstrength of nanostructured metals and alloys produced by severe plastic deformation, **R.Z. Valiev, N.A. Enikeev, M.Yu. Murashkin, S.E. Alexandrov, R.V. Goldshtein.**, Dokl. Phys., 2010, Vol. 55 (6), pp. 267.

92. Alfred Wilm and the beginnings of Duralumin, **Olivier Hardouinduparc**, Zeitschrift für Metallkunde , 2005, Vol. 96, pp. 398-404.

93. Tests on duralumin columns for aircraft construction, **John G . Lee,** 1924.

94. Investigation of the fatigue and long-term strength of flat duralumin elements of aircraft structures in certain aggressive media, **A. M. Pen'kov,V. A. Gorodetskii,**Soviet materials science a transl. of Fiziko-khimicheskaya mekhanika materialov/Academy of Sciences of the Ukrainian SSR, 1971, Vol. 4.5, pp.388-391 .

95. Aircraft construction, **Albert Toussaint, Bertrand Jean Joseph Marie,** U.S. Patent No. ,507,143, 2 Sep. 1924., Vol. 1.

96. Filled Resins and Aircraft Construction, **De Havilland G**, Journal of the Aeronautical Sciences (Institute of the Aeronautical Sciences)10 , 2012, Vol. 3.

97. Physikalisch-metallurgische Untersuchungen über magnesiumhaltige Aluminiumlegierungen, **Wilm Alfred.**, Metallurgie Zeitschrift für de gesamte Hüttenkunde, 1911, Vol. 8, pp. 225–227.

98. The Role of Vacancies in the Aging of Al-Mg-Si Alloys, **Stefan Pogatscher, Marion Werinos, Helmut Antrekowitsch, Peter J. Uggowitzer**, Materials Science Forum, 2014, Vols. 794-796, pp. 1008-1013.

99. The effect of coarse second-phase particles and fine precipitates on microstructure refinement and mechanical properties of severely deformed Al alloy, **I. Gutierrez-Urrutia, M.A. Munoz-Morris, D.G. Morris**, Materials Science and Engineering A , 2005,Vol. 394 , pp. 399–410.

100. Dynamic precipitation during severe plastic deformation of an Al–Mg–Si aluminium alloy, **Hans J. Roven, Manping Liu, Jens C. Werenskiold**, Materials Science and Engineering A , 2008, Vol. 483–484 , pp. 54–58.

101. Recovery of deformation substructure and coarsening of particles on annealing severely plastically deformed Al–Mg–Si alloy and analysis of strengthening mechanisms, **I. Gutierrez-Urrutia, M.A. Muñoz-Morris, D.G. Morris.**, Journal of Materials Research , 2006, Vol. 21, pp. 329-342.

102. Enhanced grain refinement due to deformation-induced precipitation during ambient-temperature severe plastic deformation of an Al–7%Si alloy, **J.M. García-Infanta, S. Swaminathan, C.M. Cepeda-Jiménez, T.R. McNelley**, Journal of Alloys and Compounds , 2009, Vol. 478, pp. 139–143.

103. On the effect of SPD on recycled experimental aluminium alloys Nanostructures, particle break-up and properties, **P. Szczygiel, H.J. Roven, O. Reiso**, Materials Science and Engineering A , 2005, Vols. 410–411, pp. 261–264.

104. Using ECAP to achieve grain refinement, precipitate fragmentation and high strain rate superplasticity in a spraycast aluminum alloy, **Cheng Xu, Minoru Furukawa, Zenji Horita, Terence G. Langdon**, Acta Materialia , 2003,Vol. 51 , pp. 6139–6149.

105. Microstructural development during equal channel angular pressing of hypo-eutectic Al–Si casting alloy by different processing routes, **J.M. Garc´ıa-Infanta, S. Swaminathan, A.P. Zhilyaev, F. Carreno, O.A. Ruano, T.R. McNelley**, Materials Science and Engineering A, 2008, Vol. 485 , pp. 160–175.

106. Microstructure of two-phase al–1.7 at% cu alloy deformed by equal-channel angular pressing, **M. Murayama, Z. Horita, K. Hono** , Acta materialia,2001, Vol. 49, pp. 21–29.

107. Evolution of the Structure of V95 Aluminum Alloy upon HighPressure Torsion, **I. G. Brodova, I. G. Shirinkina, A. N. Petrova, O. V. Antonova, V. P. Pilyugin** , The Physics of Metals and Metallography ,2011, Vol. 111, pp. 630–638.

108. Analysis of strengthening mechanisms in a severelyplastically-deformed Al–Mg–Si alloy with submicron grain size, **D. G. Morris, I. Gutierrez-Urrutia, M.A. Munoz Morris**, Journal of Material Science, 2007, Vol. 42, pp. 1439–1443.

109. High tensile ductility in a nanostructured metal, **Yinimin Wang, Mingwei Chen, Fenghua Zhou, En Ma** , Nature,2002, Vol. 31, pp. 419 .

110. A Study on the Combined Treatment of Cryorolling, Short-Annealing, and Aging for the Development of Ultrafine-Grained Al 6063 Alloy with Enhanced Strength and Ductility, **Sushanta Kumar Panigrahi, R. Jayaganthan**, Metallurgical and Materials **T**ransactions A,2010, Vol. 41A, pp. 2010—2675.

111. Plastic deformation and fracture of ultrafine-grained Al–Mg alloys with a bimodal grain size distribution, **G.J. Fan, H. Choo, P.K. Liaw, E.J. Lavernia** 7, Acta Materialia, 2006, Vol. 54, pp. 1759–1766.

112. Bimodal microstructure and deformation of cryomilled bulk nanocrystalline Al–7.5Mg alloy, **Z. Lee, D.B. Witkin, V. Radmilovic, E.J. Lavernia, S.R. Nutt,** Materials Science and Engineering A,2005, Vol. 410–411, pp. 462–467.

113. Al–Mg alloy engineered with bimodal grain size for high strength and increased ductility, **David Witkin, Z. Lee, R. Rodriguez, S. Nutt, E. Lavernia,** 4, Scripta Materialia, 2003, Vol. 49, pp. 297–302.

114. Tensile Deformation and Fracture Mechanism of Bulk Bimodal Ultrafine-Grained Al-Mg Alloy, **Zonghoon Lee, Velimir Radmilovic, Byungmin Ahn, Enrique J. Lavernia, Steven R. Nutt**, Metallurgical Materials Transactions A , 2010, Vol. 41A, pp. 795.

115. Room-Temperature Mechanical Behavior of Cryomilled Al Alloys, **David Witkin, Bing Q. Han, Enrique J. Lavernia,** Metallurgical And Materials Transactions A, 2006, Vol. 37A, pp. 185.

116. Dynamic observations of deformation in an ultrafine-grained Al–Mg alloy with bimodal grain structure, **Ahn Byungmin, Enrique J. Lavernia, Steven R. Nutt**, Journal of Materials Science ,2008, Vol. 43,pp.23-24.

117. Deformation behavior of bimodal nanostructured 5083 Al alloys, **B. O. Han,** Metallurgical and Materials Transactions A 2005, Vol. 36, Pp.957-965 .

118. Microstructural evolution during recovery and recrystallization of a nanocrystalline Al-Mg alloy prepared by cryogenic ball milling,**F. Zhou,** Acta Materialia, 2003, Vol. 51.10,pp.2777-2791.

119. Plastic flow properties and microstructural evolution in an ultrafine-grained Al-Mg-Si alloy at elevated temperatures, **B. P. Kashyap,** Metallurgical and Materials Transactions A 2009, Vol. 40,pp. 3294-3303.

120. An overview : fatigue behaviour of ultrafine-grained metals and alloys, **H. W. Höppel,**

International Journal of Fatigue , 2006, Vol. 28.9,pp.1001-1010.

121. Simultaneously Increasing the Ductility and Strength of Nanostructured Alloys, **Yong-Hao Zhao, Xiao-Zhou Liao, Sheng Cheng, En Ma, Yuntian T. Zhu**, Advanced Materials,2006, Vol. 18, pp. 2280–2283.

122. Microstructures and mechanical properties of ultrafine grained 7075 Al alloy processed by ECAP and their evolutions during annealing, **Y.H. Zhao, X.Z. Liao, Z. Jin, R.Z. Valiev, Y.T. Zhu,** 15, Acta Materialia,2004, Vol. 52, pp. 4589–4599.

123. Effect of aging treatment on heavily deformed microstructure of a 6061 aluminum alloy after equal channel angular pressing, **J.K Kim, H.G Jeong, S.I Hong, Y.S Kim, W.J Kim,** 8, Scripta Materialia, 2001,Vol. 45, pp. 901–907.

124. Optimization of strength and ductility of 2024 Al by equal channel angular pressing (ECAP) and post-ECAP aging, **W.J. Kim, C.S. Chung, D.S. Ma, S.I. Hong, H.K. Kim,** 4, Scripta Materialia, 2003,Vol. 49, pp. 333–338.

125. Development of ultrafine grained high strength Al–Cu alloy by cryorolling, **T. Shanmugasundaram, B. S. Murty, V. Subramanya Sarma**, Scripta materialia **,**2006, Vol. 54.pp.2013-2017.

126. Effect of cryo-rolling and annealing on microstructure and properties of commercially pure aluminium,**Rangaraju Nikhil,** Materials Science and Engineering A **,** 2005, Vol. 398,pp.246-251.

127. Development of ultrafine grained high strength age hardenable Al 7075 alloy by cryorolling, **Sushanta Kumar Panigrahi, R. Jayaganthan, Materials & Design ,**2011, Vol. 32,pp.3150-3160.

128. Optimizing the strength and ductility of the fine structured 2024 al alloy by nano precipitation, **S. Cheng, Y.H. Zhao,Y.T. Zhu, E. Ma,** Acta materialia,2007, Vol. 55, pp. 5822-5832.

129. Nanostructured high-strength molybdenum alloys with unprecedented tensile ductility, **G. Liu, G. J. Zhang, F. Jiang, X. D. Ding, Y. J. Sun, J. Sun ,E. Ma** , Nature Materials,2013, Vol. 12, pp. 344–350 .

130. Microalloying Ultrafine Grained Al Alloys with Enhanced Ductility, **L. Jiang, J.K. Li, P. M.Cheng, G. Liu, R. H. Wang, B. A. Chen, J. Y. Zhang, J. Sun, M. X. Yang, G. Yang.** , Scientific reports, 2014,Vols. 4,pp. 3605.

131. Improving the tensile ductility and uniform elongation of high-strength ultrafine-grained Al alloys by lowering the grain boundary misorientation angle, **T. Hu, K. Ma, T. D.Topping, B. Saller, A. Yousefiani,J. M. Schoenung, E. J. Lavernia**, Scripta Materialia,2014, Vols. 78-79, pp. 25-28.

132. Experimental and Numerical Investigation of the Role ofGrain Boundary Misorientation Angle on theDislocation–Grain Boundary Interactions, **Demircan Canadinc, Emre Biyikli, Thomas Niendorf, Hans Jurgen Maier** , Advanced Engineering Materials , 2011,Vol. 13, pp. 281.

133. Production of ultrafine grain sizes in aluminium sheets by severe plastic deformation using the technique of groove pressing,**A**. **Krishnaiah, Uday Chakkingal, P. Venugopal,** Scripta Materialia **,**2005, Vol. 52,pp.1229-1233.

134.Bulk Nanostructured Metals for Innovative Applications. **Z. Ruslan , P. Ilchat Sabirov, Alexander Zhilyaev, G. langdon Terence,** 10, Journal of Materials,JOM, 2012, Vol. 64, pp. 1134-1142.

135. Nanostructured materials: processing, properties and applications, **Carl. C. Koch, ,William Andrew,** 2006.

136.Performance and applications of nanostructured materials produced by severe plastic deformation, **Yuntian. T . Zhu, Terry C. Lowe, Terence G. Langdon,** Scripta Materialia**, 2**004, Vol. ,51pp.825-830 .

137. Simultaneously increasing the ductility and strength of nanostructured alloys, **Yong-Hao Zhao,** Advanced Materials-Deerfield Beach Then Weinheim**,** 2006, Vol. 18,pp.2280 .

138.http://www.britannica.com/EBchecked/topic/369081/materials-science/32300/Materials-for-medicine. [Online]

139. Bulk nanostructured materials, **Michael. J. Zehetbauer,Yuntian Theodore Zhu,** John Wiley & Sons, 2009.

140. Ti based biomaterials, the ultimate choice for orthopaedic implants–a review, **Ma. Geetha,** Progress in Materials Science ,2009, Vol. 54.3,pp.397-425.

141.Development of new metallic alloys for biomedical applications, **Niinomi Mitsuo, Masaaki Nakai, Junko Hieda,**Acta Biomaterialia, 2012, Vol. 8,pp.3888-3903.

142. Extreme grain refinement by severe plastic deformation ,A wealth of challenging science, **Y. Estrin, A.Vinogradov**, Acta materialia, 2013, Vol. 61, pp. 782-817.

143.On The Corrosion Behaviour Of Ultra-Fine Grain Copper, **A. Vinogradov, T. Mimaki, S. Hashimoto, R. Valiev** 3, , Scripta Materialia, 1999, Vol. 41, pp. 319–326.

144.Corrosion and ion release behavior of ultra-fine grained bulk pure copper fabricated by ECAP in Hanks solution as potential biomaterial for contraception, **X.X. Xu, F.L. Nie, J.X. Zhang, W. Zheng, Y.F. Zheng, C. Hu, G. Yang**, Materials Letters , 2010, Vol. 64, pp. 524–527.

145.Bio-corrosion of a magnesium alloy with different processing histories, **H. Wang, Y. Estrin, Z. Zúberová**, Materials Letters, 2008, Vol. 62, pp. 2476–2479.

146.Friction stir processing of magnesium–nanohydroxyapatite composites with controlled in vitro degradation behavior, **B. Ratna Sunil, T.S. Sampath Kumar, Uday Chakkingal, V. Nandakumar, Mukesh Doble**, Materials Science and Engineering C, 2014,Vol. 39, pp. 315–324.

147. Cellular and molecular interactions between MC3T3-E1 pre-osteoblasts and nanostructured titanium produced by high-pressure torsion, **S. Faghihi, F. Azari, A.P. Zhilyaev, J.A. Szpunar, H. Vali, M.Tabrizian,** Biomaterials, 2007, Vol. 28(27), pp. 3887-3895.

148. Accelerated growth of preosteoblastic cells on ultrafine grained titanium, **Y.Estrin, C. Kasper, S. Diederichs, R. Lapovok,** 4, Journal of Biomedical Materials Research - Part A, 2009, Vol. 90, pp. 1239-1242.

149. Nanostructured titanium for biomedical applications, **R.Z. Valiev, I.P. Semenova, V.V. Latysh, H. Rack,T.C. Lowe, J. Petruzelka, L. Dluhos, D.Hrusak, J.Sochova,** 8, Advanced Engineering Materials, 2008, Vol. 10, pp. B15-B17+702.

150. Titanium alloys for biomedical applications, **H. J Rack,J. I. Qazi,** Materials Science and EngineeringC, 2006, Vol. 26.8,pp.1269-1277 .

151. Biomedical applications of titanium and its alloys, **C. N. Elias, Jom 46-49,**2008, Vol. 60.

152. Nanostructured titanium for biomedical applications, **Ruslan Z**. **Valiev,** Advanced engineering materials**,** 2008, Vol. 10,pp B15-B17.

153. The effect of pre-processing and grain structure on the bio-corrosion and fatigue resistance of magnesium alloy AZ31, **H.Wang, Y. Estrin, H. Fu, G. Song, Z. Zúberová,** 11, Advanced Engineering Materials, 2007, Vol. 9, pp. 967-972.

154. Severe Plastic Deformation as a means of producing Ultra-Fine-Grained Net-Shaped Micro Electro-Mechanical Systems Parts, **Y. Estrin, M. Janecek, G.I. Raab, R.Z. Valiev, A. Zi**, Metallurgical And Materials Transactions A, 2007, Vol. 38A, pp. 1906-1909.

155. Fabrication of MEMS components using ultra fine grained aluminium alloys, **Xiao Guang Qiao, Nong Gao, Zakaria Moktadir, Michael Kraft, Marco J Starink,** Journal of Micromechanics and Microengineering, 2010, Vol. 20, pp. 045029.

156. Microembossing of ultrafine grained Al: microstructural analysis and finite element modeling, **X.G. Qiao, M.T. Bah, J.W. Zhang, N. Gao, Z. Moktadir, M. Kraft, M.J. Starink**, Journal of micromechanics and microengineering , 2010,Vol. 20, pp. 105002.

157. Properties of AA 6061 processed by multi axial compression/forging (MAC/F), **B.Cherukuri, R.Srinivasan,** Materials and Manufacturing Process , 2006, Vol. 21, pp. 519–25.

158. Grain refinement in an as-cast AZ61 magnesium alloy processed by multi-axial forging under the multitemperature processing procedure, **Chen Qiang,** Materials Science and Engineering A, 2012 ,vol.541,pp98-104.

159. Role of stacking fault energy in strengthening due to cryo-deformation of FCC metals, **Sarma V. Subramanya**, Materials Science and Engineering A **,** 2010, Vol. 527,pp.7624-7630.

160. Comparative Study of Microstructure and Mechanical Properties of Al 6063 Alloy Processed by Multi Axial Forging at 77K and Cryorolling, **Maruff Hussain,** Procedia Engineering , 2014, Vol. 75,pp.129-133

161. Asymmetric cryorolling for fabrication of nanostructural aluminum sheets, **Y. U.Hailiang,** Scientific reports 2 **,** 2012.

162. The improvement of strength and ductility in ultra-fine grained 5052 Al alloy by cryogenic-and warm-rolling, **U. G.Kang,** Journal of materials science, 2010, Vol. 45,pp. 4739-4744.

163. Mechanical properties and microstructural evolution of Al 6061 alloy processed by multidirectional forging at liquid nitrogen temperature, **P.Nageswara rao, Dharmendra Singh, R.Jayaganthan.** , Materials and Design, 2014,Vol. 56l, pp. 97–104.

164. Effect of rolling temperature on microstructure and mechanical properties of 6063 Al alloy, **S. K. Panigrahi, R. Jayaganthan,** Material Science and Engineering A , 2008, Vol. 492 , pp. 300-305.

165. Effect of annealing on thermal stability, precipitate evolution, and mechanical properties of cryorolled Al 7075 alloy, **S.K. Panigrahi, R.Jayaganthan,** Metallurgical and Materials Transactions A, Physical Metallurgy and Materials Science, 2011,Vol. 42, pp. 3208-3217.

166. **Gang, U.G**, Mater Trans JIM, 2009, Vol. 50, pp. 82–86.

167. Effect of annealing and aging treatment on mechanical properties of ultrafine grained Al 6061 alloy. **P. N. Rao, S. K. Panigrahi, R. Jayaganthan**, Material Science and Technology, 2010, Vol. 26, pp. 371–374.

168. Effect of annealing on microstructure and mechanical properties of Al 6061 alloy processed by cryorolling, **P. Nageswara Rao, D. Singh, R. Jayaganthan**, Material Science and Technology , 2013, Vol. 39, pp. 76-82.

169. Effects of warm rolling and ageing after cryogenic rolling on mechanical properties and microstructure of Al 6061 alloy, **P.Nageswara rao, R.Jayaganthan**, Materials and Design, 2012, Vol. 39, pp. 226–233.

170. Dynamic recrystallisation and dynamic precipitation in AA6061 aluminium alloy during hot deformation, **X. H. Fan, M. Li, D. Y. Li, Y. C. Shao, S. R. Zhang, Y. H. Peng**, Material Science and Technology, 2014, Vol. 30, pp. 1263-1272.

171. Enhanced Ductility in Ultrafine-Grained Al Alloys Produced by SPD Techniques, **R. Z. Valiev, M. Y. Murashkin, B. Straumal**, Material Science Forum , 2009, Vols. 633–634, pp. 321–332.

172. Bulk nanostructured materials from severe plastic deformation, **R.Z. Valiev, R.K. Islamgaliev, I.V. Alexandrov**, Progress in Material Science, 2000, Vol. 45, pp. 103-189.

173. Structure of grains and grain boundaries in cryo-mechanically processed Ti alloy, **A. Dasgupta, S. Murugesan, S. Saroja, M. Vijayalakshmi, M. Luysberg, M. Veron, E. Rauch, T. Jayakumar** , Journal of Material Science , 2013,Vol. 48, pp. 4592–4598.

174. Mechanical properties and corrosion behaviour of nanocrystalline Ti–5Ta–1.8Nb alloy produced by cryo-rolling, **P. Bhaskar, A. Dasgupta, V. S. Sarma, U. K. Mudali, S. Saroja**, Material Science and Engineering A , 2014,Vol. 616 , pp. 71-77.

175. Microstructure and mechanical properties of ultra fine grained Cu-Zn and Cu-Al alloys produced by cryorolling and annealing, **V. Subramanya Sarma, K. Sivaprasad, D. Sturm, M. Heilmaier**, Material Science and Engineering A , 2008, Vol. 489, pp. 253-258.

176. The precipitation sequence in Al–Mg–Si alloys, **G.A. Edwards, K. Stiller, G.L.Dunlop, M.J. Couper,** 11, Acta Materialia, 1998,Vol. 46, pp. 3893-3904.

177. Precipitation hardening processes in an Al–0.4%Mg–1.3%Si–0.25%Fe aluminum alloy, **A.K. Guptha, D.J. Lloyd, S.A Court**, Material sceince and Engineering A, 2001,Vol. 301A, pp. 140-146.

178. Pre-Precipitate Clusters And Precipitation Processes In Al-Mg-Si Alloys, Acta materialia , 1999 ,Vol. 47, pp. 1537-1548,.

179. The influence of composition and natural aging on clustering during preageing in Al- Mg-Si alloys, **M. Torsæter, H.S. Hasting, W. Lefebvre, C.D. Marioara, J.C. Walmsley, S.J. Andersen, R.Holmestad**, Journal of Applied Physics, 2010,Vol. 108, pp. 073527.

180. Optimizing the strength and ductility of fine structured 2024 Al alloy by nano-precipitation, **S. Cheng, Y.H. Zhao, Y.T. Zhu, E. Ma,** 17 , Acta materialia, 2007, Vol. 55, pp. 5822–5832.

181. Studies on potentiodynamic polarization behaviour of Cryorolled Al-Mg-Si Alloy, **N. N. Krishna, B. Gopi, K. Sivaprasad, and V. Muthupandi**, Key to Engineering Materials , 2013, Vol. 545, pp. 153-157.

182. Effect of rolling temperature on microstructure and mechanical properties of cryorolled Al-Mg-Si alloy reinforced with 3wt% TiB2 In Situ Composite, **B. Gopi, N. Naga Krishna, K. Sivaprasad, K. Venkateswarlu,** Advanced Material Research, 2012, Vol. 584, pp. 556-560.

183. A Comparative study on mechanical properties of Al 7075 alloy processed by rolling at cryogenic temperature and room temperature, **S. K. Panigrahi, R. Jayaganthan,** Material Science Forum **,** 2008, Vol. 584–586, pp. 734-740.

184. Effect of ageing on microstructure and mechanical properties of bulk, cryorolled, and room temperature rolled Al 7075 alloy, **S. K. Panigrahi, R. Jayaganthan**, Journal of Alloys and Compounds, 2011, Vol. 509, pp. 9609-9616.

185. Effect of cryorolling and warm rolling on precipitation evolution in Al 6061 alloy, **P.Nageswara Rao, B.Viswanadh,R. Jayaganthan,** 12, , Materials Science and Engineering A, 2014, Vol. 606, pp. 1–10.

186. Low-Temperature Differential Scanning Calorimetry of an Al-Mg-Si Alloy, **C. S. T Chang, J. Banhart ,**7, Metallurgical and Materials Transactions A, 2011,Vol. 42, pp. 1960-1964.

187. Analytical solution for the Kissinger equation, **P. Roura, J. Farjas**, Journal of Materials Research, 2009,Vol. 24 , pp. 3095-3098.

188. The effect of cold deformation on the kinetics of the β″ precipitates in an Al-Mg-Si alloy, R**. S. Yassar, D. P. Field, H. Weiland**, Metallurgical and Material Transactions A , 2005,Vol. 36, pp. 2059-2065.

189. A theoritical and experimental study of aluminium alloy 6061-SiC metal matrix composite to identify the operative mechanism for accelerated ageing, **I.Dutta, D.L. Bourell, Latimer,** Materials Science and Engineering A, 1989, Vol. 112, pp. 67-77.

190. Effect of cold rolling on the aging kinetics of Al2O3 6061 Al composite by differential scanning calorimetric technique, **Huei-Long Lee, Wun-Hwa Lu, Sammy Lap-Ip Chan**, Scripta Metallurgica et Materiala, 1991 , Vol. 25 , pp. 2165-2170.

191. Effect of cold rolling on the aging kinetics of Al composite by differential scanning calorimetric technique, **H.-L. Lee, W.-H. Lu, S. L.-I. Chan,** Scripta Metallurgica and Materialia, 1991, Vol. 25 , pp. 2165–2170.

192. Strength and biaxial formability of cryo-rolled 2024 aluminium subject to concurrent recovery and precipitation, **M. Weiss, A. S. Taylor, P. D. Hodgson, N. Stanford**, Acta Materialia, 2013, Vol. 61, pp. 5278–5289.

193. Effect of rolling temperature on the evolution of defects and properties of an Al–Cu alloy, **V.S. Sharma, W.W. Jian, J. Wang, H. Conrad, Y.T. Zhu,** Journal of Material Science , 2010, Vol. 45 , pp. 4846–4850.

194. Discussion of the Theories of Line Broadening, **G. K. Williamson, W. H. Hall**, Acta Metallurgica , 1953,Vol. 1, pp. 22–31.

195. Pre-aging to improve bake hardening in a twin-roll cast Al–Mg–Si alloy, **Y Birol,** Material Science and Engineering A, 2005, Vol. 391, pp. 175–180.

196. The effect of coarse second-phase particles and fine precipitates on microstructure refinement and mechanical properties of severely deformed Al alloy, **I. Gutierrez-Urrutia, M.A. Munoz-Morris, D.G. Morris,** Materials Science and Engineering A , 2005, Vol. 394, pp. 399–410.

197. On the effect of SPD on recycled experimental aluminium alloys: Nanostructures, particle break-up and properties, **P. Szczygiel, H.J. Roven, O. Reiso,** Materials Science and Engineering A , 2005, Vols. 410–411, pp. 261–264.

198. Grain boundaries in ultrafine grained materials processed by severe plastic deformation and related phenomena, **X. Sauvage, G. Wilde, S.V. Divinski, Z. Horita, R.Z. Valiev**, Materials Science and Engineering A, 2012, Vol. 540, pp. 1–12.

199. Influence of equal-channel angular pressing on precipitation in an Al–Zn–Mg–Cu alloy, **G. Sha, Y.B. Wang, X.Z. Liao, Z.C. Duan, S.P. Ringer, T.G. Langdon**, Acta Materialia , 2009, Vol. 57, pp. 3123–3132.

200. The effect of severe plastic deformation on precipitation in supersaturated Al–Zn–Mg alloys, **J. Gubicza, I. Schiller, N.Q. Chinh, J. Illy, Z. Horita, T.G. Langdon,** Materials Science and Engineering A , 2007, Vols. 460–461, pp. 77–85.

201. The formation of nanograin structures and accelerated room-temperature theta precipitation in a severely deformed Al–4 wt.% Cu alloy, **Y. Huang, J.D. Robson, P.B. Prangnell,** Acta Materialia ,2010, Vol. 58, pp. 1643–1657.

202. The improvement of strength and ductility in ultrafine grained 5052 Al alloy by cryogenic and warm rolling, **U.G.Kang, J.C. Lee, S.W. Jeong, W.J. Nam,** Journal of Material Science, 2010, Vol. 45, pp. 4739-4744.

203. Structure and Mechanical Properties of Aluminum Alloy 6061 Subjected to Equal-Channel Angular Pressing in Parallel Channels, **M. Yu. Murashkin, E. V. Bobruk, A. R. Kil'mametov, R. Z. Valiev** , The Physics of Metals and Metallography, 2009,Vol. 108, pp. 415–423.

204. A calorimetric study of precipitation in commercial aluminium alloy, **I. Dutta, S. M. Allen.** , Journal Of Materials Science Letters , 1991, Vol. 10 , pp. 323-326 .

205. Influence of extrusion temperature on the aging behavior of 6061Al-15 vol%SiCw composites, **A. Borrego, J. Ibanez, V. Lopez, M. Lieblich, G. Gonzales-Doncel**, Scripta Materialia, 1996, Vol. 34, pp. 471–478.

206. The effect of sample preparation on the DSC analysis of 6061 alloy, **Y.Birol,** 24, Journal of Materials Science, 2005, Vol. 40, pp. 6357-6361.

207. A calorimetric and metallographic study of precipitation process in AA6061 and its composites, **Y. Song, T.N. Baker,** Material Science and Engineering A, 1995, Vol. 201, pp. 251–260.

208. Precipitation hardening in aluminum alloy 6022, **W.F. Miao, D.E. Laughlin**, Scripta Materialia, 1999, Vol. 40, pp. 873–878.

209. 6061 Aluminum alloy-SiC particulate composite: acomparison between aging behavior in T4 and T6 treatments, **P. Appendino, C. Badini,** Material Science and Engineering A, 1991, Vol. 135, pp. 275–279.

210. Effect of cryorolling and annealing on microstructure and properties of commercially pure aluminium, **N.Rangaraju, T. Raghuram, B.V. Krishna, K.P. Rao, P. Venugopal**, Material Science and Engineering A, 2005, Vol. 398, pp. 246-251.

211. Effect of cryorolling on the structure and the mechanical properties of ultrafine-grained nickel, **E. V Naidenkin, K. V., Ivanov, E. V Golosov**, Russian Metallurgy, 2014, Vol. 4, pp. 303–307.

212. The effect of cryorolling strain on precipitation kinetics of Al 7075 alloy, **R.Jayaganthan, Sushanth Kumar Panigrahi,** Materials Scinece Forum, 2008, Vol. 584-586, pp. 911-916.

213. Development of ultrafine-grained Al 6063 alloy by cryorolling with the optimized initial heat treatment conditions, **Sushanth Kumar Panigrahi, R. Jayaganthan**, Materials and Design, 2011, Vol. 32, pp. 2172–2180.

214. Development of ultrafine grained high strength Al–Cu alloy by cryorolling, **T. Shanmugasundaram, B.S. Murty, V.S. Sarma**, Scripta Materialia, 2006, Vol. 54, pp. 2013–2017.

215. Asymmetric cryorolling for fabrication of nanostructural aluminum sheets, **H. Yu, C.Lu, K.Tieu, X. Liu,Y. Sun, Q.Yu, C. Kong,** Scientific Reports, 2012, Vol. 2, pp. 772.

216. Optimizing the strength and ductility of the fine structured 2024 al alloy by nano precipitation, **S.Cheng, Y.H. Zhao,T.T. Zhu, E.Ma,** Acta materialia, 2007, Vol. 55, pp. 5822-5832.

217. Effects of ARB and ageing processes on mechanical properties and microstructure of 6061 aluminum alloy, **Mohammad Reza Rezaei, Mohammed Reza Toroghinejad, Fakhreddin Ashrafizadeh** , Journal of Material Processing and Technology, 2011,Vol. 211, pp. 1184–90.

218. Eight routes to improve the tensile ductility of bulk nanostructured metals and alloys, **E.Ma**, JOM, 2006, Vol. 58, pp. 49-53.

219. Mechanisms controlling the artificial aging of Al–Mg–Si Alloys, **S. Pogatscher, H. Antrekowitsch, H. Leitner, T. Ebner, P.J. Uggowitzer**, Acta Materialia, 2011,Vol. 59, pp. 3352-3363.

220. Electron microscopy studies of the age-hardening behaviors in 6005A alloy and microstructural characterizations of precipitates, **W. Yang, L. Huang, R. Zhang, M. Wang, Z. Li, Y. Jia, R. Lei, X. Sheng**, Journal of Alloys and compounds, 2012, Vol. 514, pp. 220-233.

221. **S.D. Dumolt, D.E. Laughlin, J.C. Williams**, Scripta Materialia, 1984, Vol. 18, pp. 1347.

222. **W.F. Smith,** Metallurgical Transactions, 1973, Vol. 4, pp. 2435.

223. **C. Ravi, C. Wolverton**, Acta Materialia, 2004, Vol. 52, pp 4213.

224. **K. Yamada, T. Sato, A. Kamio** , Material Science Forum, 2000,Vol. 331–337, pp. 669.

225. Positive effect of natural pre-ageing on precipitation hardening in Al–0.44at% Mg–0.38 at% Si alloy, **C.S.T. Chang, I. Wieler, N. Wanderka, J. Banhart** , Ultramicroscopy, 2009,Vol. 109 , pp. 585–592.

226. Three dimensional atom probe characterization of nanoclusters responsible for multistep ageing behavior of an Al-Mg-Si alloy, **A. Serizawa, S.Hirosawa, T.Sato**, Metallurgical and Materials Transactions A,2008, Vol. 39A, pp. 243-251.

227. **A. Luo, D.J. Lloyd, A. Gupta, W.V. Youdelis**, Acta Metallurgica and Materials, 1993, Vol. 41 (3).

228. Pre-straining to improve the bake hardening response of a twin-roll cast Al-Mg-Si alloy, **Birol Yucel**, Scripta materialia, 2005, Vol. 52, pp. 169-173.

229. **Y.Birol,** Mater. Sci. Eng. A,2005, Vol. 391, pp. 175–180.

230. On the precipitation-Hardening behaviour of the Al-Mg-Si-Cu alloy AA611, **S.Esmaeili, X. Wang, D.J. Lloyd, W.J.Poole,** Metallurgical and Materials Transactions A, 2003,Vol. 34A, pp. 751.

231. Influence of Pre-Straining and Pre-Ageing on the Age-Hardening Response of Al-Mg-Si Alloys, **Yong Yan, Zeqin Liang, John Banhart**, Material Science Forum,2014, Vols. 794-796 , pp. 903-908.

232. The determination of the activation energy varying with the precipitated fraction of metastable phase in an Al–Si–Mg alloy using non-isothermal dilatometry, **Mourad Ibrahim Daoudi, Abdelhafid Triki, Abdelkrim Redjaimia, Chihaoui Yamina**, Thermochimica Acta,2014, Vol. 577 , pp. 5– 10 .

233. Study of the formation kinetics of Metastable phases in quenched Al-Mg-Si Alloys,**A. A. Vasilyev, N. L. Kuzmin, A. S. Gruzdev,** 8, Physics of the Solid State,2011, Vol. 53, pp. 1658-1663.

234. **H.E. Kissinger,** Analytical Chemistry, 1957, Vol. 40, pp. 1702.

235. Effect of pre-aging and maturing on the precipitation hardening of an Al–Mg–Si alloy, **T. Abid, A. Boubertakh, S. Hamamda**, Journal of Alloys and Compounds, 2010,Vol. 490, pp. 166–169.

236. Achieving ultrafine-grained structure in a pure nickel by friction stir processing with additional cooling, **P. Xue, B.L. Xiao, Z.Y. Ma**, Materials and Design , 2014,Vol. 56, pp. 848-851.

237. Precipitation phenomena, thermal stability and grain growth kinetics in an ultra-fine grained Al 2014 alloy after annealing treatment, **A. Dhal, S.K. Panigrahi, M.S. Shunmugam**, Journal of Alloys and Compounds, 2015, Vol. 649, pp. 229-238.

238. Formation and reversion of clusters during natural aging and subsequent artificial aging in an Al–Mg–Si alloy, **Y. Aruga, M. Kozuka, Y. Takaki, T.Sato**, Materials Science and Engineering A,2015, Vol. 631, pp. 86–96.

239. Recent development in aluminium alloys for the automotive industry, **W. M. Zhuang, L. Bottema, J. Wittebrood, A. D. Smet, P. Haszler, A. Vieregge,** Material Science and Engineering A ,2000, Vol. 280(1), pp. 37-49.

240. Grain refinement limit and mechanical properties of 6063 alloy inoculated by Al–Ti–C (B) master alloys, **E. Wang, T. Gao, J. Nie, X. Liu,** Journal of Alloys and Compounds,2014, Vol. 594, pp. 7–11 .

241. Production of Al–Ti–B master alloys from Ti sponge and KBF4, **Y.Birol,** Journal of Alloys and Compounds ,2007, Vols. 440(1–2), pp. 108-112.

242. Principles of equal-channel angular pressing as a processing tool for grain refinement, **R. Z. Valiev, T. G. Langdon,** Progress in Materials Science ,2006, Vol. 51, pp. 881–981.

243. Elongation increase in ultra-fine grained Al–Fe–Si alloy sheets, **H.W. Kim, S.B Kang, N. Tsuji, Y. Minamino,** Acta Materialia,2005, Vol. 53(6), pp. 1737–1749.

244. Evolution of sub-micron grain size and weak texture in magnesium alloy Mg–3Al–0.4Mn by a modified multi-axial forging process, **S. Biswas, S. Suwas,** Scripta Materialia,2012, Vol. 66, pp. 89–92.

245. Multidirectional forging of AZ91 magnesium alloy and its effects on microstructures and mechanical properties, **K. B. Nie, K. K. Deng, X. J. Wang,F. J. Xu, K.Wu, M. Y Zheng,** Material Science and Engineering A , 2015,Vol. 624, pp. 157–168.

246. Effect of ageing on microstructure and mechanical properties of a multi-directionally forged Mg– 6Al–1Zn alloy, **H.Miura, T. Maruoka, J.J. Jonas ,** Material Science and Engineering A,2013, Vol. 563, pp. 53.

247. Microstructure and mechanical properties of multi directionally forged Mg-Al-Zn alloy, **H. Miura, T. Maruoka, J.J. Jonas,** Scripta materialia,2012, Vol. 66, pp. 49-51.

248. Dynamic processes for nanostructure development in Cu after severe cryogenic rolling deformation,**Y .Wang, T. Jiao, E. Ma,** Materials Transactions ,2003, Vol. 44 (10), pp. 1926–1934 .

249. Microstructural evolution and recrystallization behavior in copper multi-directionally forged at 77 K, **Y. Nakao, H. Miura , T. Sakai,** Advanced Materials Research ,2007, Vol. 15–17, pp. 649–654.

250. Microstructural studies of Al 5083 alloy deformed through Cryorolling,**D.Singh,P.N.rao, R. Jayaganthan**, Advanced Materials Research ,2012, Vol. 585, pp. 376–380.

251. Effect of cryorolling and ageing on microstructure, mechanical properties and corrosion behavior of Al-Cu-Mg-Si alloy,**P.N**. **rao, M.Gopi,R. Jayaganthan**, Banaras Metallurgist ,2014 Vol. 19, pp. 19-25.

252. Ultrafine grain formation in face centered cubic metals during severe plastic deformation,**T. Sakai, H.Miura, X. Yang,** Material Science and Engineering A ,2009, Vols. 499(1–2), pp. 2–6.

253.Influence of specimen dimensions on the tensile behavior of ultrafine-grained Cu,**Y.H. Zhao,**

.Z.Guo,Q. Wei,A.M. Dangelewicz,C. Xu, Y.T.Zhu,T.J. Langdon, Y.Z. Zhou,E.J.

Lavernia,Scripta Materialia, 2008,Vol. 59(6), pp. 627–630.

254. The sequence of precipitation in the Al-Mg-Si-Cu alloy AA6111, **X. Wang, S. Esmaeili,D.J. Lloyd**,Metallurgical and Material Transactions A,2006, Vol. 37, pp. 2691–2699.

255. Precipitation kinetics of Al-1.12 Mg2Si-0.35 Si and Al-1.07 Mg2Si-0.33 Cu alloys, **A.Gaber, M.A. Gaffar, M.S. Mostafa, E.F. AboZeid**, Journal of Alloys and Compounds, 2007,Vol. 429, pp. 167-175.

256. The influence of temperature and storage time at RT on nucleation of the β″ phase in a 6082 Al–Mg– Si alloy,**C. Marioara, S. Andersen, J. Jansen, H. Zandbergen**, Acta Materialia,2003, Vol. 51(3), pp. 789–796 .

.